

## 2.0 Analytical Model

Two models were used in the dynamic impact runs for the borobond design of the ES-3100 shipping container; a detailed model and a simplified model. A detailed model included the drum closure details, CV details and generally a finer element mesh. The detailed model was used for all the runs, except the study which evaluated the response of the drum to various punch angles. A simplified model was used to investigate the variation in punch angles. The detailed model is discussed in Section 2.1 and the simplified model is discussed in Section 2.2.

Design drawings were used to develop the ES-3100 analytical models. The reference 5.5 AutoSketch software was used as an aid in the creation of the TrueGrid input file. The running of TrueGrid created the bulk of the LS-Dyna input file (e.g., the nodal data, element data, contact surfaces, etc). The LS-Dyna command lines and material properties were created in a separate file and edited into the TrueGrid created LS-Dyna input file. The resulting file was a complete LS-Dyna input file which was then submitted for execution.

### 2.1 Model Description - Detailed Model

Figure 2.1.1 shows the typical detailed model assembly for the ES-3100. All of the entities shown (rigid surface, crush plate, shipping package and punch) exist in the model, however, only the entities of concern in an impact were active in that impact. In the 4-foot impact and 30-foot impact only the shipping package and the rigid plate were in contact. The crush plate and the punch existed in the model, however, there was no contact between them and the shipping package. During the crush impact, the crush plate contacts the shipping package, which then contacts the rigid plate. During the crush impact, the punch exists, but is not contacted. During the punch impact, the crush plate and the rigid surface are deleted from the model, allowing contact to be made between the shipping package and the punch.

Figure 2.1.2 shows the components of the detailed model in an exploded view. The element mesh is not included in Figure 2.1.1, nor in Figure 2.1.2 for clarity. Representative element meshes for the detailed model are shown in Figures 2.1.3 and 2.1.4.

Various impact configurations of the ES-3100 detailed model are documented in this calculation. Figure 2.1.5 shows icons representing the impact configurations run for the design effort. The 4-foot impact and the punch impact are not as structurally demanding as is the 30-foot free fall impact, nor the 30-foot crush impact. Therefore, only the 30-foot impact and the crush impact were performed in the design effort runs. Figure 2.1.6

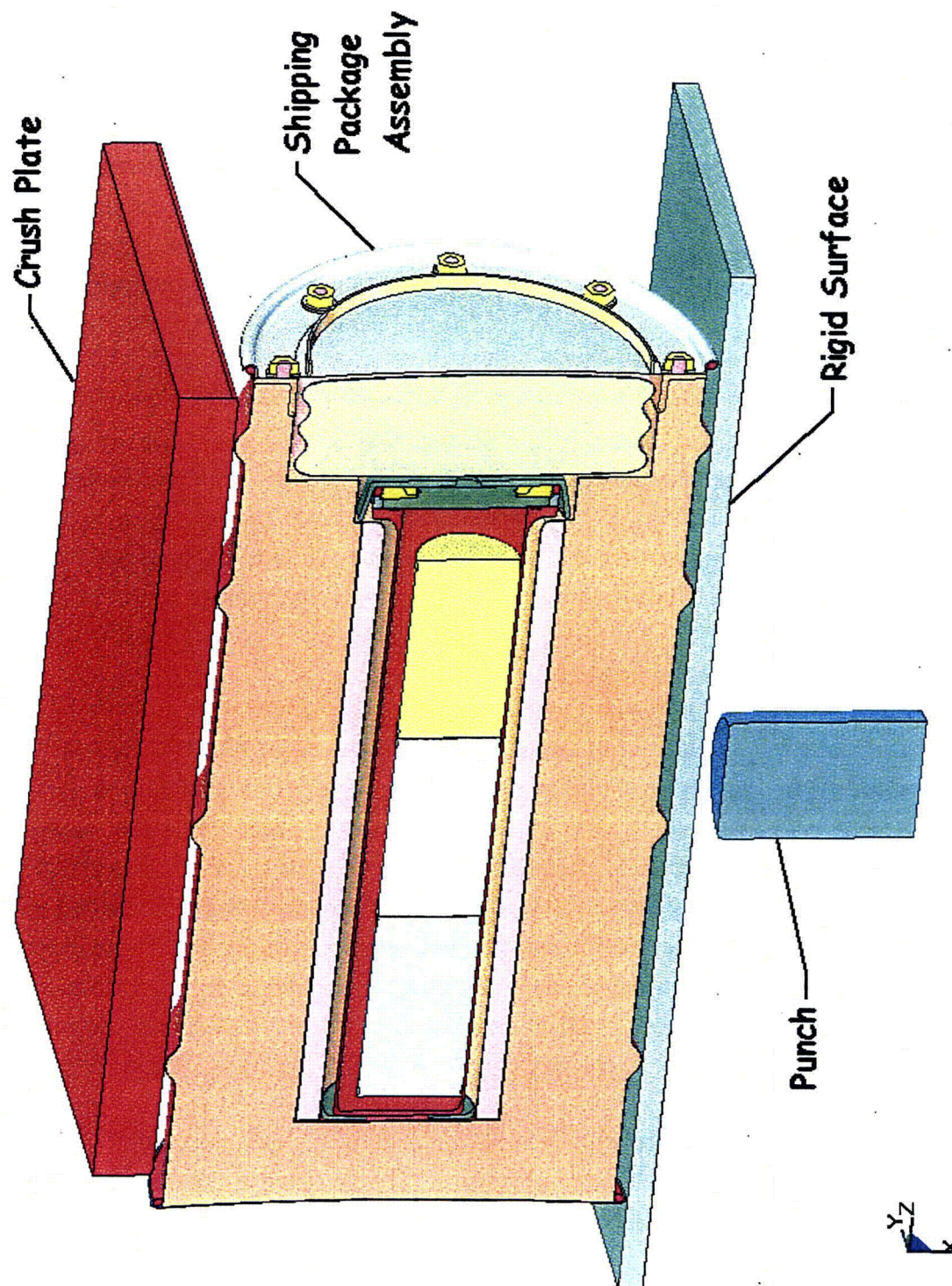


Figure 2.1.1 - Typical ES-3100 Detailed Model Assembly



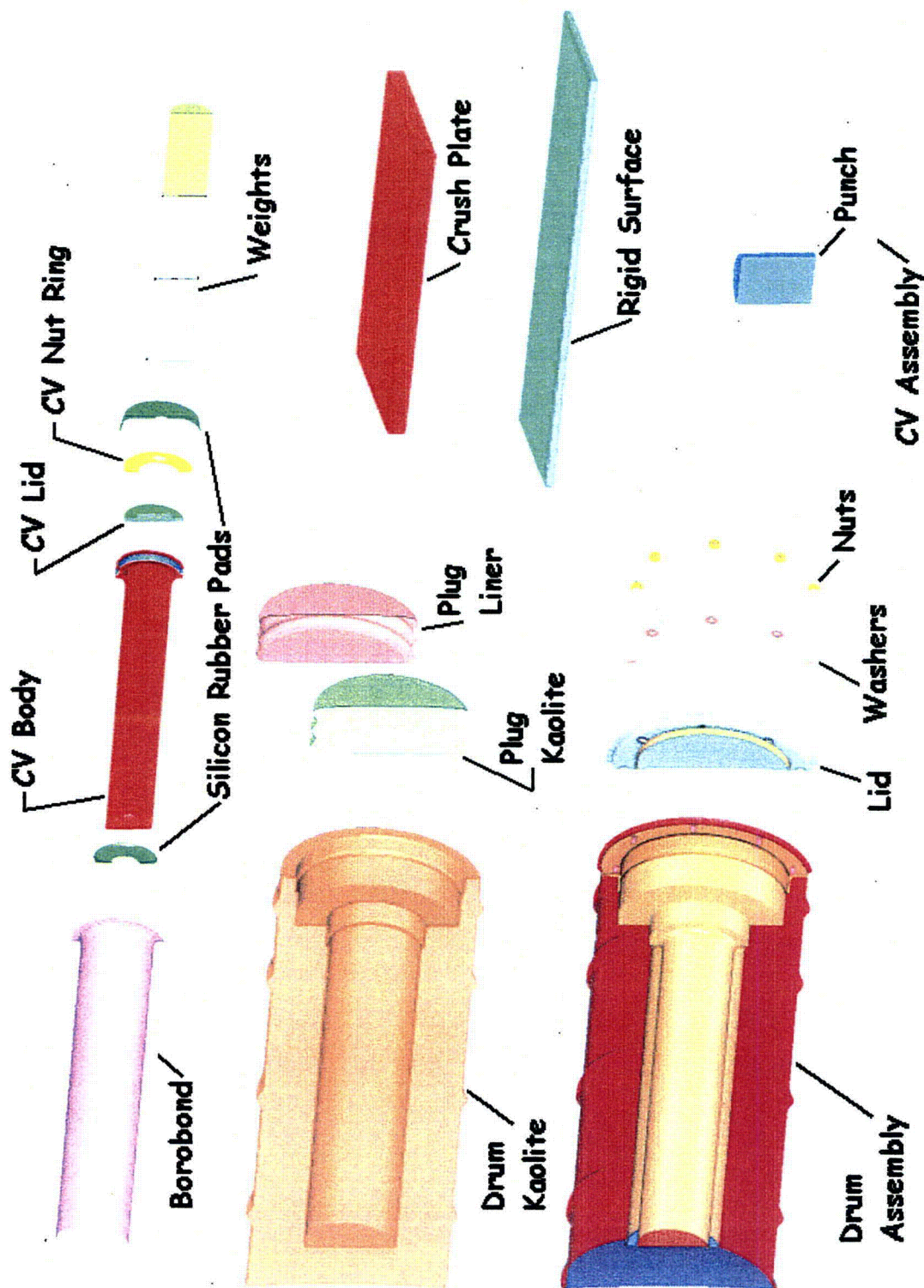


Figure 2.1.2 - ES-3100 Detailed Model Components



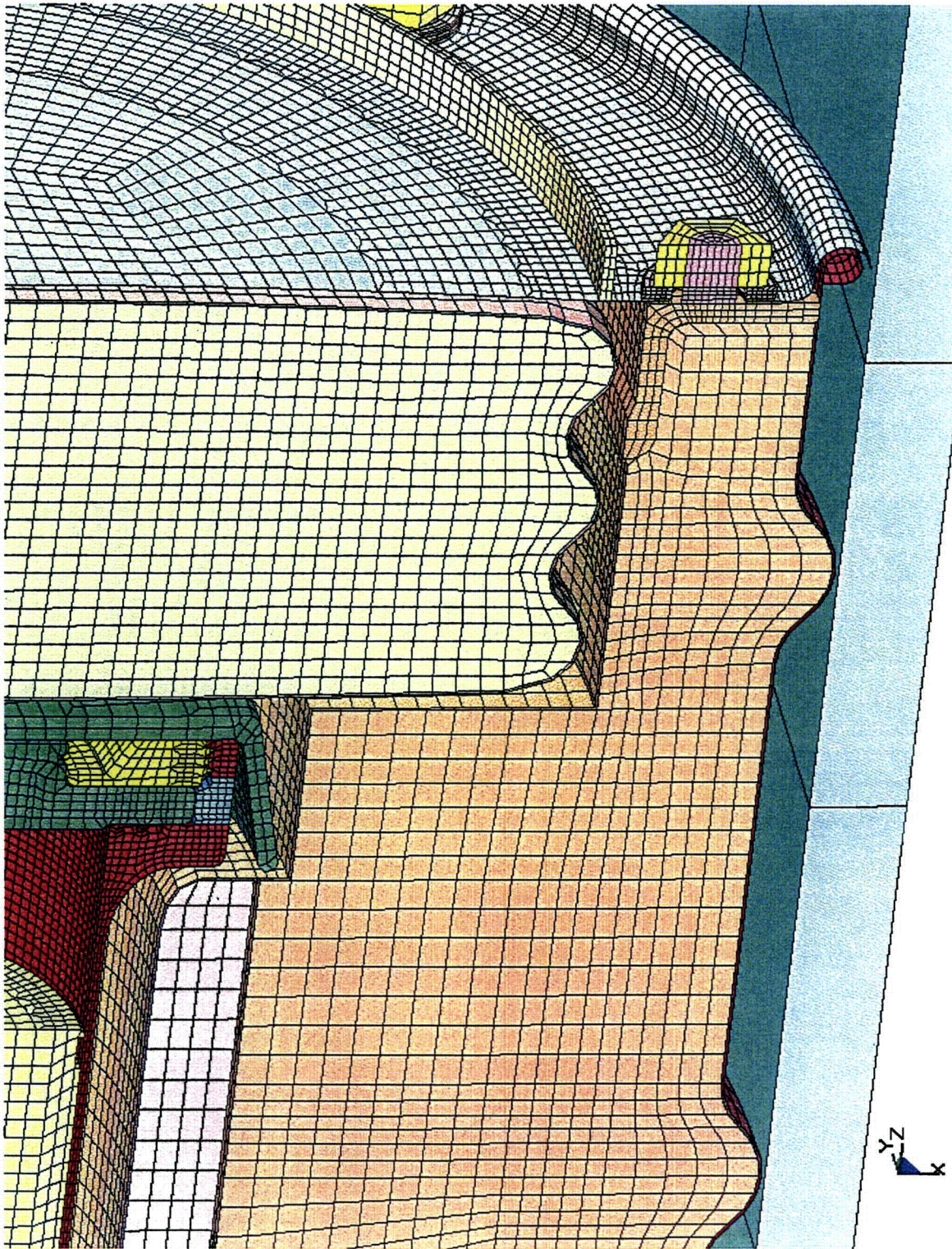


Figure 2.1.3 - Typical Element Mesh in the Upper Container Region of the Detailed Model



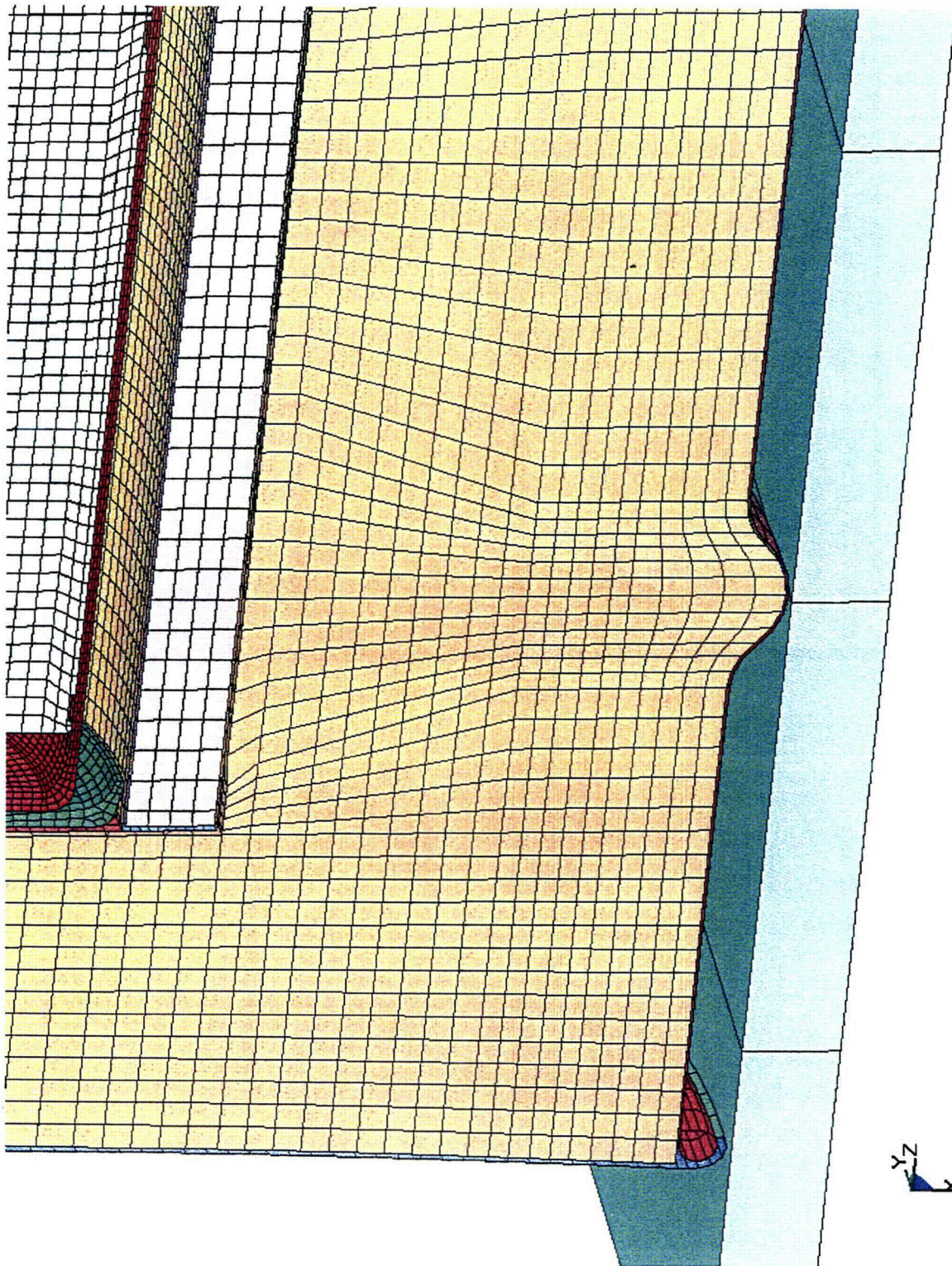


Figure 2.1.4 - Typical Element Mesh in the Lower Container Region of the Detailed Model



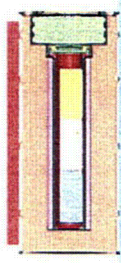
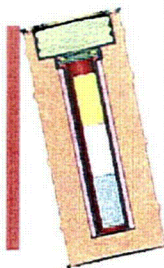
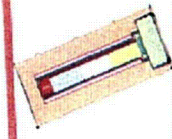
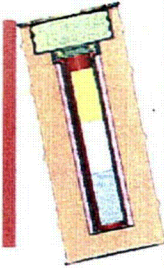
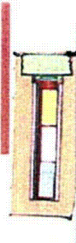


ES-3100 Dynamic Analysis						
30-Foot Impact		Crush		30-Foot Impact		
Side (run1g, 1ga)		Centered (run1g)			12 Degree Slapdown(run4g,ga) Bolts on Symmetry Plane	
		Offset (run1ga)				
Lid Corner (run2e)		Bottom Corner (run2e)			12 Degree Slapdown (run4h) Bolts off Symmetry Plane	
		Top End Down (run3b)				
		Bottom End Crush (run3b)		Offset (run4h)		
				Centered (run4ga)		
				Offset (run4g)		

Figure 2.1.5 - LS-Dyna Design Runs for Successive 30-Foot and 30-Foot Crush Impacts

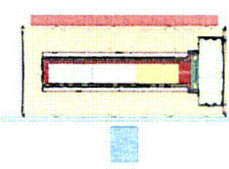
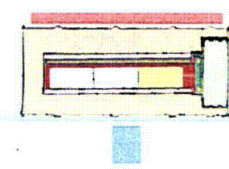
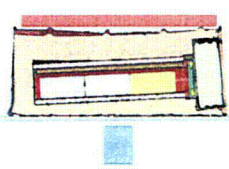
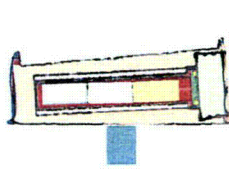
ES-3100 Dynamic Analysis			
4-Foot Impact	30-Foot Impact	30-Foot Crush Impact	40-Inch Puncture Impact
Side (Run1hl, 1hh)	Side (Run1hl, 1hh)	Side (Run1hl, 1hh)	Side (Run1hl, 1hh)
			

Figure 2.1.6 - Four Successive Impacts with the ES-3100 Bounding Kaolite Stiffness Models

shows icons representing the configurations run for the successive 4-foot + 30-foot + 30-foot crush + 40-inch punch impacts. The Figure 2.1.6 impacts were performed with the upper (-40°F, run1hh) and lower bound (100°F, run1hl) kaolite properties (see Section 2.3.5). The Figure 2.1.5 design runs were made with averaged kaolite properties (see Section 2.3.5). The run numbers (e.g., run1g, etc) are listed in Table 2.1.1 along with a verbal description of the impacts. Table 2.1.1 also identifies the Kaolite material model used for each run (see Section 2.3.5 for definition of the material properties).

Cumulative damage to the shipping package is obtained through successive impact restart solutions of LS-Dyna. At the beginning of the first impact, the initial velocity is assigned to the appropriate model nodes for the first impact. The solution is initiated and is considered over, when the kinetic energy reaches a constant value (after a minimum is reached) and when the rebound velocity reaches a constant value. Consideration was also given to the motion of the masses internal to the CV with regard to a primary impacts against the CV wall. When a run is considered over, the solution is halted and a restart file is written by LS-Dyna. The restart file captures the state of the container assembly at that point in the execution (including nodal velocities and element strains). A restart input file (text file) is then created which defines changes to be made to the model. The restart input file is used to redefine the velocity for the nodes of interest in a successive impact, or delete materials (components) if desired. The redefined velocity becomes the initial velocity, for the successive impact. The successive impact solution is then initiated with the restart file written by the halting of the previous impact and the restart input file. The velocities used in this analysis are: 193 in/sec for the 4-foot impact; 528 in/sec for the 30-foot impact; and 176 in/sec for the 40-inch punch impact.

Table 2.1.1 - Description of the ES-3100 Impacts Using the Detailed Model

Run ID	Description	Kaolite Model <sup>†</sup>
Run1g	30-foot side impact + 30-foot crush with plate centered on drum	Average stiffness, 22.4 lb/ft <sup>3</sup>
Run1ga	30-foot side impact + 30-foot crush with plate centered on CV flange	Average stiffness, 22.4 lb/ft <sup>3</sup>
Run1hl	4-foot side impact + 30-foot side impact + 30-foot crush impact + 40-inch punch impact	Lower bound stiffness, 27 lb/ft <sup>3</sup>
Run1hh	4-foot side impact + 30-foot side impact + 30-foot crush impact + 40-inch punch impact	Upper bound stiffness, 27 lb/ft <sup>3</sup>
Run2e	30-foot CG over lid corner impact + 30-foot crush on bottom corner	Average stiffness, 22.4 lb/ft <sup>3</sup>
Run3b	30-foot top end impact + 30-foot bottom end crush	Average stiffness, 22.4 lb/ft <sup>3</sup>
Run4g	30-foot, 12° slapdown with lid studs on plane of symmetry + 30-foot crush with plate centered on CV flange	Average stiffness, 22.4 lb/ft <sup>3</sup>
Run4ga	30-foot, 12° slapdown with lid studs on plane of symmetry + 30-foot crush with plate centered on drum	Average stiffness, 22.4 lb/ft <sup>3</sup>
Run4h	30-foot, 12° slapdown with lid studs off plane of symmetry + 30-foot crush with plate centered on the CV flange	Average stiffness, 22.4 lb/ft <sup>3</sup>
Run4ha	30-foot, 12° slapdown with lid studs off plane of symmetry + 30-foot crush with plate centered on the drum	Average stiffness, 22.4 lb/ft <sup>3</sup>
† - Defined in Section 2.3.5		



In the successive design impacts (Figure 2.15), a 30-foot impact was followed by a 30-foot crush impact. For these runs, the initial velocities of the shipping package assembly nodes were all defined as 528 in/sec in a direction normal and toward the rigid surface. When the initial impact was over, the run was halted and the velocities of the shipping package assembly nodes were all re-defined as 0.0 in/sec in the restart input file. This file also defined the velocity of the crush plate nodes as 528 in/sec in a direction towards the shipping package.

For the bounding kaolite stiffness runs (Figure 2.1.6), the impacts were successive 4-foot, 30-foot, 30-foot crush and 40-inch punch impacts. The 4-foot, 30-foot and 30-foot crush impacts were carried out as defined previously. The successive punch impact was initiated with the restart input file deleting the crush plate and the rigid plate from the model. The restart input file also redefined the velocity of the shipping package nodes to be towards the punch. This allowed the shipping package to pass through the original position of the rigid surface and impact the punch.

Table 2.1.2 gives the shipping package component masses and weights used in the detailed model analyses. Summations for assembly weights are also listed along with a total assembly weight. As discussed in the Section 2.3 on material models, an initial mass based on preliminary information supplied by the designer is adjusted to match expected hardware weights. This adjustment is required due to the faceted element faces on the inner and outer radius surfaces and the fact that small details are not explicitly modeled (holes, notches, etc). The total weight (full model) of the model is about 427.85 pounds, with 22.4 lb/ft<sup>3</sup> kaolite. The mass moment of inertia for the package is 90.84 in\*lb\*sec<sup>2</sup> about the global Y axis and the CG is located at Z = 22.4 inches.

Contact surfaces are used to allow adjacent components to separate, bear and/or slide along an adjacent surface. The contact used between the metal components of the model is a LS-Dyna single surface contact. Each node is reactive against every other element in the defined set. The contact between the borobond and its stainless steel liners; and the kaolite and its stainless steel liners is a surface to surface contact. All package nodes are defined as reactive to the rigid surface.

Table 2.1.2 - Analysis Weights for ES-3100

Material Number	Component Description	Run1g-Side		Run1h-Side		Run1hh-Side		Run2e-Lid Comer		Run3b-Lid End		Run4g- Slapdown		Run4h- Slapdown	
		mass *	weight **	mass *	weight **	mass *	weight **	mass *	weight **	mass *	weight **	mass *	weight **	mass *	weight **
m 1	CV body	2.73E-02	21.10	2.73E-02	21.10	2.73E-02	21.10	2.73E-02	21.10	2.73E-02	21.10	2.73E-02	21.10	2.73E-02	21.10
m 2	CV body at flange	1.73E-03	1.34	1.73E-03	1.34	1.73E-03	1.34	1.73E-03	1.34	1.73E-03	1.34	1.73E-03	1.34	1.73E-03	1.34
m 3	CV lid	9.57E-03	7.39	9.57E-03	7.39	9.57E-03	7.39	9.57E-03	7.39	9.57E-03	7.39	9.57E-03	7.39	9.57E-03	7.39
m 4	CV screw ring	4.27E-03	3.30	4.27E-03	3.30	4.27E-03	3.30	4.27E-03	3.30	4.27E-03	3.30	4.27E-03	3.30	4.27E-03	3.30
m 5	angle	1.69E-02	13.02	1.69E-02	13.02	1.69E-02	13.02	1.69E-02	13.02	1.69E-02	13.02	1.69E-02	13.02	1.69E-02	13.02
m 6	drum	6.02E-02	46.50	6.02E-02	46.50	6.02E-02	46.50	6.02E-02	46.50	6.02E-02	46.50	6.02E-02	46.50	6.02E-02	46.50
m 7	drum bottom head	1.22E-02	9.42	1.22E-02	9.42	1.22E-02	9.42	1.22E-02	9.42	1.22E-02	9.42	1.22E-02	9.42	1.22E-02	9.42
m 8	weld drum to drum bottom head	1.18E-04	0.09	1.18E-04	0.09	1.18E-04	0.09	1.18E-04	0.09	1.18E-04	0.09	1.18E-04	0.09	1.18E-04	0.09
m 9	liner overlap to angle (0.03)	1.36E-04	0.11	1.36E-04	0.11	1.36E-04	0.11	1.36E-04	0.11	1.36E-04	0.11	1.36E-04	0.11	1.36E-04	0.11
m 10	liner (0.06)	3.95E-02	30.51	3.95E-02	30.51	3.95E-02	30.51	3.95E-02	30.51	3.95E-02	30.51	3.95E-02	30.51	3.95E-02	30.51
m 11	liner bottom (0.120) (see m 27 for	1.40E-03	1.08	1.40E-03	1.08	1.40E-03	1.08	1.40E-03	1.08	1.40E-03	1.08	1.40E-03	1.08	1.40E-03	1.08
m 12	lid shells (0.06)	7.25E-03	5.59	7.25E-03	5.59	7.25E-03	5.59	7.25E-03	5.59	7.25E-03	5.59	7.25E-03	5.59	7.25E-03	5.59
m 13	thin lid shell at bolts	1.37E-05	0.01	1.37E-05	0.01	1.37E-05	0.01	1.37E-05	0.01	1.37E-05	0.01	1.37E-05	0.01	1.37E-05	0.01
m 14	lid solids at the lid bolts	5.03E-05	0.04	5.03E-05	0.04	5.03E-05	0.04	5.03E-05	0.04	5.03E-05	0.04	5.03E-05	0.04	5.03E-05	0.04
m 15	lid stiffener	1.39E-03	1.07	1.39E-03	1.07	1.39E-03	1.07	1.39E-03	1.07	1.39E-03	1.07	1.39E-03	1.07	1.39E-03	1.07
m 16	drum bolts	5.06E-04	0.39	5.06E-04	0.39	5.06E-04	0.39	5.06E-04	0.39	5.06E-04	0.39	5.06E-04	0.39	5.06E-04	0.39
m 17	drum bolt nuts	1.20E-03	0.93	1.20E-03	0.93	1.20E-03	0.93	1.20E-03	0.93	1.20E-03	0.93	1.20E-03	0.93	1.20E-03	0.93
m 18	drum bolt washers	4.71E-04	0.36	4.71E-04	0.36	4.71E-04	0.36	4.71E-04	0.36	4.71E-04	0.36	4.71E-04	0.36	4.71E-04	0.36
m 19	plug liner	1.29E-02	10.00	1.29E-02	10.00	1.29E-02	10.00	1.29E-02	10.00	1.29E-02	10.00	1.29E-02	10.00	1.29E-02	10.00
m 20	plug kaolite	1.26E-02	9.70	1.26E-02	9.70	1.26E-02	9.70	1.26E-02	9.70	1.26E-02	9.70	1.26E-02	9.70	1.26E-02	9.70
m 21	drum kaolite	1.43E-01	110.08	1.43E-01	110.08	1.43E-01	110.08	1.43E-01	110.08	1.43E-01	110.08	1.43E-01	110.08	1.43E-01	110.08
m 22	drum borobond	5.66E-02	43.70	5.66E-02	43.70	5.66E-02	43.70	5.66E-02	43.70	5.66E-02	43.70	5.66E-02	43.70	5.66E-02	43.70
m 24	lower internal cv mass	4.75E-02	36.69	4.75E-02	36.69	4.75E-02	36.69	4.75E-02	36.69	4.75E-02	36.69	4.75E-02	36.69	4.75E-02	36.69
m 25	middle internal cv mass	4.75E-02	36.69	4.75E-02	36.69	4.75E-02	36.69	4.75E-02	36.69	4.75E-02	36.69	4.75E-02	36.69	4.75E-02	36.69
m 26	upper internal cv mass	4.75E-02	36.69	4.75E-02	36.69	4.75E-02	36.69	4.75E-02	36.69	4.75E-02	36.69	4.75E-02	36.69	4.75E-02	36.69
m 27	liner bottom solids	9.87E-04	0.76	9.87E-04	0.76	9.87E-04	0.76	9.87E-04	0.76	9.87E-04	0.76	9.87E-04	0.76	9.87E-04	0.76
m 29	visual rigid plane	7.80E-04	0.60	7.80E-04	0.60	7.80E-04	0.60	7.80E-04	0.60	7.80E-04	0.60	7.80E-04	0.60	7.80E-04	0.60
m 30	crush plate	1.42E+00	1099.99	1.42E+00	1099.99	1.42E+00	1099.99	1.42E+00	1099.99	1.42E+00	1099.99	1.42E+00	1099.99	1.42E+00	1099.99
m 31	punch	8.24E-02	63.62	8.24E-02	63.62	8.24E-02	63.62	8.24E-02	63.62	8.24E-02	63.62	8.24E-02	63.62	8.24E-02	63.62
m 32	silicon rubber	1.65E-03	1.27	1.65E-03	1.27	1.65E-03	1.27	1.65E-03	1.27	1.65E-03	1.27	1.65E-03	1.27	1.65E-03	1.27
dyna total model weight		2.06E+00	1592.05	2.06E+00	1592.05	2.06E+00	1592.05	2.06E+00	1592.05	2.06E+00	1592.05	2.06E+00	1592.05	2.06E+00	1592.05
CV lid and nut ring			10.68		10.68		10.68		10.68		10.68		10.68		10.68
CV body wt			22.44		22.44		22.44		22.44		22.44		22.44		22.44
CV total wt			33.12		33.12		33.12		33.12		33.12		33.12		33.12
plug liner and kaolite			19.70		21.69		21.69		19.70		19.70		19.70		19.70
liner + angle			45.49		45.49		45.49		45.49		45.49		45.49		45.49
drum body + kaolite + borobond4			256.94		279.90		279.90		256.94		256.94		256.94		256.94
drum + lid + plug + kaolite + borobond4			284.65		309.60		309.60		284.65		284.65		284.65		284.65
internal cv masses			110.08		110.08		110.08		110.08		110.08		110.08		110.08
Total Package Weight			427.85		452.79		452.79		427.85		427.85		427.85		427.85
Crush Plate Weight			1099.99		1099.99		1099.99		1099.99		1099.99		1099.99		1099.99
Punch Weight			63.62		63.62		63.62		63.62		63.62		63.62		63.62
Visual Rigid Plane			0.60		0.60		0.60		0.60		0.60		0.60		0.60
Total Model Weight			1592.05		1617.00		1617.00		1592.15		1592.07		1592.15		1592.15

\* - Mass is for the 1/2 model and is units of (pound \* second^2) / inch

\*\* - Weight is for the total package (2 x model weight) and is in units of pounds.

Friction factors are used in the contact surfaces of the models. Generally speaking, a static coefficient of 0.3 and a dynamic value of 0.2 is used. For the silicon rubber parts, a static coefficient of 0.6 and a dynamic value of 0.5 is assumed. The general factors of 0.3 (static) and 0.2 (dynamic) are also used for the shipping package contact with the rigid surface.

The design of the ES-3100 and the impact configurations are symmetrical. An analytical half model is used with conditions of symmetry defined for all nodes initially on the plane of symmetry. The drum bolting and the CV nut ring are modeled with surfaces initially in contact, but not pre-loaded. The CV is not pressurized. Gravity is included in the models.

The model typically used for a drum welded stud which secures the lid is shown in Figure 2.1.7. The mesh footprint in the stud is mirrored in the angle such that there is a one-to-one match of the stud nodes to angle nodes on the mating surface. The lower nodes on the studs are allowed to merge with the angle nodes. This is structurally conservative at the stud/angle intersection due to the fact that in the stud arc welding process a shoulder boss (area greater than the nominal stud area) is formed. The radius of the modeled studs is such that the faceted area of the stud model equates to the tensile stress area of the studs. Similarly to the stud/angle nodes, the nut/stud nodes are positioned and allowed to merge. The lid is modeled with shell elements, however, at the radius around each stud a transition to brick elements is made. This allows frictional bearing of the lid thickness onto the stud shank to be modeled. This modeling approach has been used and accepted for NNSA-licensed shipping packages that were subject to independent review and verification analysis (i.e., DPP-2 and ES-2100).

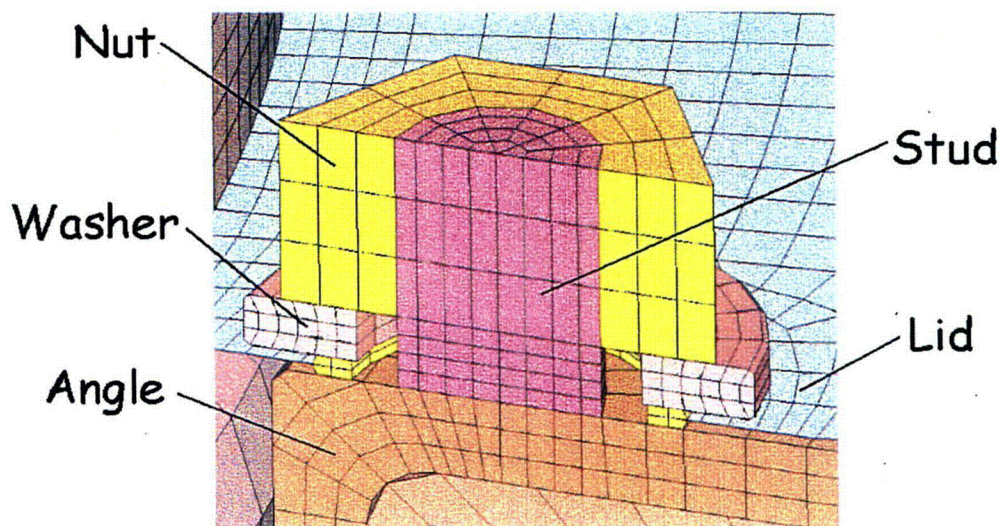


Figure 2.1.7 - Localized Model of a Stud



## 2.2 Model Description - Simplified Model

A series of punch impact runs were made on a simple model of the ES-3100 shipping container by varying the angle between the container liner and the punch, see Figure 2.2.1. In Figure 2.2.1, the position of the punch relative to the drum is shown with the angles in degrees. The purpose of the punch runs was to determine the response of the stainless steel drum liner due to the angled punch impacts. A series of eight, angled drops as shown in Figure 2.2.2 and described in Table 2.2.1 were made. In Figure 2.2.2, the punch is held stationary and the drum is positioned relative to the punch. The center of gravity of the shipping package was located directly above the side of the punch as shown in Figure 2.2.1. The initial velocity of the container is parallel to the axis of the punch as shown in Figure 2.2.2.

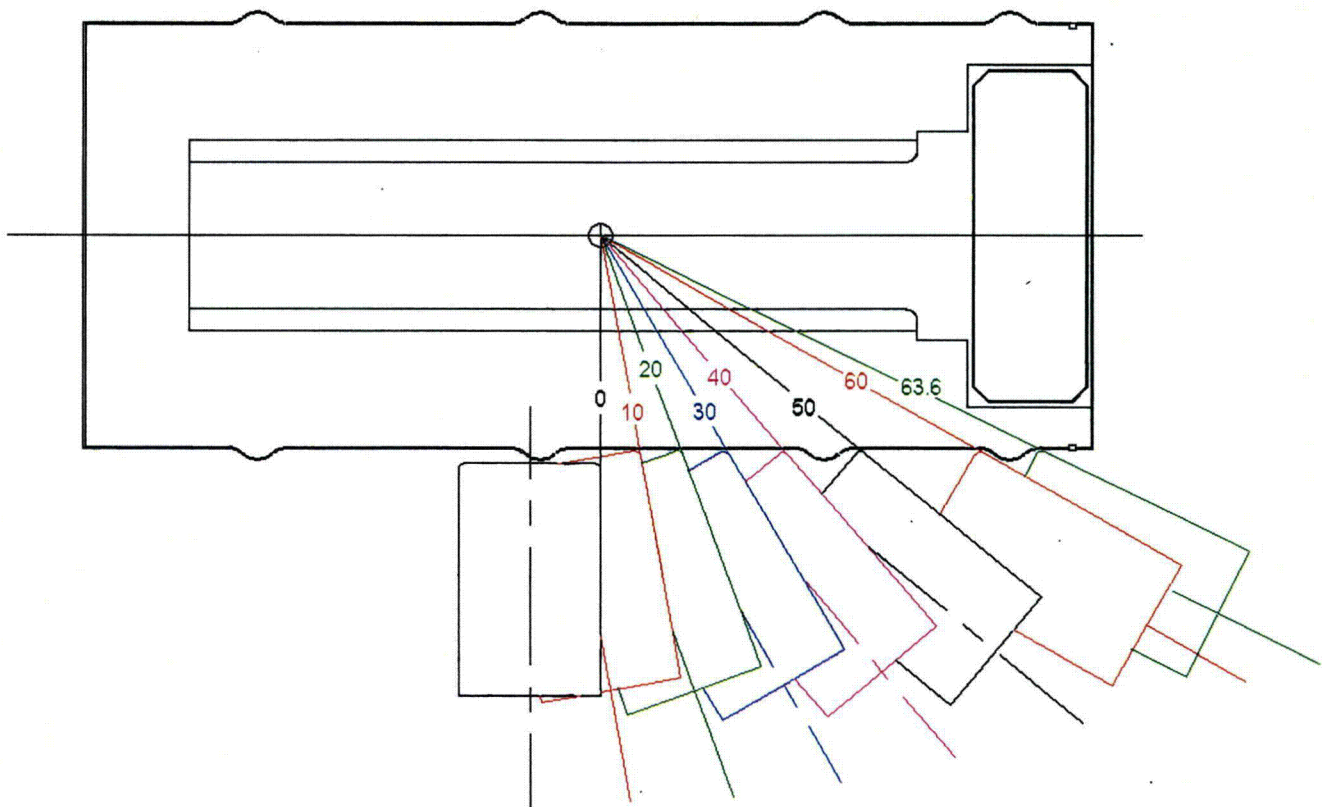


Figure 2.2.1 - Punch Angles on the Drum Liner

A simplified model of the ES-3100 was derived from the more detailed model (described in Section 2.1) for this series of runs. The model detail needed in the 4-foot, 30-foot, crush, and successive punch impact is not needed for the series of punch impacts. The purpose of the series of punch impacts is to evaluate the response of the drum skin to various punch angles.

The detailed model (section 2.1) was simplified (see below) to form the simple model. The detailed model was simplified except for the drum skin and the drum kaolite mesh nearest the punch impact. Figure 2.2.3 shows the simplified shipping package model used for the series of punch impacts. Figure 2.2.4 shows an exploded view of the simple model components.

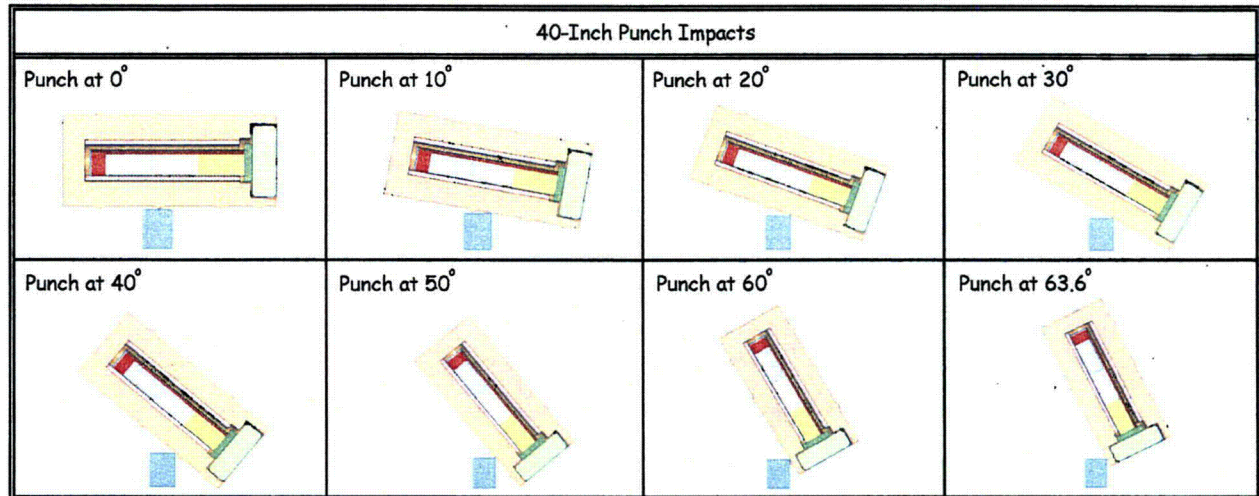


Figure 2.2.2 - ES-3100 Punch Configurations for the Series of Punch Impacts

Table 2.2.1 - Description of the ES-3100 Impacts with the Simplified Model Summarized in this DAC

Run ID <sup>†</sup>	Description <sup>†</sup>	Kaolite Model
Punch at 0°	40-inch punch impact at 0°	Average stiffness, 22.4 lb/ft <sup>3</sup> (note the density is altered slightly so that the punch model weights approximate the full model runs)
Punch at 10°	40-inch punch impact at 10°	
Punch at 20°	40-inch punch impact at 20°	
Punch at 30°	40-inch punch impact at 30°	
Punch at 40°	40-inch punch impact at 40°	
Punch at 50°	40-inch punch impact at 50°	
Punch at 60°	40-inch punch impact at 60°	
Punch at 63.6°	40-inch punch impact at 63.6°	

<sup>†</sup> - Angles in degrees, measured from a perpendicular to the drum axis as shown in Figure 2.2.1



3100 RUN-P000 APRIL 2004 KQH  
Time = 0

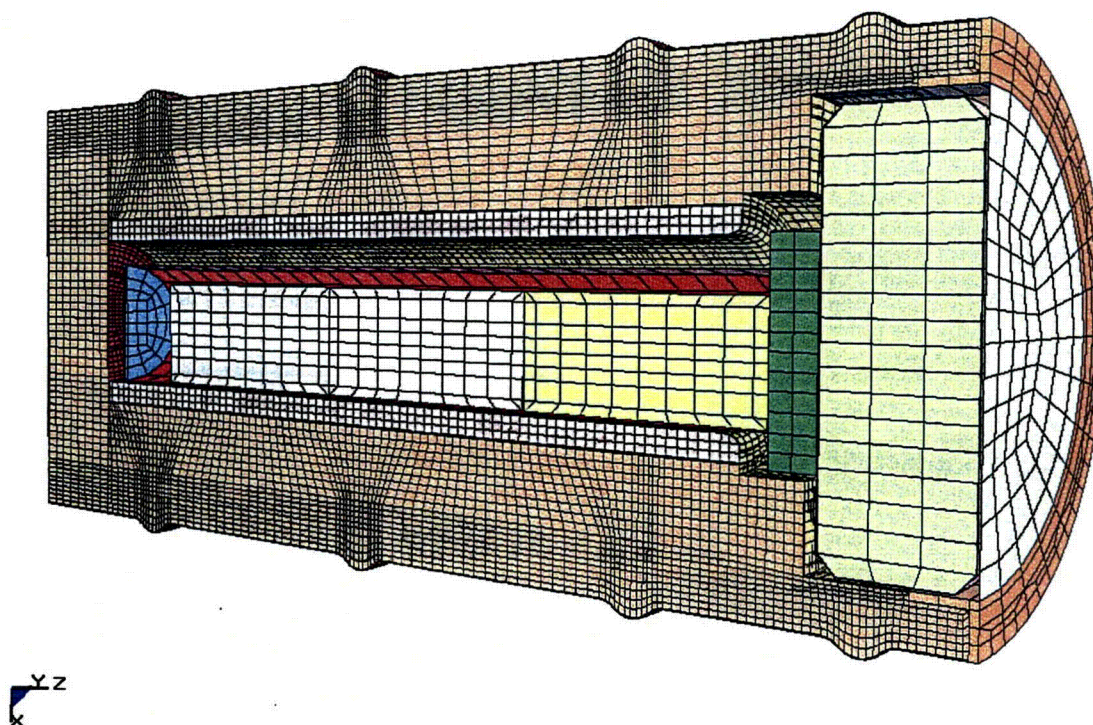


Figure 2.2.3 - Simplified ES-3100 Shipping Package Model for the Series of Punch Impacts



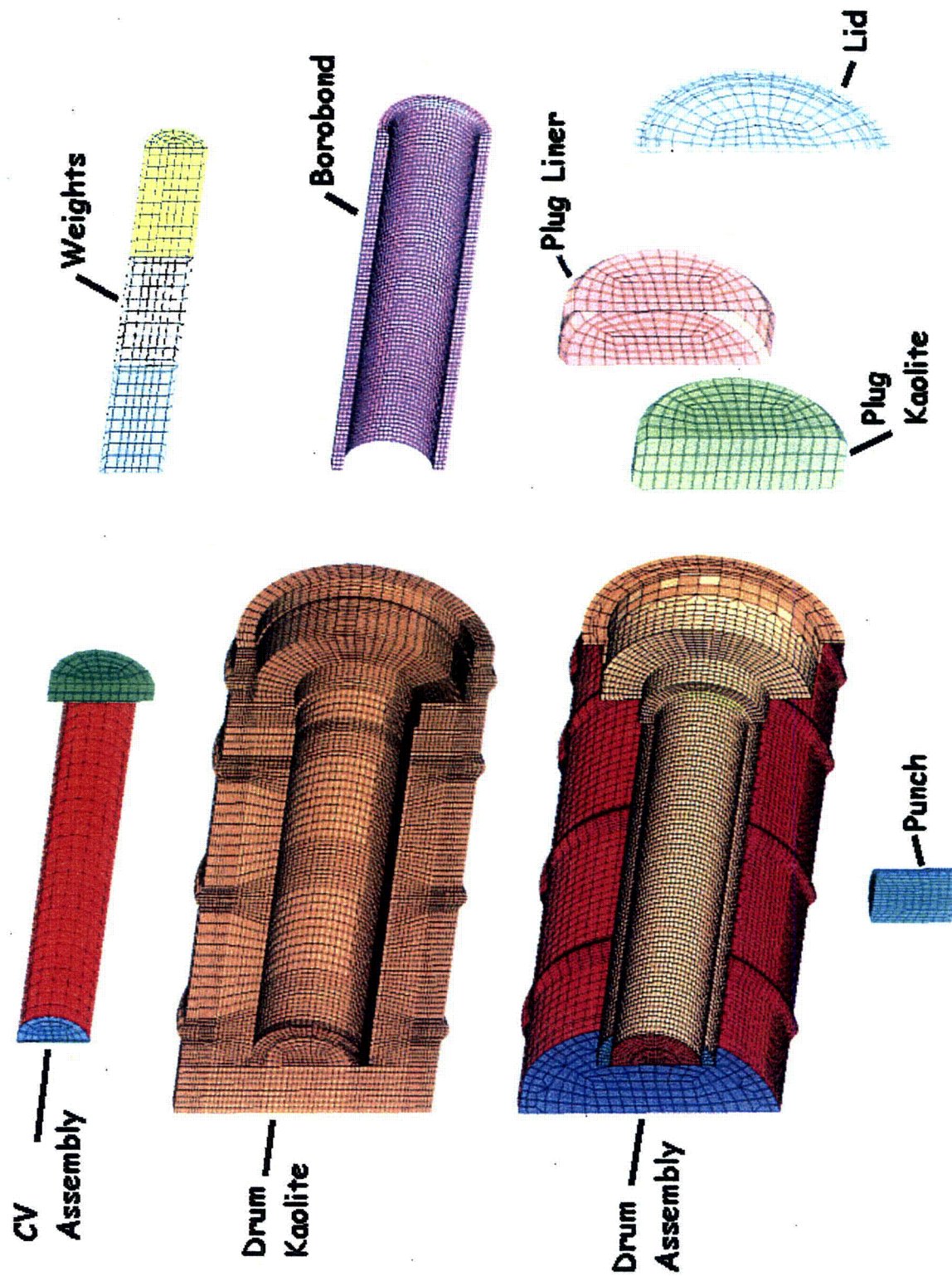


Figure 2.2.4 - Exploded View of the ES-3100 Simple Model

Since the concern is the response of the drum skin to the punch, detail in the shipping container components remote from this concern is not warranted and only the mass/stiffness effects on the region of concern become important. In general, there is a simplification of the element mesh (coarser element mesh) away from the punch impact location. Items such as the CV, the plug and the drum lid retention details were greatly simplified in modeling detail (compare Figures 2.2.3 and 2.2.4 verses Figures 2.1.1 through 2.1.4). The CV was simplified to a simple cylinder (shell elements) with a simple solid lid. The drum lid attachment details were replaced by a simple flat lid whose nodes were allowed to merge with the angle nodes. The container plug was also simplified to a simple disk with chamfered corners. This simple model allowed a savings on computer run time and storage allotment without sacrificing the item of concern, the response of the drum liner due to the angled punch.

An effort was made in the geometrical/mesh simplification to maintain the mass distribution of the container as close as is reasonable to the detailed model. Table 2.2.2 shows the weights for all the punch impacts. The total weight for the simple model package assembly was 427.91 pounds with the 22.4 lb/ft<sup>3</sup> kaolite. The mass inertia about the global Y axis for the simple model is 89.64 in\*lb\*sec<sup>2</sup> and the CG is located at Z= 23.0 inches.

Material Number	Component Description	mass*	weight**
1	CV Body	2.6336E-02	20.33
2	CV Bottom Head	2.7398E-03	2.12
3	CV Flange/Lid	1.5492E-02	11.96
4	removed for punch runs	0.0000E+00	0.00
5	Angle	1.9249E-02	14.86
6	Drum	6.0236E-02	46.60
7	Drum Bottom	1.2318E-02	9.51
8	removed for punch runs	0.0000E+00	0.00
9	removed for punch runs	0.0000E+00	0.00
10	Liner	3.9641E-02	30.60
11	Liner Bottom	1.3361E-03	1.03
12	Lid	8.6358E-03	6.67
13	removed for punch runs	0.0000E+00	0.00
14	removed for punch runs	0.0000E+00	0.00
15	removed for punch runs	0.0000E+00	0.00
16	removed for punch runs	0.0000E+00	0.00
17	removed for punch runs	0.0000E+00	0.00
18	removed for punch runs	0.0000E+00	0.00
19	Plug Liner	1.2949E-02	10.00
20	Plug Kaolite	1.2573E-02	9.71
21	Drum Kaolite	1.4265E-01	110.13
22	Borobond	5.6607E-02	43.70
24	CV Lower Inner Weight	4.7530E-02	36.69
25	CV Middle Inner Weight	4.7530E-02	36.69
26	CV Upper Inner Weight	4.7530E-02	36.69
27	Liner Kaolite Cavity Bottom	9.3847E-04	0.72
28	removed for punch runs	0.0000E+00	0.00
29	removed for punch runs	0.0000E+00	0.00
30	removed for punch runs	0.0000E+00	0.00
31	Punch	8.2405E-02	63.62
32	removed for punch runs	0.0000E+00	0.00
pkg			427.91
punch			63.62
total		6.3670E-01	491.53
* - Mass is for the 1/2 model and is units of (pound * second^2) / inch			
** - Weight is for the total package (2 x model weight) and is in units of pounds.			

### 2.3 Material Models

The LS-Dyna material models used in the ES-3100 analytical model are shown in the Table 2.3.1 index. Note that the designation 304L (capital L) is used for clarity.

Table 2.3.1 - Material Model Index for the ES-3100 LS-Dyna Model			
LS-Dyna Part #	Part Description	Material Description	Described in DAC Section
1	CV Body	304L	2.3.1
2	CV Body Neck	304L	2.3.1
3	CV Lid	304L	2.3.1
4	CV Nut Ring	A-479 Nitronic-60	2.3.2
5	Angle	304	2.3.3
6	Drum	304	2.3.3
7	Bottom Head	304	2.3.3
8	Attachment Shell Elements	304	2.3.3
9	Attachment Shell Elements	304	2.3.3
10	Liner	304	2.3.3
11	Liner Bottom	304	2.3.3
12	Lid Shell Elements	304	2.3.3
13	Attachment Shell Elements	304	2.3.3
14	Lid Solid Elements	304	2.3.3
15	Lid Stiffener	304	2.3.3
16	Studs	304	2.3.3 <sup>†</sup>
17	Stud Nuts	Bronze	2.3.4
18	Stud Washers	304	2.3.3
19	Plug Liner	304	2.3.3
20	Plug Kaolite	Kaolite 1600	2.3.5
21	Drum Kaolite	Kaolite 1600	2.3.5
22	Borobond	Borobond 4	2.3.6
23	Not Used	Not Used	Not Used
24	Lower Internal CV Mass	Mild Steel	2.3.7
25	Middle Internal CV Mass	Mild Steel	2.3.7
26	Upper Internal CV Mass	Mild Steel	2.3.7
27	Liner Bottom	304	2.3.3
28	Not Used	Not Used	Not Used
29	Visual Rigid Plane	Rigid	2.3.8
30	Crush Plate	Mild Steel	2.3.7
31	Punch	Mild Steel	2.3.7
32	Silicon Rubber Pads	Silicon Rubber	2.3.9
† - An elastic/plastic model with material failure is used for the studs as explained in the noted section.			



Density values listed in Section 2.3 were used as initial values for the material weights. Once the model was completed and initial runs made, the initial density was then ratioed such that the preliminary weights obtained from the designer were matched by the analysis results. Table 2.1.2 shows the resulting component and assembly weights for the detailed model.

The material presented in this section is for room temperature (about 70°) unless otherwise stated. Section 2.3.5 presents Kaolite data at room temperature in section 2.3.5.1, 100°F in section 2.3.5.2 and -40°F in section 2.3.5.3.

### 2.3.1 304L Stainless Steel

The material 304L is used for the CV components except the nut ring. A software database obtained from Lawrence Livermore National Lab personnel is used to obtain the 304L material data which is reproduced below.

Material density . . . . .	0.28600	lb/in**3
Young's Modulus . . . . .	2.800E+07	psi
Shear Modulus . . . . .	1.085E+07	psi
Bulk Modulus . . . . .	2.222E+07	psi
Poisson's ratio . . . . .	0.2900	
Yield stress at offset . . .	32000.0	psi
Engineering ultimate stress.	85000.0	psi
Elongation at failure . . .	57.00	%
Yield offset . . . . .	0.20000	%
----- Calculated values -----		
Strain Hardening equation	s = s0 e**m	
Equation constants	s0 = 160455	m = 0.27916
Yield point	sy = 21735	ey = 0.00078
Ultimate (Engineering)	Su = 85000	Nu = 0.32202
Ultimate (True)	sut= 112372	eut= 0.27916
Failure (True)	sft= 168989	eft= 1.20397
Energy to ultimate	24605 in-lb/in**3	

The LS-Dyna power law plasticity model (\*MAT\_POWER\_LAW\_PLASTICITY) is used for 304L. The material model is:

$$\sigma = K\epsilon^m$$

were,  $K$  = strength coefficient = 160455 (psi)

$m$  = hardening exponent = 0.27916

The density listed in the reference was an initial density (0.286 lb/in<sup>3</sup>) and equates to an initial mass density of 7.4093e-4 lb\*sec<sup>2</sup>/in<sup>4</sup>.

### 2.3.2 A-479 Nitronic-60

The CV nut ring is modeled with A-479 Nitronic-60 properties. The Reference 5.4 was used to obtain the following material data for the S21800 material.

Tensile Strength	95 ksi
Yield Strength	50 ksi
Elongation	35%

The modulus of elasticity is assumed to be 26.2e6 psi.

From this data the following tangent modulus was calculated for the LS-Dyna, \*MAT\_PLASTIC\_KINEMATIC material model.

$$\epsilon = \frac{\sigma}{E} = \frac{50000psi}{26.2e6psi} = 0.00192in/in$$

$$E_{tan} = \frac{95000psi - 50000psi}{0.35 - 0.00192} \approx 129000psi$$

A poisson's ratio of 0.298 was used. A density of 0.2754 lb/in<sup>3</sup> was initially used. This equates to an initial mass density of 7.1347 lb\*sec<sup>2</sup>/in<sup>4</sup>.



### 2.3.3 304 Stainless Steel

The general shipping container components were modeled as 304 stainless steel. The LS-Dyna material model \*MAT\_POWER\_LAW\_PLASTICITY was used for the general container components. The 304 material data was obtained from a software database obtained from Lawrence Livermore National Lab personnel and is reproduced below.

Material density . . . . .	0.29000	lb/in**3
Young's Modulus. . . . .	2.810E+07	psi
Shear Modulus. . . . .	1.089E+07	psi
Bulk Modulus . . . . .	2.230E+07	psi
Poisson's ratio. . . . .	0.2900	
Yield stress at offset . . .	34000.0	psi
Engineering ultimate stress.	87000.0	psi
Elongation at failure. . . .	57.00	%
----- Calculated values -----		
Strain Hardening equation	s = s0 e**m	
Equation constants	s0 = 162738	m = 0.27208
Yield point	sy = 23729	ey = 0.00084
Ultimate (Engineering)	Su = 87000	Nu = 0.31269
Ultimate (True)	sut= 114204	eut= 0.27208
Failure (True)	sft= 167370	eft= 1.10866

Similar to section 2.3.1, the power law coefficients for the 304 model used for the general shipping container components were:

$$K = \text{strength coefficient} = 162738 \text{ (psi)}$$

$$m = \text{hardening exponent} = 0.27208$$

The 0.290 lb/in<sup>3</sup> density equates to 7.513 e-4 lb\*sec<sup>2</sup>/in<sup>4</sup> for the initial mass density.

The drum studs were modeled using the \*MAT\_PLASTIC\_KINEMATIC material model in LS-Dyna using the following 304 material properties. This material model allowed material failure to be used for the studs. With material failure, LS-Dyna removes elements which reach the defined failure strain. The following elastic-plastic model was derived from the above material properties.

$$\text{Modulus of Elasticity} = 2.81\text{e}7 \text{ psi}^\dagger$$

$$\text{Poisson's Ratio} = 0.29$$

$$\text{Yield} = 34000 \text{ psi}$$

$$\text{Plastic Modulus} = 93180 \text{ psi}$$

$$\text{Failure Strain} = 0.57 \text{ in/in}$$

The modeling of the drum studs with engineering stress/strain data curve is conservative from a design standpoint. This approach has been used and accepted for NNSA-licensed shipping packages that were subject to independent review and verification analysis (i.e., DT-22 and DT-23).

† - Note: the value of  $2.9e7$  psi (vs  $2.81e7$  psi) was inadvertently used in the analysis for the modulus of elasticity. This is seen to cause minimal concern due to the minimal energy absorption in the elastic range.



## 2.3.4 Bronze

The drum lid nuts are made of bronze. A software database obtained from Lawrence Livermore National Lab personnel was used to obtain the material data which is reproduced below.

Material . . . .	bronze commercial	cu.9 zn.1	½ hard
Material density . . . . .	0.31800	lb/in**3	
Young's Modulus. . . . .	1.700E+07	psi	
Shear Modulus. . . . .	6.391E+06	psi	
Bulk Modulus . . . . .	1.667E+07	psi	
Poisson's ratio. . . . .	0.3300		
Yield stress at offset . . .	45000.0	psi	
Engineering ultimate stress.	52000.0	psi	
Elongation at failure. . . .	15.00	%	
----- Calculated values -----			
Strain Hardening equation	$s = s_0 e^{m \epsilon}$		
Equation constants	$s_0 = 70989$	$m = 0.09191$	
Yield point	$s_y = 40775$	$e_y = 0.00240$	
Ultimate (Engineering)	$S_u = 52000$	$N_u = 0.09626$	
Ultimate (True)	$s_{ut} = 57006$	$e_{ut} = 0.09191$	

The LS-Dyna power law model was used for the bronze material. The coefficients used were:

$K = \text{strength coefficient} = 70989(\text{psi})$

$m = \text{hardening exponent} = 0.09191$

The density of  $0.318 \text{ lb/in}^3$ , or  $8.2371\text{e-}4 \text{ lb*sec}^2/\text{in}^4$  was the initial mass density.

## 2.3.5 Kaolite 1600

Kaolite 1600 properties were used to model the drum and plug kaolite. The LS-DYNA honeycomb material model (\*MAT\_HONEYCOMB) used for the ES-3100 has been shown to be a good representation of the Kaolite material and approved for NNSA-licensed shipping packages that were subject to independent review and verification analysis (i.e., DPP-2 and ES-2100). There have been several testing programs to determine the structural properties of Kaolite since 1995. Each time new data is obtained, it is compared to the old data to maintain enveloping upper and lower bound stiffness curves. The lower stress/strain portion of the curves presented in this section is shown in Figure 2.3.5.1 below. Each curve shown in Figure 2.3.5.1 is documented in the following sub-sections. The Kaolite test data was obtained from constrained test specimens. For the constrained Kaolite test data, the material data is the same for uniaxial and volumetric strain.

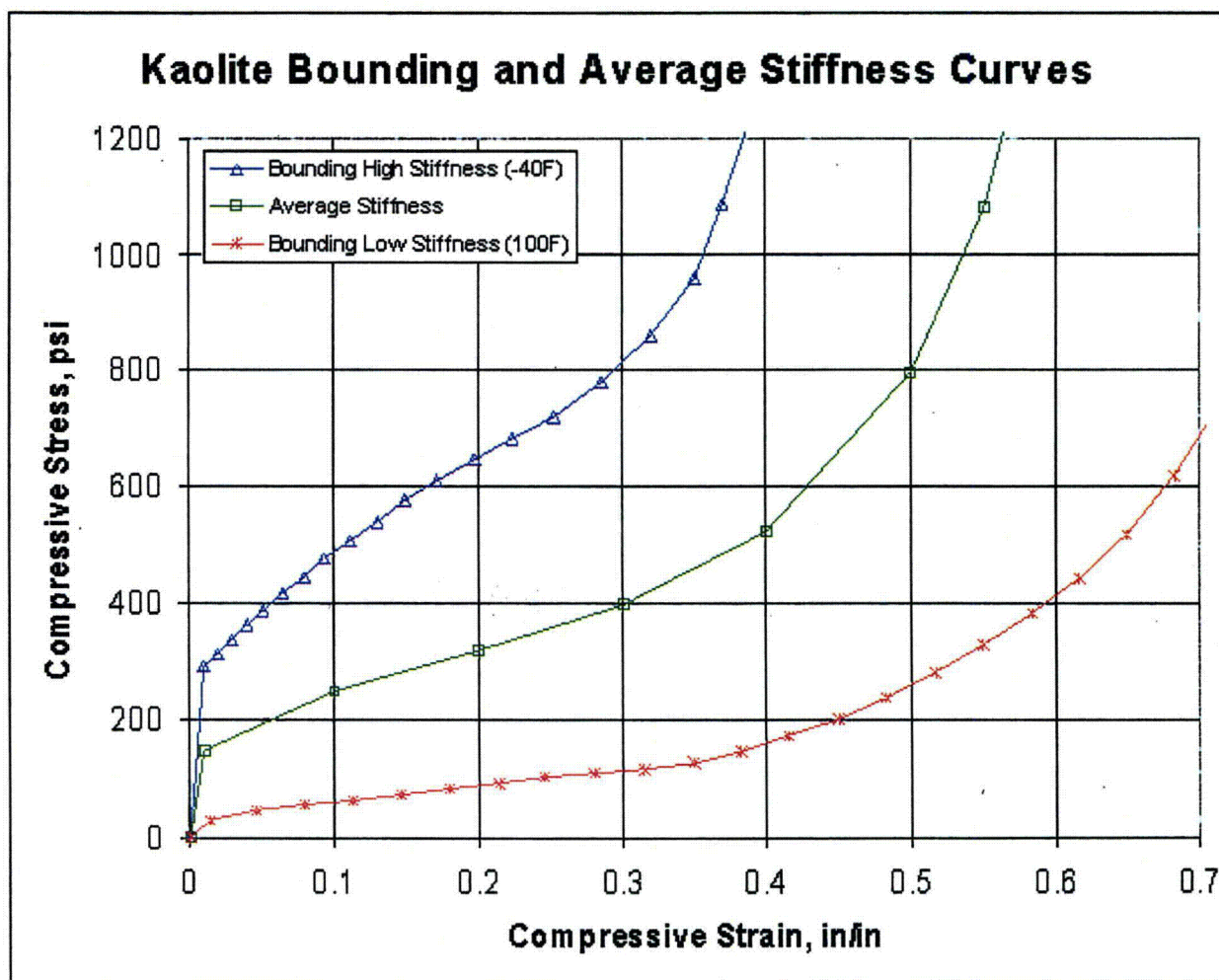


Figure 2.3.5.1 - Bounding Kaolite and Average Stiffness Curves



## 2.3.5.1 Kaolite 1600 - Averaged Stiffness

A Y12 report gives test data for constrained Kaolite 1600 material at 100°F and -40°F. The maximum peaks from the -40°F high density samples defined an upper bound load deflection curve. The minimum peaks to the 100°F low density samples defined a lower bound load deflection curve. The upper and lower curves were averaged to obtain the average stiffness results. The averaged results up to about 60% strain are then derived from test results for the LS-DYNA material model. The curve is extrapolated above 60% strain, to give a "lock-up" region (collapsing of voids). LS-Dyna does not extrapolate data curves, therefore, the curves must envelope all expected values and assumed values extend the curve well into the lock-up range. Figure 2.3.5.1 shows the lower portion of the averaged stiffness curve. The digital values for the points defined in the LS-DYNA material model are given below in Table 2.3.5.1.1.

Table 2.3.5.1.1 - Digital Load Curve for Kaolite 1600					
Strain, in/in	Stress, psi	Strain, in/in	Stress, psi	Strain, in/in	Stress, psi
0.00	0.0	0.40	523.	0.70	5000. <sup>†</sup>
0.01	148.	0.50	797.	0.75	10000. <sup>†</sup>
0.10	248.	0.55	1079.	0.775	20000. <sup>†</sup>
0.20	317.	0.60	1553.	0.79	30000. <sup>†</sup>
0.30	396.	0.65	2500. <sup>†</sup>	0.8	40000. <sup>†</sup>
<sup>†</sup> - Assumed values to obtain lockup					

The Young's Modulus for the compacted kaolite material is taken as the slope of the last two data points.

$$\frac{40000 \text{ psi} - 30000 \text{ psi}}{0.79 \text{ in/in} - 0.80 \text{ in/in}} = 1.0 \text{e}6 \text{ psi}$$

The initial slope is taken as the uncompressed modulus of elasticity.

$$E_{\text{uncompressed}} = \frac{148.11 \text{ psi} - 0.0 \text{ psi}}{0.01 - 0.0} = 14811 \text{ psi}$$

Assuming a low poisson's ratio (0.01), the shear modulus is,

$$G = \frac{E}{2(1+\nu)} = \frac{14811 \text{ psi}}{2(1+0.01)} \approx \frac{14811 \text{ psi}}{2} = 7405 \text{ psi}$$

Full compaction is also assumed at a relative volume of 0.20 (this corresponds with the 80% strain assumed data point). The mass density used for the nominal kaolite runs in the analysis is 3.3583e-5 lb\*sec<sup>2</sup>/in<sup>4</sup>, which equates to 22.4lb/ft<sup>3</sup>.

## 2.3.5.2 Kaolite 1600 - Lower Bound Stiffness

The kaolite lower bounding stiffness model shown in Figure 2.3.5.1, originated in the ES2LM shipping container calculation and is associated with 100°F. The digital values for the points which define in the LS-Dyna lower bound stiffness curve are given in Table 2.3.5.2.1.

Table 2.3.5.2.1 - Digital Load Curve for Kaolite 1600, Lower Bound		
Strain, in/in	Stress, psi	Origin
0.00	0.0	Test Data and ES2LM Shipping Container Calculation
0.0132	29.	
0.0456	48.	
0.0792	56.	
0.1128	64.	
0.1464	75.	
0.1800	83.	
0.2136	93.	
0.2460	105.	
0.2796	109.	
0.3144	117.	
0.3480	127.	
0.3816	148.	
0.4140	174.	
0.4488	202.	
0.4824	237.	
0.5160	281.	
0.5496	330.	
0.5832	381.	
0.6168	443.	
0.6492	520.	
0.6828	619.	
0.7140	744.	
0.7476	896.	
0.7800	1099.	
0.7944	1205.	
0.8200	3000.	Assumed <sup>†</sup>
0.8700	10000.	Assumed <sup>†</sup>
0.9000	40000.	Assumed <sup>†</sup>
† - Assumed to provide "lock-up"		

The Young's Modulus for the compacted kaolite material is taken as the slope of the last two data points.

$$\frac{40000\text{psi} - 10000\text{psi}}{0.90\text{in/in} - 0.87\text{in/in}} = 1.0e6\text{psi}$$

The initial slope is taken as the uncompressed modulus of elasticity.

$$E_{\text{uncompressed}} = \frac{29.\text{psi} - 0.0\text{psi}}{0.0132 - 0.0} = 2197\text{psi}$$

Assuming a low poisson's ratio, the shear modulus is,

$$G \approx \frac{E}{2} = 1099\text{psi}$$

A low poisson's ratio is assumed, 0.01. Full compaction is also assumed at a relative volume of 0.10. The density used is 27 lb/ft<sup>3</sup>, or 4.0479e-5 lb\*sec<sup>2</sup>/in<sup>4</sup>.

### 2.3.5.3 Kaolite 1600 Upper Bound Stiffness

The upper bound stiffness of the kaolite 1600 material is an enveloping curve obtained from two sets of material test data. Table 2.3.5.3.1 shows the digital values of the curve.

The Young's Modulus for the compacted kaolite material is taken as the slope of the last two data points.

$$\frac{40000\text{psi} - 22000\text{psi}}{0.88\text{in/in} - 0.85\text{in/in}} = 6.0e5\text{psi}$$

The initial slope is taken as the uncompressed modulus of elasticity.

$$E_{\text{uncompressed}} = \frac{292.1\text{psi} - 0.0\text{psi}}{0.01 - 0.0} = 29210\text{psi}$$

Assuming a low poisson's ratio, the shear modulus is,

$$G \approx \frac{E}{2} = 14605\text{psi}$$

A density of 27 lb/ft<sup>3</sup> is used as in the low stiffness run. A low poisson's ratio is assumed, 0.01. Full compaction is also assumed at a relative volume of 0.12.



Table 2.3.5.3.1 - Upper Bounding Kaolite Curve		
Strain, in/in	Stress, psi	Origin
0	292.1	Summer 2004 Material Testing
0.01	292.1	
0.019	313.3	
0.029	336.1	
0.04	360.5	
0.051	386.6	
0.064	414.3	
0.079	443.6	
0.094	474.5	
0.111	506.9	
0.13	540.7	
0.15	575.7	
0.172	611.6	
0.197	647.9	
0.224	684.1	
0.253	719.6	
0.285	780	assumed for smooth transition†
0.32	860	
0.3504	958	DPP2 Shipping Container Calculation
0.3696	1086	
0.3888	1231	
0.45	2000	assumed for lock-up†
0.5	3000	
0.6	6000	
0.7	10000	
0.8	16000	
0.85	22000	
0.88	40000	
† - Assumed values for transition and lock-up		

2.3.6 Borobond 4 Casting Material

The following soil and foam model is used for the borobond 4 casting material. The model is obtained from work done on the Y12, HEU storage pallet and the subsequent physical testing.

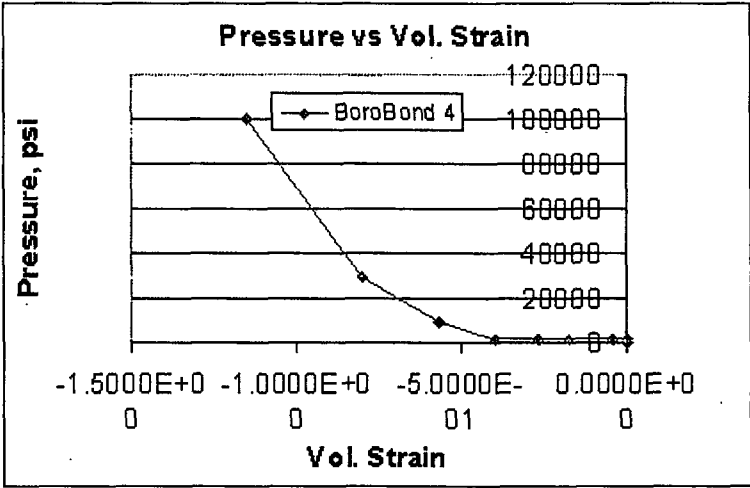


Figure 2.2.3 - Pressure vs Volumetric Strain

The following material data was used for the model of the Borobond 4 casting material.

LS-Dyna Material Model	*MAT_SOIL_AND_FOAM
Density	1.7991e-4 lb-sec <sup>2</sup> /in <sup>4</sup> (120 lb/ft <sup>3</sup> )
Shear Modulus	1.019e6 psi
Bulk Modulus	2.491e6 psi
A <sub>0</sub>	1.008e7 (psi) <sup>2</sup>
A <sub>1</sub>	0
A <sub>2</sub>	0
Tensile Cutoff	309.3 psi
Pressure vs Volumetric Strain Data:	

Pressure, psi	Volumetric Strain, in <sup>3</sup> /in <sup>3</sup>
0	0
1833.3	-7.387e-4
1850	-4.2363e-2
1866	-1.7334e-1
1883	-2.6993e-1
1900	-3.9631e-1
10000	-5.6503e-1
30000	-7.9972e-1
100000	-1.1536

### 2.3.7 Mild Steel

AISI 1020 carbon steel was used to obtain properties for a typical or nominal low carbon steel. A software database obtained from Lawrence Livermore National Lab personnel was used to obtain the material data for AISI 1020 and is reproduced below.

Material . . . . .	steel carbon AISI 1020 plate bar sheet strip to 18 in.
Young's Modulus. . . . .	3.000E+07 psi
Shear Modulus. . . . .	1.163E+07 psi
Bulk Modulus . . . . .	2.381E+07 psi
Poisson's ratio. . . . .	0.2900
Yield stress at offset . . .	30000.0 psi
Engineering ultimate stress.	55000.0 psi
Elongation at failure. . . .	25.00 %

A modulus of elasticity of 2.9e7 (vs 3.0e7 psi) was inadvertently used in the analysis for this material. This material model was used for the inner CV weights, the crush plate and the punch. This is seen to be of minimal concern due to the fact that the components which use this modulus are not of concern themselves, it is their effect on the package/CV that is of concern.

A density of about 490 lb/ft<sup>3</sup> is also initially assumed, which equates to a mass density of 7.35 lb-sec<sup>2</sup>/in<sup>4</sup>. This initial mass value was then adjusted based on the expected component weight.

Using the ultimate (55000 psi) and yield (30000 psi); the failure strain of 0.25 and assuming a 2% offset, a simple bi-linear tangent modulus of 1.0e5 is assumed.

$$E_{\tan} = \frac{55000 \text{ psi} - 30000 \text{ psi}}{0.25 - 0.002} \approx 1.0e5 \text{ psi}$$

### 2.3.8 Rigid Plane

The following properties were assigned to the rigid plane (for contact surface concerns):

Modulus of Elasticity = 28e6 psi  
Poisson's Ratio = 0.29

A relatively low value of density was also specified for the rigid plane, 1e-6 lb\*sec<sup>2</sup>/in<sup>4</sup>. Each node of the rigid plane was restrained from rotation and translation in the material definition.



### 2.3.9 Silicon Rubber

The pads outboard of the CV bottom and top are used to isolate the CV with regards to a transportation vibration concern. The following properties were assumed for the silicon rubber pads:

$$E \approx 150000 \text{ psi}$$

$$\text{Density} = 0.0446 \text{ lb/in}^3 = 1.1554 \text{ e-4 lb*sec}^2/\text{in}^4$$

A modulus of elasticity for the silicon rubber of about 150 psi can be obtained from Figure 35.13 of reference 5.6 (relative magnitude can be mimicked by various sources on the internet). However, this low E value will not allow a stable solution of LS-Dyna. The value of  $E = 150000 \text{ psi}$  results in a stable solution. The silicon rubber piece at the CV lid/flange and the piece at the base of the CV offer only bearing to the CV. A stiffer silicon material would tend to minimize the bearing footprint on the CV, hence force higher stresses/strains in the CV. Initial runs show this to be the case, up to the point that the softer ( $E = 150 \text{ psi}$ ) solution fails. Therefore, the value of  $E = 150000 \text{ psi}$  is used due to the fact that it tends to be conservative with respect to the CV and it allows a stable solution of LS-Dyna.

The density shown above is assumed and was found by averaging several nominal silicon rubber values obtained from the internet.

The shear modulus was calculated as:

$$G = \frac{E}{2(1+\nu)} = \frac{150000 \text{ psi}}{2(1+0.463)} = 51260 \text{ psi}$$

The LS-Dyna \*MAT\_BLATZ-KO\_RUBBER was used to model the silicon rubber components. The model defines the poisson's ratio as 0.463.

### 3.0 Solution Results

In this section, the results of the different analyses are presented. A voluminous amount of data can be obtained for each and every run presented in this DAC. An attempt is made to present the response story of each impact, yet not to overburden the reader, nor the expense of this report with similar images/data. Components of relatively low strain, or whose strain contour patterns are similar to other impacts which have been presented, may be presented digitally in a table (maximum) and not visually in an image. In the bounding kaolite runs, an effort was made to present the same images for comparison purposes.

Results from run1g are presented in detail as are results from the crush impact of run1ga. An effort is made to abbreviate the results of the other runs due to repetition. Only configuration and strain results of note, or uniqueness due to the configuration are included in the other runs. For ease of reading, the plots in sub-sections of Section 3.0 will be shown after the discussion in each section. Time is generally given in seconds, displacements in inches and velocity in inches/seconds.

The kinetic energy and velocity time history plots are nodal averages for the set of nodes that make up the body of concern (e.g., the shipping package for 4-foot impacts or the crush plate for crush impacts). Therefore, the plots are an averaged value to represent the body of concern.

The element mesh is generally not included on package assembly views such as Figure 3.0.1. The element mesh is generally quite small and its inclusion would make it more difficult to observe the components. In close up images, the element mesh is generally included.

The effective plastic strain level contour plots in the shell elements are surface strains (bending/peak strains) unless otherwise noted. Maximum, or in effect, bending strain is the default in LS-Post fringe plotting of shell elements. The maximum value for the plotted elements is given in the title block in the upper left corner of each fringe plot. The maximum fringe value (shown in the upper right hand corner of each fringe plot) may be redefined by the analyst and may or may not reflect the maximum value shown in the left, title block corner. In some fringe plots, the range may be adjusted to show regions in excess of a specific level. Note that shell elements are modeled at the centerline of the thickness. Therefore, in time history plots, one-half the shell thickness needs to be added/subtracted to obtain the desired metal surface for each node.

The nodes on the plane of symmetry and near the rigid plane are termed at "0°". The nodes initially on the Y plane are termed at "90°". And the nodes on the plane of symmetry

and typically nearer the crush plate are termed "180°". This terminology is typically used only in the side and slapdown impacts and denotes the circumferential positions.

The global coordinate system is the default system in LS-Dyna and is the coordinate system of default in this calculation. The global system is centered on the package centerline, at the bottom of the package as shown in Figure 3.0.1 (if the package were sitting on a flat floor, the surface of the floor would define  $Z = 0.0$ ). The global XZ axes define the plane of symmetry. The global coordinate system triad icon is shown on most images in this section; offset by default in LS-Post for visual purposes. A local coordinate system was defined for the CV assembly due to lid/body flange separation concerns. The local system used is shown in Figure 3.0.2 and moves with the three defining nodes on the CV body and lid. The local X direction is in the direction of CV lid separation at the O-ring location in the flange. The local CV coordinate system is used in the lid separation time history plots in the results sections.

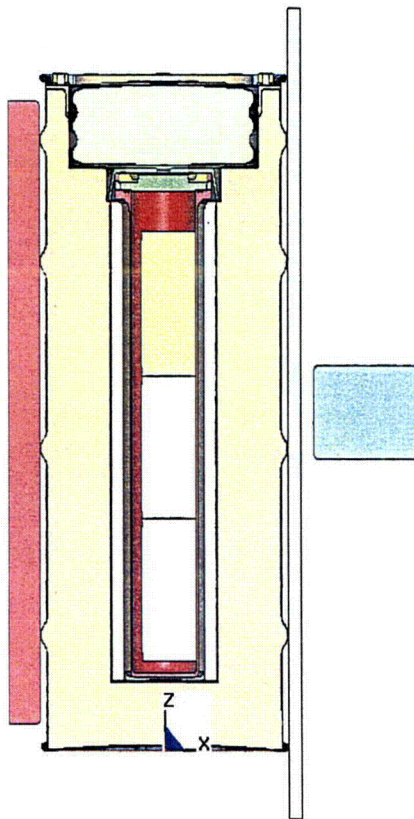


Figure 3.0.1 - Global Coordinate System

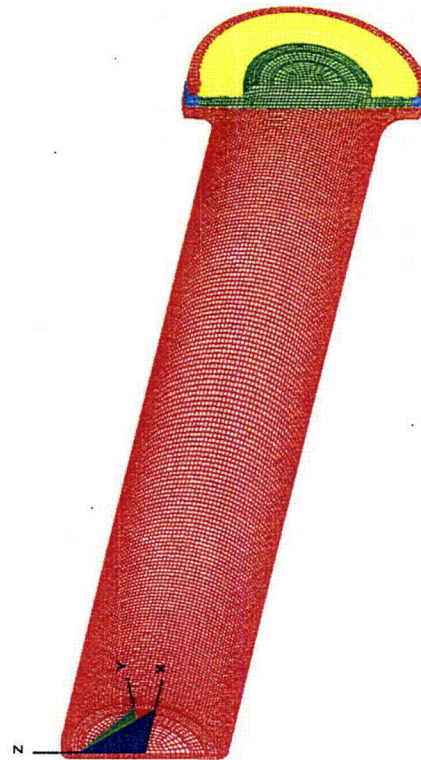


Figure 3.0.2 - CV Local Coordinate System



A study of the slapdown angle was performed using a computer code obtained from Los Alamos National Lab. The code considers a simplified, deformable body whose slapdown angle can be varied through multiple runs. The response of interest was the velocity of the secondary impacting end as it strikes the rigid surface.

To obtain all the input constants needed by the slapdown code, trial runs of the ES-3100 model were made. From the trial run, the load on the rigid surface and the deflection of the ES-3100 package ends were used to obtain the simple spring constants. The overall body dimensions, center of gravity location, mass moment of inertia and container mass were also input to the slapdown code. Figure 2.1.7 shows the results of the slapdown study. The friction factor between the rigid surface and the container was varied between 0.0 and 0.3. An angle of  $12^\circ$  was found to maximize the secondary impact and was chosen for the slapdown angle for the ES-3100.

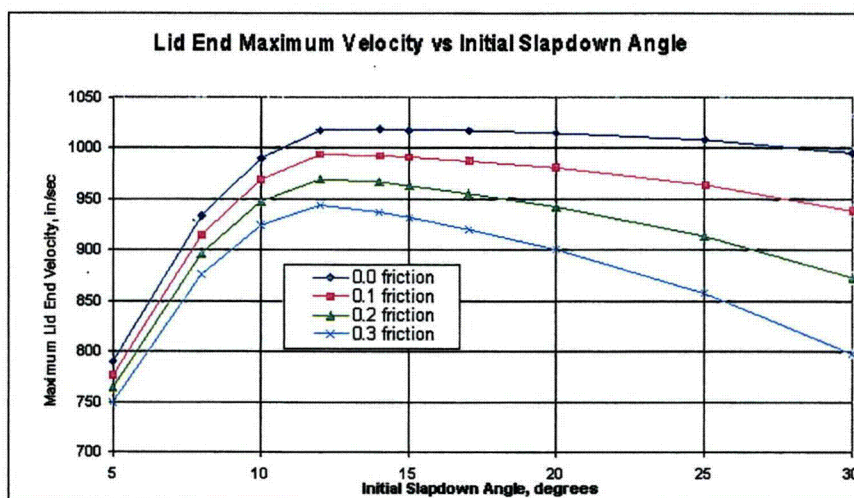


Figure 2.1.7 - Secondary Velocity Maximum from the Slapdown Study

### 3.1 Run1g - Side

Run1g is a design run with a 30-foot side impact (run time from 0 to about 0.0085 seconds) followed by a 30-foot, centered crush impact (from about 0.0085 to 0.025 seconds).

Figure 3.1.1 shows the initial configuration of the model. Note that the punch was in the model, but a punch impact was not included in this run. Figure 3.1.2 shows the configuration of the model after the 30-foot impact. Figure 3.1.3 shows the lid region of the model after the 30-foot impact. Figure 3.1.4 shows the final configuration in the bottom region of the drum nearest the 30-foot impact with the rigid plane.

The effective plastic strain in the CV body at the end of the 30-foot impact is shown in Figure 3.1.5 to be a maximum of 0.0346 in/in. The maximum effective plastic strain occurs near the bottom head as shown in one of the enlarged views in the figure. Figure 3.1.6 shows the maximum effective plastic strain in the CV lid to be 0.0002 in/in for the 30-foot impact. The nut ring remained elastic during the 30-foot impact and is not shown in an image.

The effective plastic strain in the drum angle for the 30-foot impact is shown in Figure 3.1.7. The maximum strain is found to be 0.0682 in/in nearest the rigid plane. Figure 3.1.8 shows the maximum effective plastic strain in the drum to be 0.2218 in/in near the location of the angle and rigid plane. Figure 3.1.9 shows the effective plastic strain in the drum bottom head to be a maximum of 0.2444 in/in. The maximum effective plastic strain in the liner is 0.1189 in/in as given in Figure 3.1.10. The maximum is localized at the junction of the borobond/kaolite liner, near the CV flange, opposite the impact (180°). Figure 3.1.11 shows the maximum effective plastic strain in the drum lid to be 0.3580 in/in and occurs near the stud nearest the impact (0°). The maximum effective plastic strain in the lid stiffener is 0.0060 in/in and is not shown in a Figure. The maximum effective plastic strain in the drum studs is shown in Figure 3.1.12 to be 0.1171 in/in. The maximum effective plastic strain in the drum stud nuts is 0.0005 in/in and in the washers is 0.1628 in/in. The maximum effective plastic strain in the plug liner is 0.08260 in/in. Figures for the nuts, washers and plug liner are not shown.

The time history for the kinetic energy of the package assembly in the 30-foot impact is shown in Figure 3.1.13. Figure 3.1.14 shows the assembly X velocity time history. A constant rebound velocity was obtained at 0.0085 seconds, so the solution was halted at that point. The abrupt response near 0.0085 seconds in both figures is a precipitate of the successive impact restarts (redefining the velocities for the successive impact).

A restart of the LS-Dyna solution is used to create the crush impact. The state of the shipping package at time = 0.0085 seconds was written to a restart file at the end of the 30-foot impact. A second file, the restart input file (user defined) was used to extend the solution to 0.025 seconds, redefine the shipping container nodal velocity to 0.0 in/sec, and

redefine the crush plate nodal velocity to 528 in/sec. With the restart file and the restart input file, the crush impact solution was initiated on the 30-foot damaged container.

The initial configuration of the crush impact was the final configuration of the 30-foot impact as shown in Figure 3.1.2. The final configuration for the crush impact is shown in Figure 3.1.15. Figure 3.1.16 shows a view of the lid region near the rigid plane after the crush impact (0°). Figure 3.1.17 shows the upper lid region (180°). Figure 3.1.18 shows the lower bottom region (0°) and Figure 3.1.19 shows the upper bottom region after the crush impact (180°).

Figure 3.1.20 shows the maximum effective plastic strain in the CV body after the crush impact to be 0.0348 in/in. This is approximately the value after the 30-foot impact. The internal weights bare on the CV side wall forcing the local elevated strain region. Figure 3.1.21 shows the effective plastic strain in the CV lid to be a maximum of 0.0002 in/in. The CV nut ring remains elastic during the crush impact.

Figure 3.1.22 shows the maximum effective plastic strain in the drum angle due to the crush impact to be 0.0945 in/in. The maximum effective plastic strain in the drum is 0.3028 in/in as shown in Figure 3.1.23. Elevated regions of plastic strain occur in localized crimped regions at each end of the crush plate and at the attachment of the angle to the drum near the rigid surface (0°). Figure 3.1.24 shows the effective plastic strain in the drum bottom head. The maximum in the bottom head is 0.2945 in/in. The maximum effective plastic strain in the liner is 0.2063 in/in as shown in Figure 3.1.25. The maximum value occurs at the borobond/kaolite liner junction at 180°, as in the initial 30-foot impact.

The maximum effective plastic strain in the lid due to the crush impact occurs at the base of the hole for the upper stud (180°), near the crush plate. The maximum is 0.6430 in/in as shown in Figure 3.1.26. The membrane strain maximum is 0.4475 in/in and is very localized to the upper stud hole (similar to the bending shown in Figure 3.1.26). If failure were to occur it would be very localized to the lower region of the upper stud hole (near the crush plate - possible surface cracking). There is a lack of a general region of high strain in the lid which would promote an extended tear, or ripping of the lid.

Figure 3.1.27 shows the drum studs with a maximum effective plastic strain of 0.1937 in/in due to the crush impact. Not shown in figures: the maximum effective plastic strain in the lid stiffener is 0.0303 in/in; the maximum effective plastic strain in the drum stud nuts is 0.0005 in/in; the maximum effective plastic strain in the drum stud washers is 0.1628 in/in and the maximum effective plastic strain in the plug liner is 0.1212 in/in.

Figure 3.1.28 shows the kinetic energy time history for the crush plate. Figure 3.1.29



shows the X velocity time history for the plate.

The location of the nodes chosen to investigate the separation of the CV lid and the body flange at the O-rings are shown in Figure 3.1.30. The nodes are at 45° positions around the half model. The nodes are at the inside radius of the inner O-ring groove on the body and are at comparable positions on the opposite, lid surface. Figure 3.1.31 shows the separation time history for the node pairs. A positive value in the plot indicates separation (gap). The plot is quite noisy with ringing (contact chatter) of the node pair separations, but its purpose is to show relative magnitudes of separation in the model. From the figure, it can be seen that a gap spike of almost 0.004 in is obtained in the 30-foot impact just before 0.005 seconds. In the crush impact, spikes of almost 0.005 in in gap separation are seen. When the solution was halted, spikes on the order of 0.004 in are evident (there is no damping in the model other than friction). The ringing maximum is approximately 0.004 in and its minimum is about 0.00 in at the end of the solution (sinusoidal in nature). The ringing would then be about a mid-point value of 0.002 in. An implicit solution, or relaxed state is not obtained. In a relaxed state, if a permanent set were obtained in the flange region, then the average gap would be about 0.002 in, or less would be expected.

Figure 3.1.32 shows the kaolite nodes on the plane of symmetry chosen to obtain the kaolite thickness response to the impacts. Figure 3.1.33 shows the time history thickness at the nodal pairs shown. The thickness is obtained by subtracting one node X-coordinate time history from another nodes. The time in Figure 3.1.33 is in seconds and the X coordinate is the relative value in inches. For example, curve "A" represents the kaolite thickness on the plane of symmetry between the angle and the drum, nearest the crush plate. From Figure 3.1.33 it can be seen that the curve "A" thickness initially is about 1.75 inches and remains at that value for the 30-foot impact. The crush impact is seen to reduce the kaolite thickness to just under 1.0 inches for curve "A". The correlation of nodes, Figure 3.1.33 curve letter and a description of the location is given in Table 3.1.1.

Table 3.1.1 - Location of Kaolite Thickness Measurements

Model Direction	Description	Figure 3.1.33 Curve	Figure 3.1.32 Nodes
-X	Liner at Base of Angle / Drum	A	191112 / 206004
	Liner at Base of Plug Cavity / Drum	B	188411 / 200529
	Liner at Top of CV Cavity / Drum	C	224181 / 200522
	Liner at Second Drum Roll from the Lid / Drum Roll Extreme	D	222721 / 361713
	Liner at Second Drum Roll from the Bottom / Drum Roll Extreme	E	218049 / 350033
	Liner at First Drum Roll from the Bottom / Drum Roll Extreme	F	213377 / 338353
	Liner at Base of CV Cavity / Drum	G	210749 / 334338
+X	Liner at Base of CV Cavity / Drum	H	333258 / 209669
	Liner at First Drum Roll from the Bottom / Drum Roll Extreme	I	338281 / 213305
	Liner at Second Drum Roll from the Bottom / Drum Roll Extreme	J	349961 / 217977
	Liner at Second Drum Roll from the Lid / Drum Roll Extreme	K	361641 / 222649
	Liner at Top of CV Cavity / Drum	L	199946 / 223677
	Liner at Base of Plug Cavity / Drum	M	199953 / 187835
	Liner at Base of Angle / Drum	N	205932 / 191040

Figure 3.1.34 shows nodes in the drum, drum bottom and drum lid which will be used to define the diameter changes in the outer surfaces of the shipping package. Figure 3.1.35 gives the relative X coordinate values (diameter changes) for the nodes on the plane of symmetry. From the plot it is seen that the minimum diameter reaches approximately 14.5 inches and then rebounds slightly. This minimum is at the lower barrel roll in the drum. From Figure 3.1.35 it is seen that the barrel roll diameters decrease from top to bottom. The greater deflection of the crush plate nearer the bottom of the package is evident in the Figure 3.1.15 final configuration plot. Figure 3.1.36 gives the Y coordinate time history response of the nodes at the Y extreme of the shipping package (see Figure 3.1.34). The values in Figure 3.1.36 are relative to the plane of symmetry and therefore need to be doubled to obtain the diameter changes. The correlation of nodes, curve numbers and a description of the location are given in Table 3.1.2. The ovalization of the package is also evident in comparing Figures 3.1.35 and 3.1.36.

Table 3.1.2 - Nodal Locations for Drum Diameter Time Histories				
Description	Diameter (X Direction)		Radius (Y Direction)	
	Figure 3.1.35 Curve	Figure 3.1.34 Nodes	Figure 3.1.36 Curve	Figure 3.1.34 Nodes
Lid Roll	A	133634 / 133778	A	133706
First Drum Roll Below Lid	B	98158 / 98230	B	98194
Second Drum Roll Below Lid	C	100202 / 100274	C	100238
Second Drum Roll Above Bottom	D	102976 / 103048	D	103012
First Drum Roll Above Bottom	E	105750 / 105822	E	105786
Bottom Attachment Roll to Drum	F	108889 / 108961	F	108925

Figure 3.1.37 shows nodes chosen to obtain liner diameter time histories. Figure 3.1.38 shows the diameter time histories for the node pairs. Table 3.1.3 shows the location of the nodal pairs along the length of the liner.

Table 3.1.3 - Nodal Locations for Liner Diameter Time Histories		
Curve	Node Pairs	Distance Above Base of Liner (in)
A	122522 / 122666	0.0
B	123259 / 129667	5.0
C	123276 / 129684	10.3
D	123292 / 129700	15.3
E	123309 / 129717	20.6
F	123324 / 129732	25.2
G	123340 / 129748	30.2



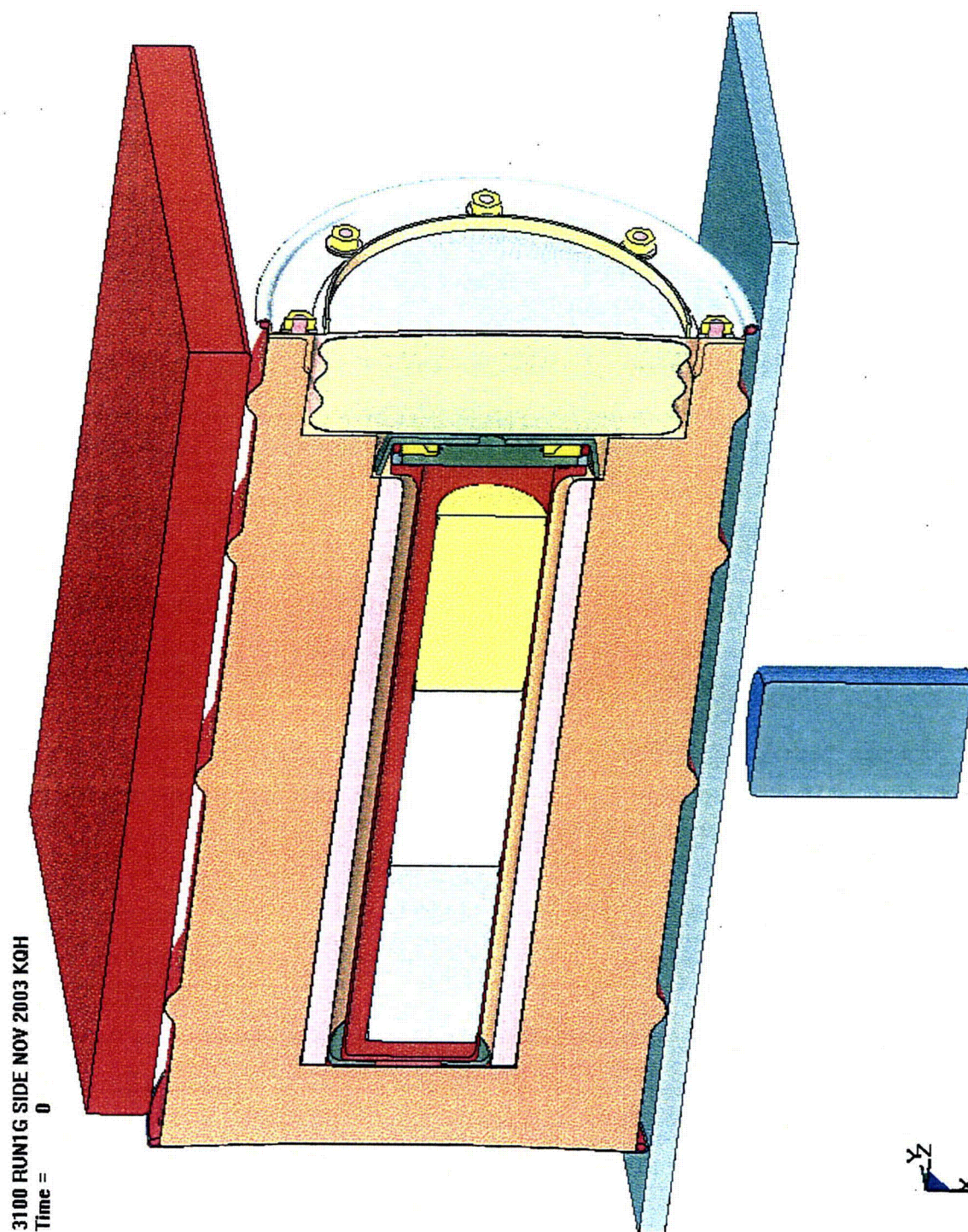


Figure 3.1.1 - Run1g, Initial Configuration



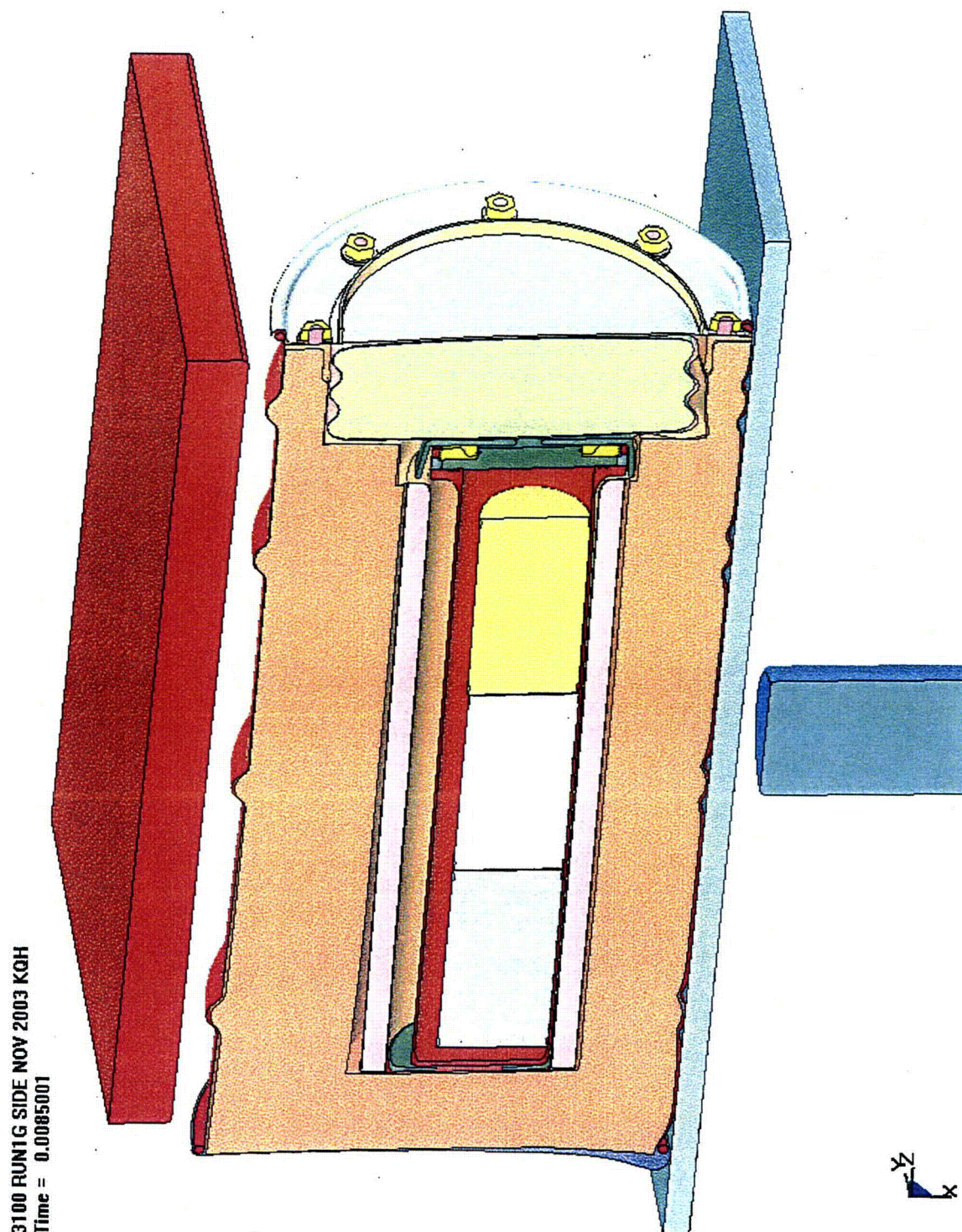


Figure 3.1.2 - Run1g, 30-Foot Impact, Final Configuration



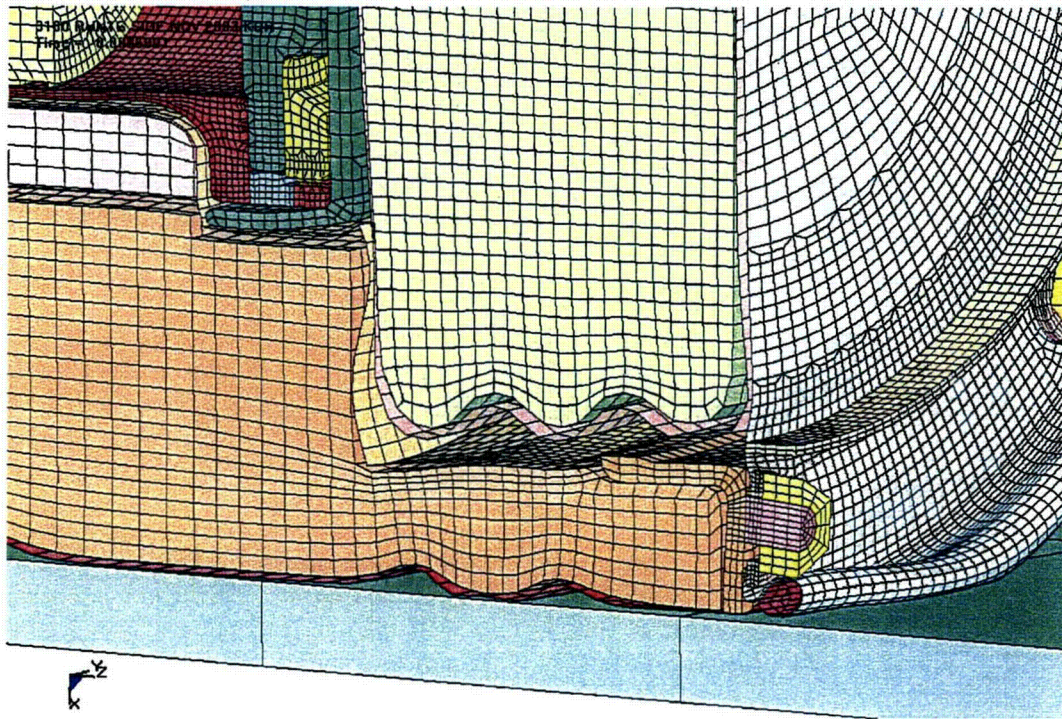


Figure 3.1.3 - Run1g, 30-Foot Impact, Configuration of the Drum Bolted Region

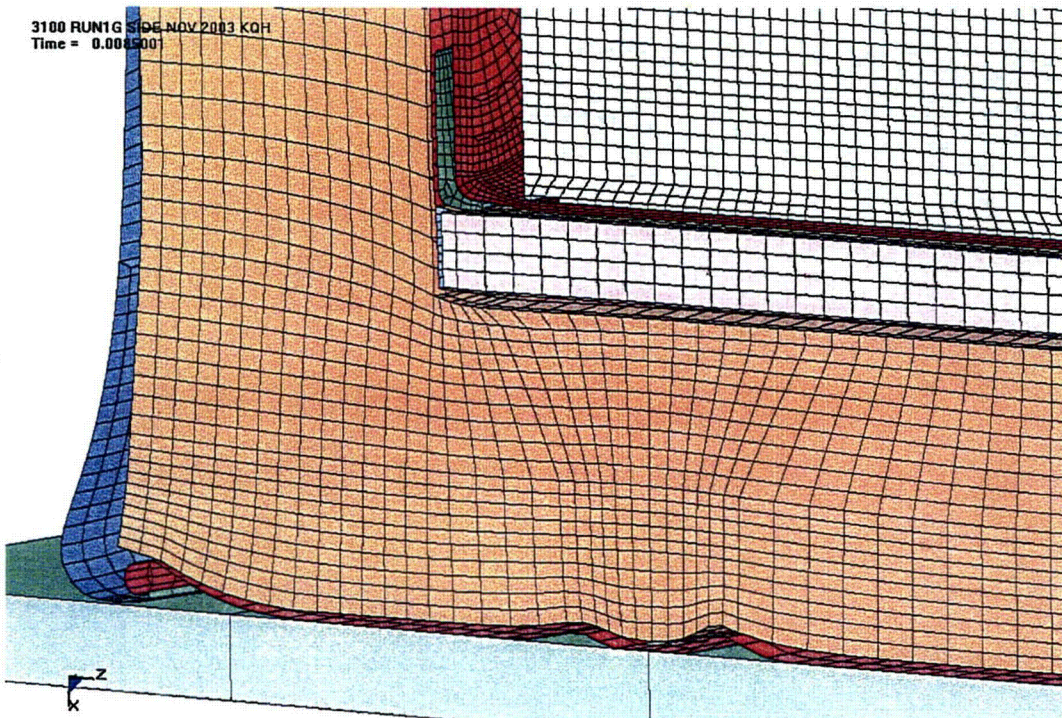


Figure 3.1.4 - Run1g, 30-Foot Impact, Configuration of the Bottom Drum Corner



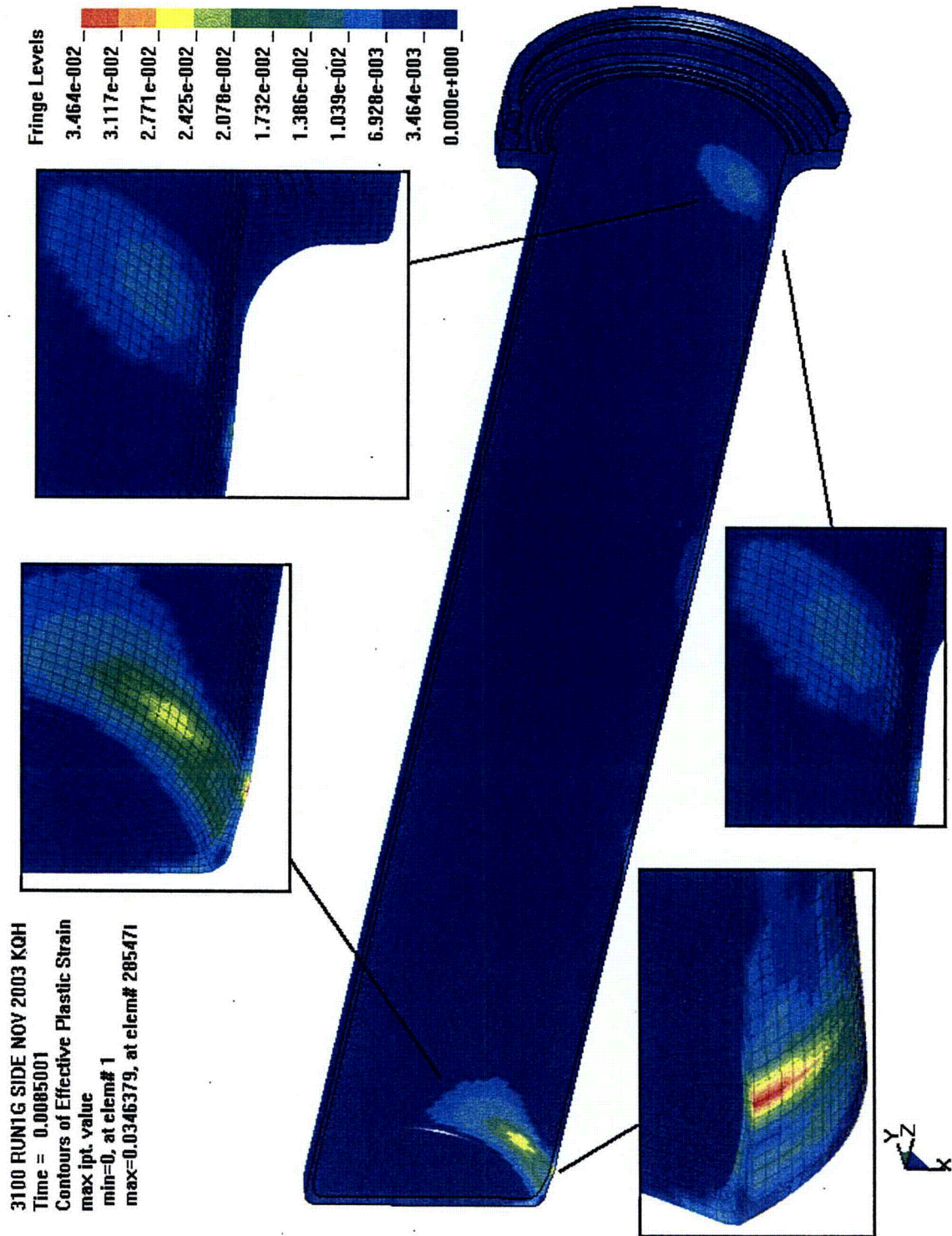
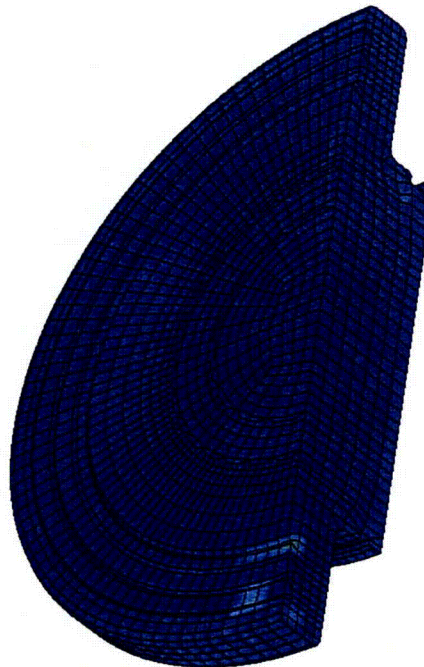


Figure 3.1.5 - Run1g, 30-Foot Impact, Effective Plastic Strain in the CV Body



3100 RUN1G SIDE NOV 2003 KQH  
Time = 0.0085001  
Contours of Effective Plastic Strain  
max lpt. value  
min=0, at elem# 51809  
max=0.000174097, at elem# 565471



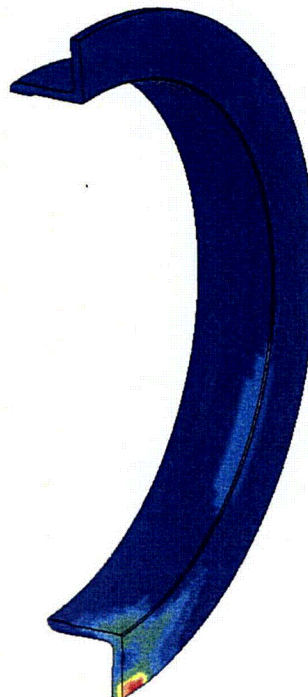
Fringe Levels

1.741e-004  
1.567e-004  
1.393e-004  
1.219e-004  
1.045e-004  
8.705e-005  
6.964e-005  
5.223e-005  
3.482e-005  
1.741e-005  
0.000e+000



Figure 3.1.6 - Run1g, 30-Foot Impact, Effective Plastic Strain in the CV Lid

3100 RUN1G SIDE NOV 2003 KQH  
Time = 0.0085001  
Contours of Effective Plastic Strain  
max lpt. value  
min=0, at elem# 60885  
max=0.0682127, at elem# 632111



Fringe Levels

6.821e-002  
6.139e-002  
5.457e-002  
4.775e-002  
4.093e-002  
3.411e-002  
2.729e-002  
2.046e-002  
1.364e-002  
6.821e-003  
0.000e+000



Figure 3.1.7 - Run1g, 30-Foot Impact, Effective Plastic Strain in the Drum Angle



Figure 3.1.8 - Run1g, 30-Foot Impact, Effective Plastic Strain in the Drum Outer Liner

3100 RUN1G SIDE NOV 2003 KQH  
Time = 0.0085001  
Contours of Effective Plastic Strain  
max lpt. value  
min=0, at elem# 15012  
max=0.24441, at elem# 151951

Fringe Levels

2.444e-001  
2.200e-001  
1.955e-001  
1.711e-001  
1.466e-001  
1.222e-001  
9.776e-002  
7.332e-002  
4.888e-002  
2.444e-002  
0.000e+000



Figure 3.1.9 - Run1g, 30-Foot Impact, Effective Plastic Strain in the Drum Bottom Head

3100 RUN1G SIDE NOV 2003 KQH  
Time = 0.0085001  
Contours of Effective Plastic Strain  
max lpt. value  
min=0, at elem# 17724  
max=0.118866, at elem# 218681

Fringe Levels

1.189e-001  
1.070e-001  
9.509e-002  
8.321e-002  
7.132e-002  
5.943e-002  
4.754e-002  
3.565e-002  
2.377e-002  
1.189e-002  
0.000e+000

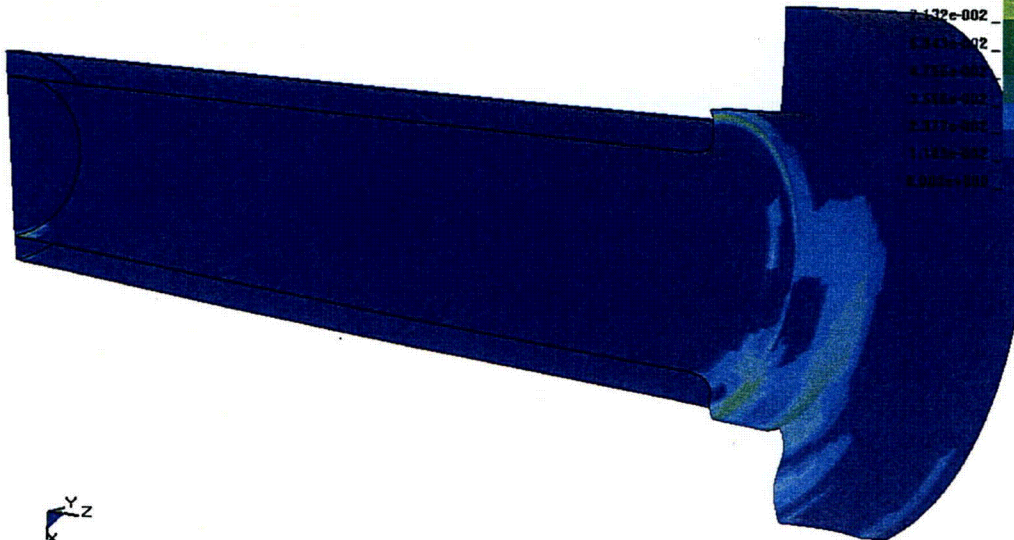


Figure 3.1.10 - Run1g, 30-Foot Impact, Effective Plastic Strain in the Liner



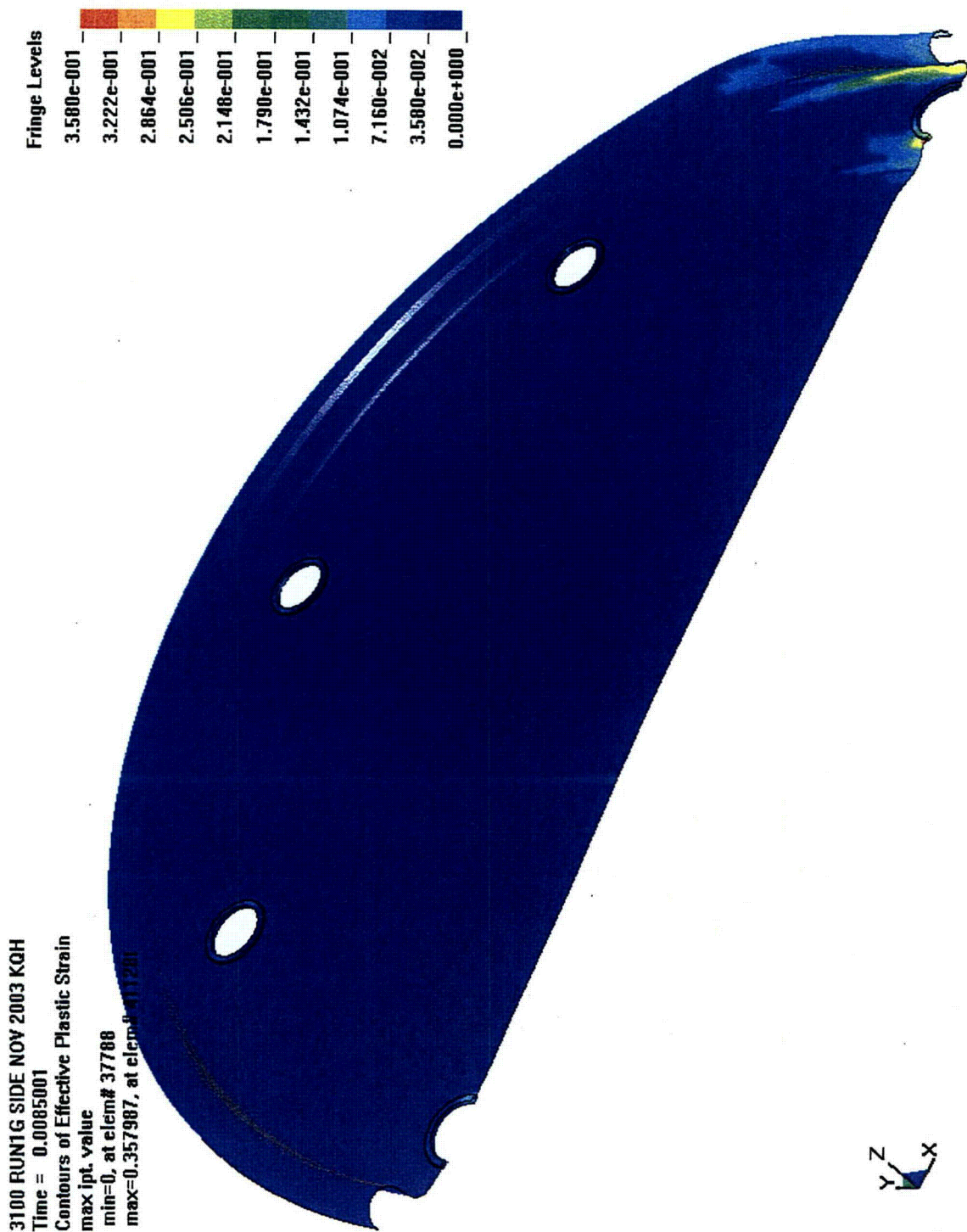


Figure 3.1.11 - Run1g, 30-Foot Impact, Effective Plastic Strain in the Drum Lid



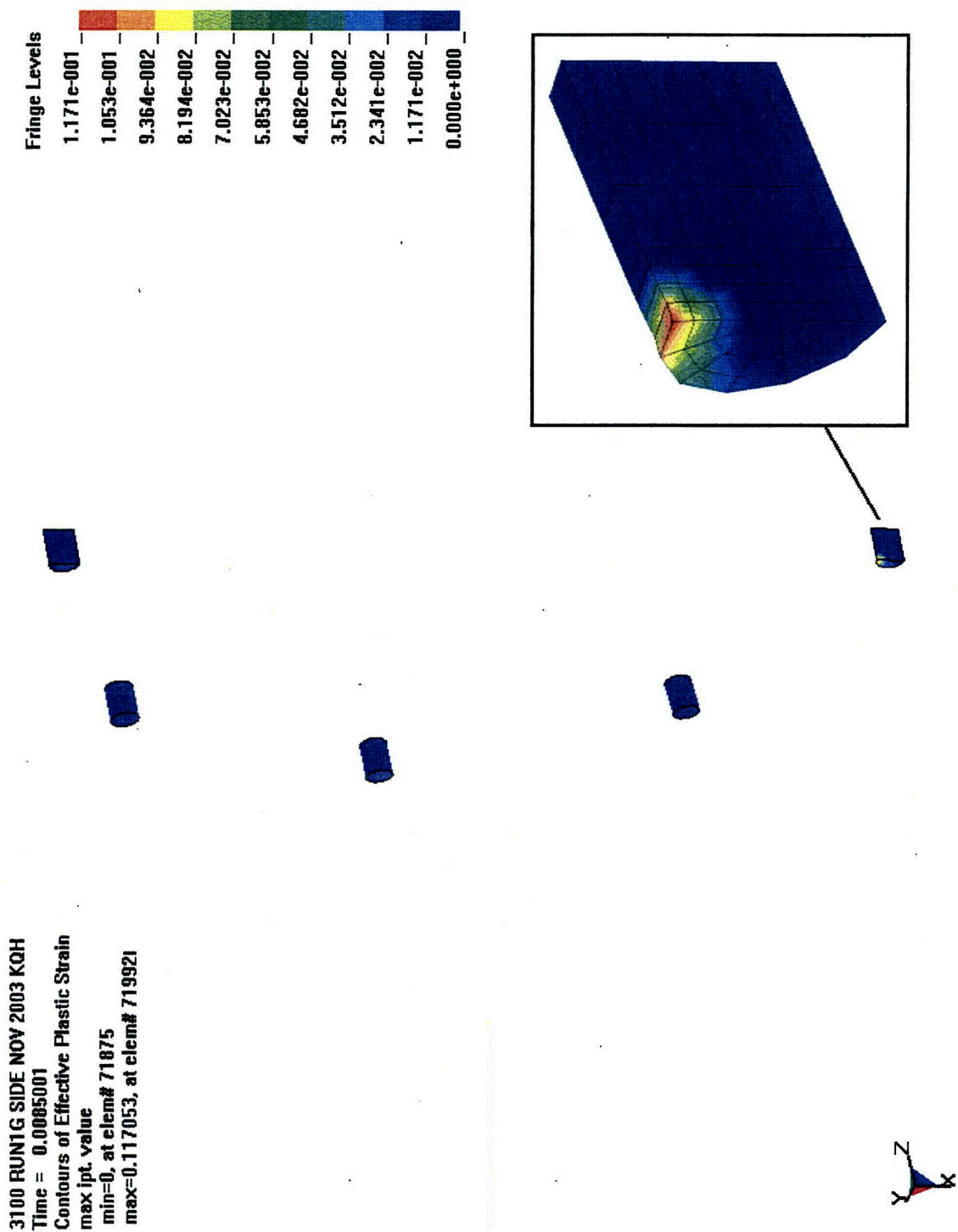


Figure 3.1.12 - Run1g, 30-Foot Impact, Effective Plastic Strain in the Drum Studs

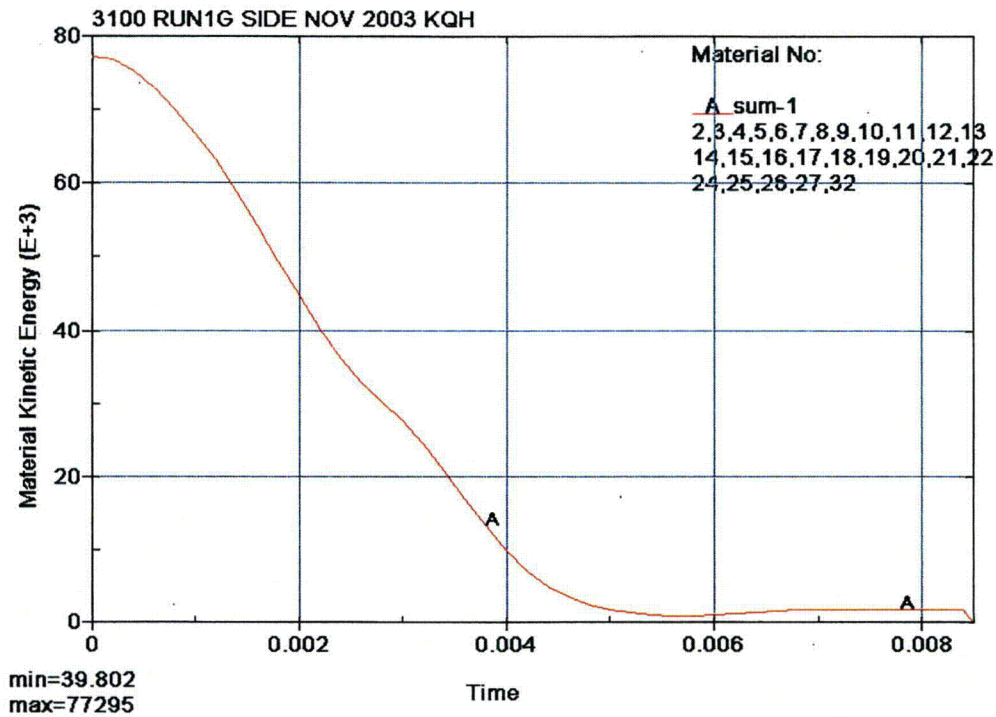


Figure 3.1.13 - Run1g, 30-Foot Impact, Kinetic Energy Time History

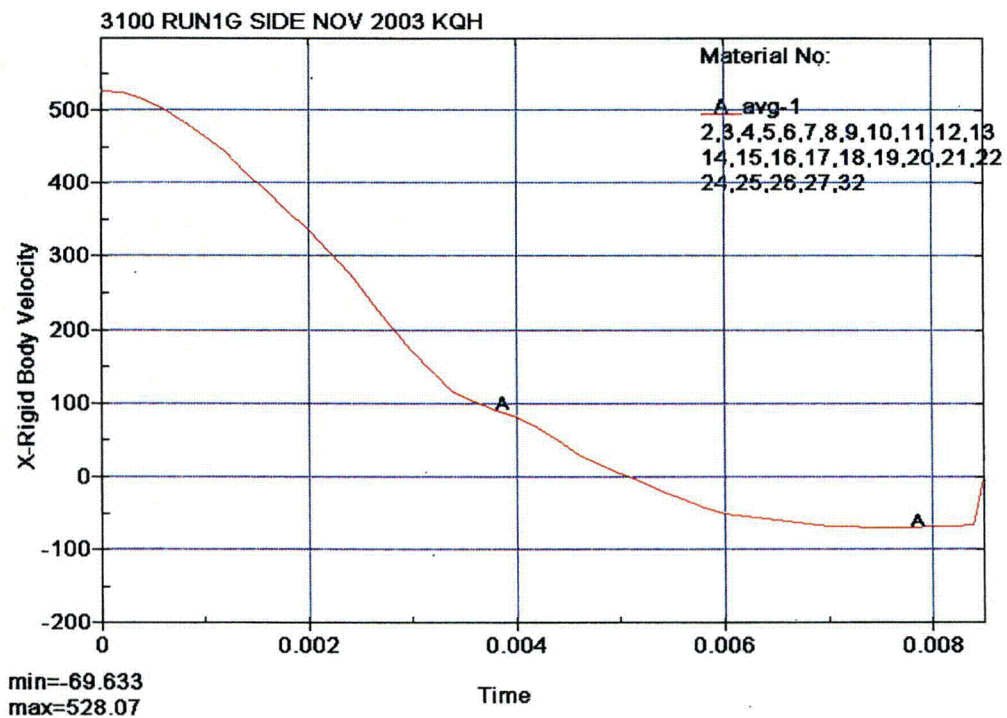


Figure 3.1.14 - Run1g, 30-Foot Impact, X Velocity Time History

3100 RUN1G SIDE NOV 2003 KQH  
Time = 0.025

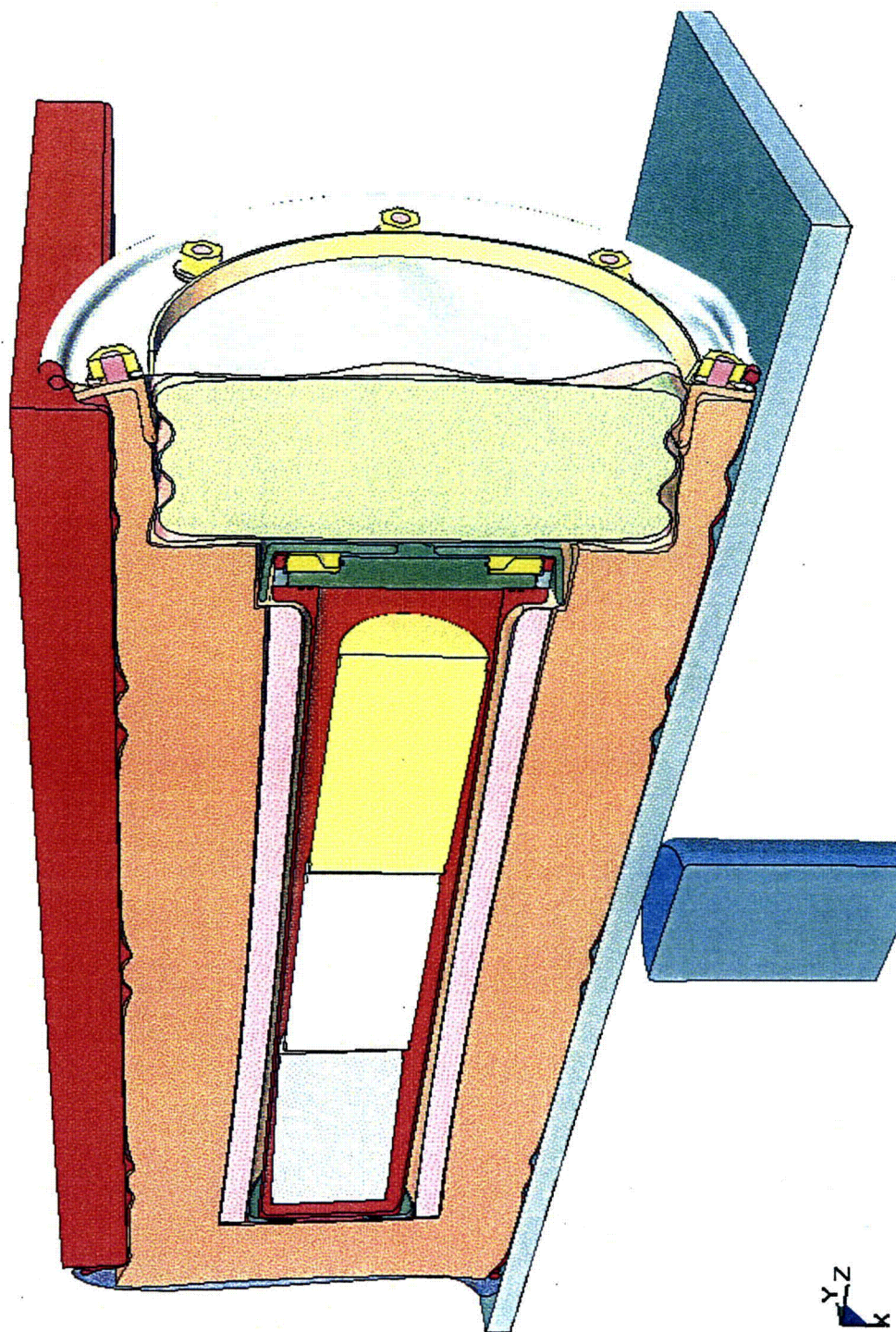


Figure 3.1.15 - Run1g, Crush Impact, Final Configuration



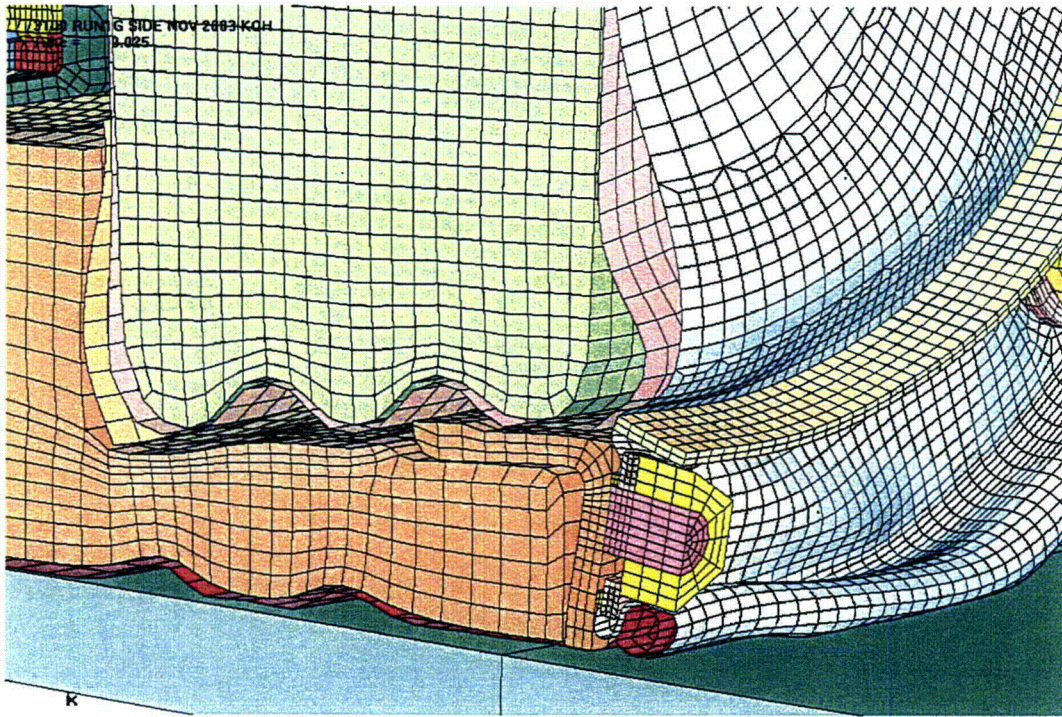


Figure 3.1.16 - Run1g, Crush Impact, Configuration of the Lower Lid Region

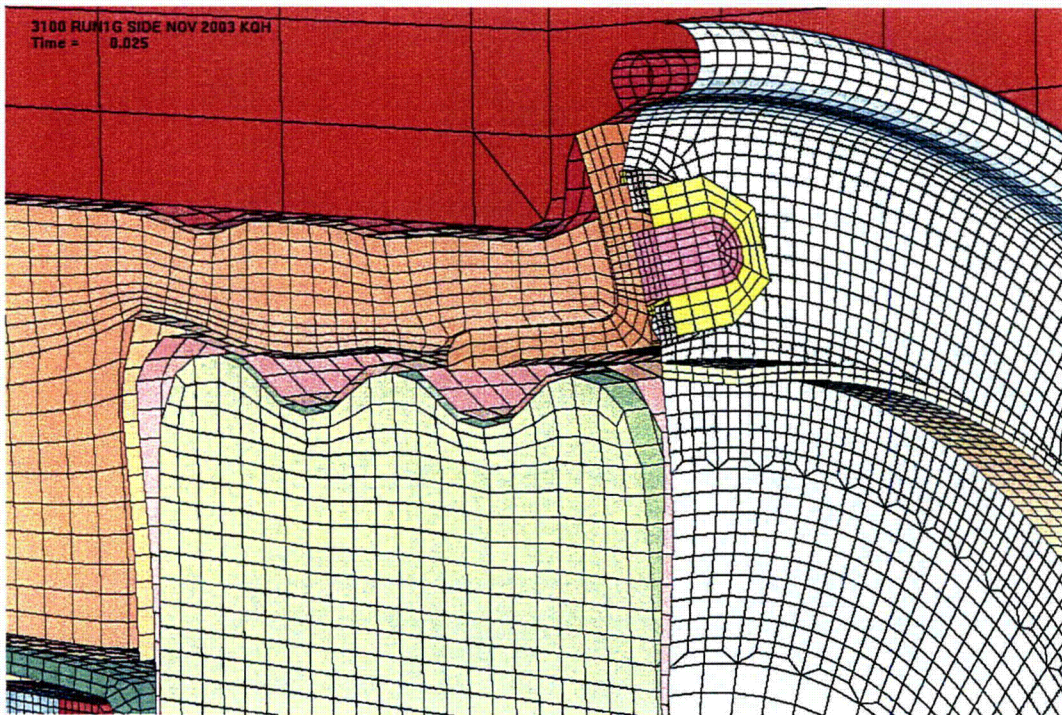


Figure 3.1.17 - Run1g, Crush Impact, Configuration of the Upper Lid Region



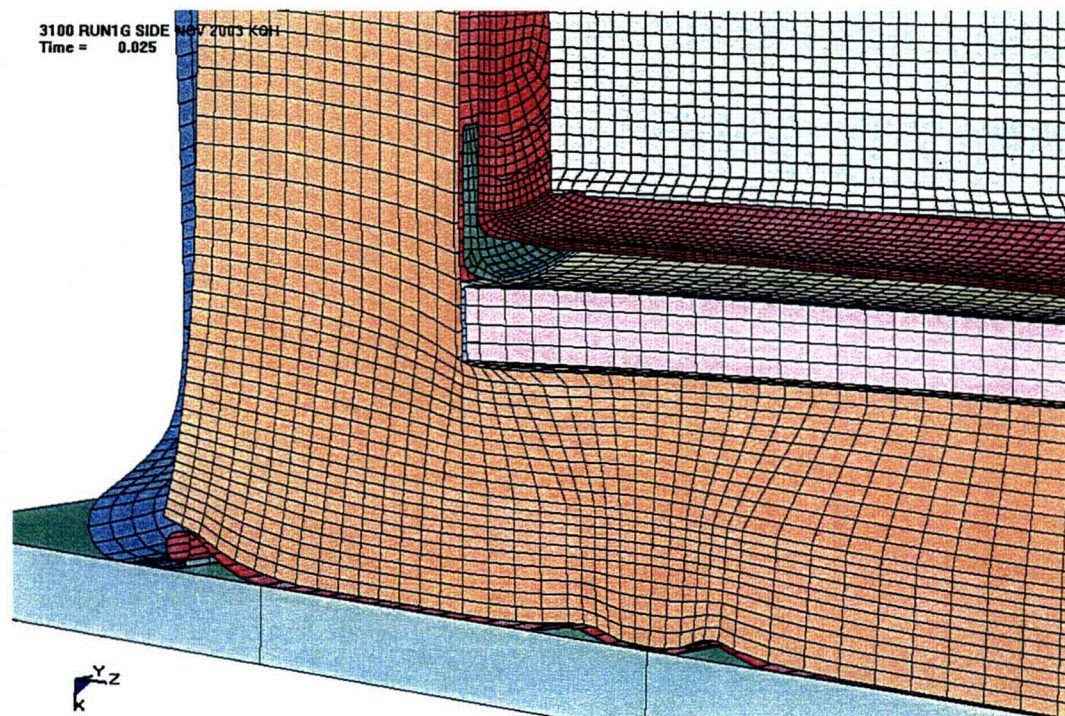


Figure 3.1.18 - Run1g, Crush Impact, Configuration of the Lower Bottom Region

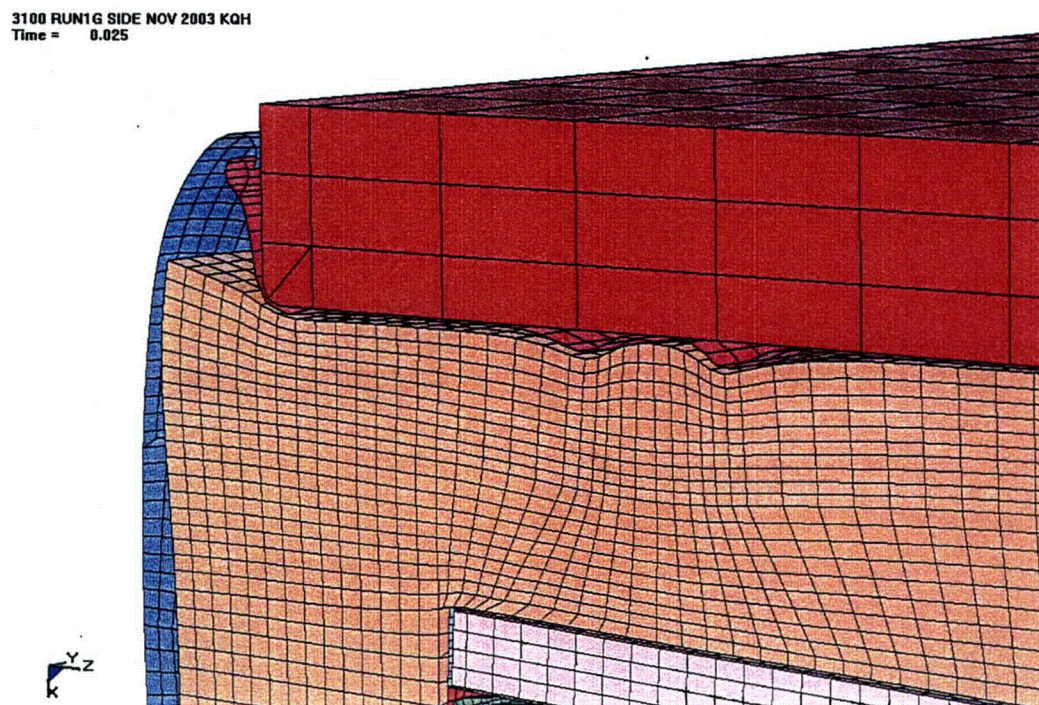


Figure 3.1.19 - Run1g, Crush Impact, Configuration of the Upper Bottom Region



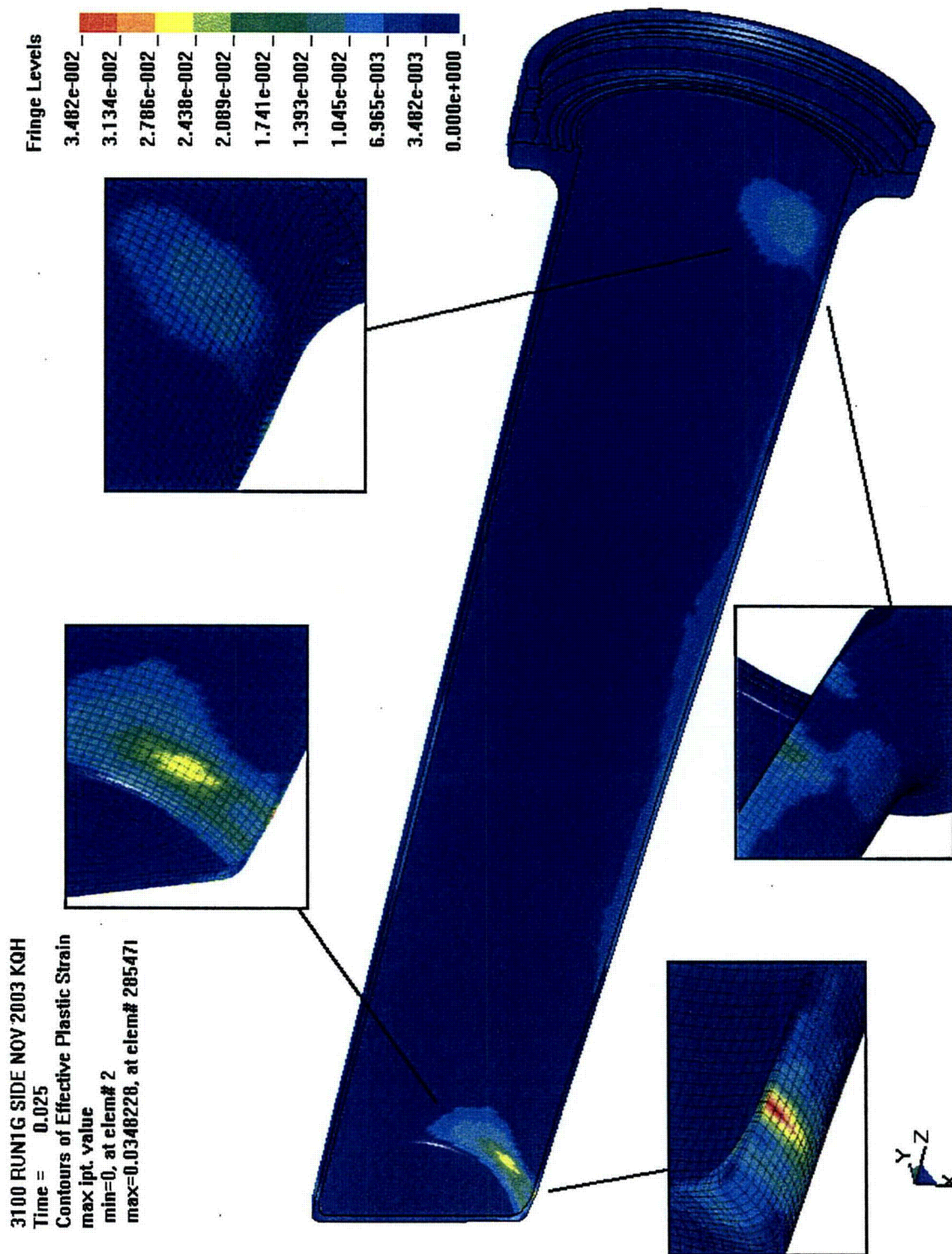
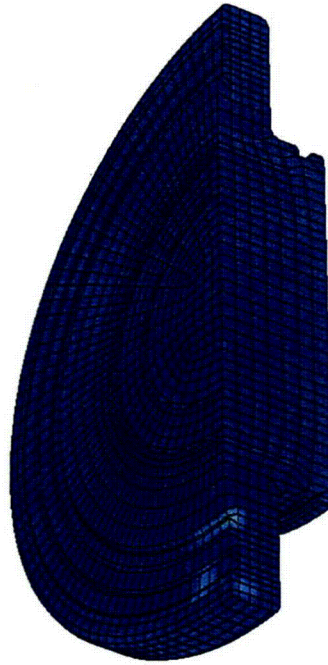


Figure 3.1.20 - Run1g, Crush Impact, Effective Plastic Strain in the CV Body

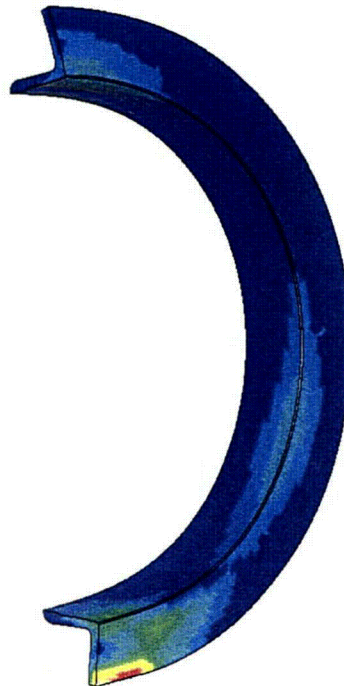
3100 RUN1G SIDE NOV 2003 KQH  
Time = 0.025  
Contours of Effective Plastic Strain  
max lpt. value  
min=0, at elem# 51809  
max=0.000174097, at elem# 565471



Fringe Levels  
1.741e-004  
1.567e-004  
1.393e-004  
1.219e-004  
1.045e-004  
8.705e-005  
6.964e-005  
5.223e-005  
3.482e-005  
1.741e-005  
0.000e+000

Figure 3.1.21 - Run1g, Crush Impact, Effective Plastic Strain in the CV Lid

3100 RUN1G SIDE NOV 2003 KQH  
Time = 0.025  
Contours of Effective Plastic Strain  
max lpt. value  
min=0, at elem# 61134  
max=0.0944739, at elem# 632631



Fringe Levels  
9.447e-002  
8.503e-002  
7.558e-002  
6.613e-002  
5.668e-002  
4.724e-002  
3.779e-002  
2.834e-002  
1.889e-002  
9.447e-003  
0.000e+000

Figure 3.1.22 - Run1g, Crush Impact, Effective Plastic Strain in the Drum Angle



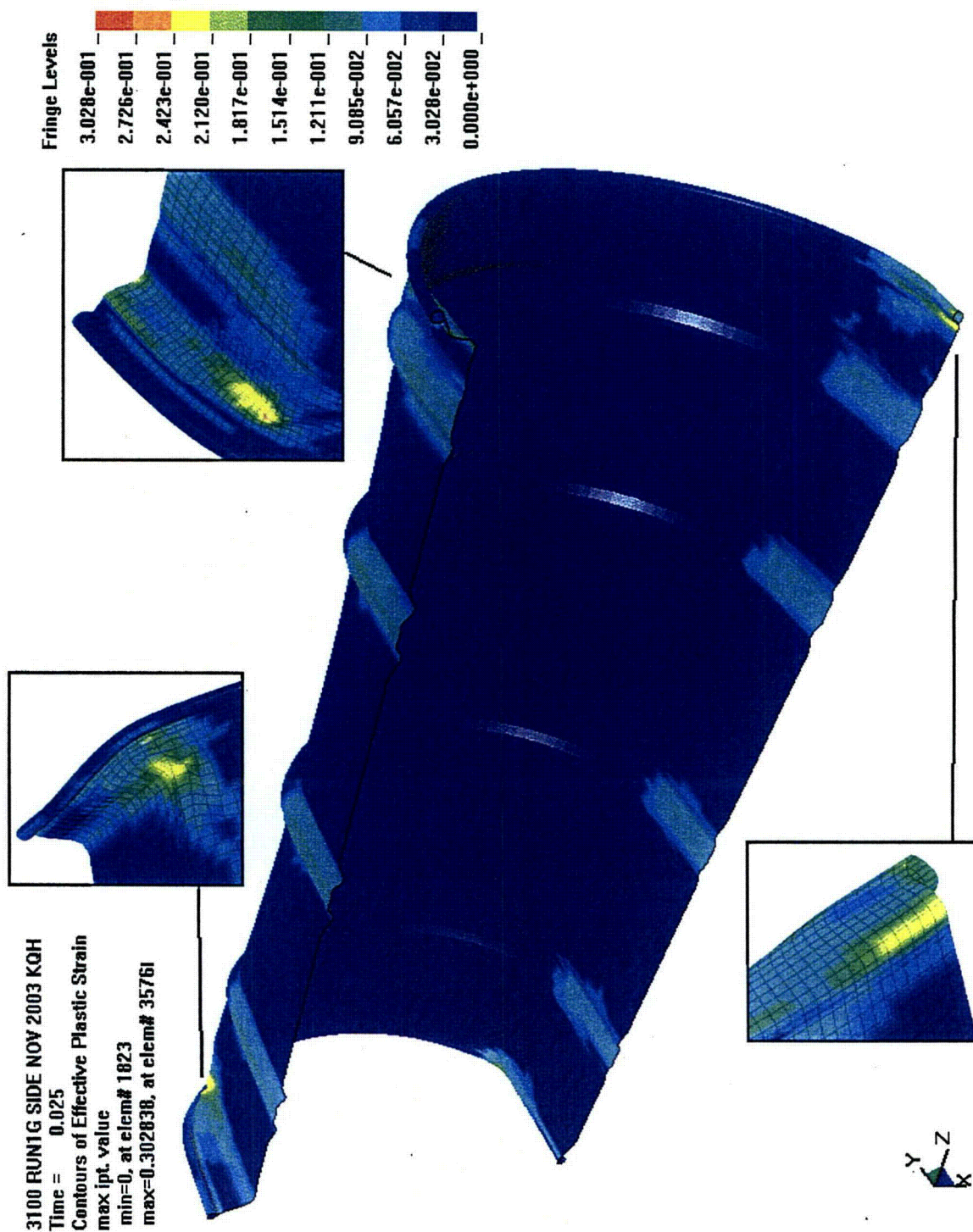


Figure 3.1.23 - Run1g, Crush Impact, Effective Plastic Strain in the Drum



3100 RUN1G SIDE NOV 2003 KQH  
Time = 0.025  
Contours of Effective Plastic Strain  
max lpt. value  
min=0, at elem# 16057  
max=0.294509, at elem# 150731

Fringe Levels

2.945e-001  
2.651e-001  
2.356e-001  
2.062e-001  
1.767e-001  
1.473e-001  
1.178e-001  
8.835e-002  
5.890e-002  
2.945e-002  
0.000e+000



Figure 3.1.24 - Run1g, Crush Impact, Effective Plastic Strain in the Drum Bottom Head

3100 RUN1G SIDE NOV 2003 KQH  
Time = 0.025  
Contours of Effective Plastic Strain  
max lpt. value  
min=0, at elem# 22081  
max=0.206269, at elem# 218681

Fringe Levels

2.063e-001  
1.856e-001  
1.650e-001  
1.444e-001  
1.238e-001  
1.031e-001  
8.251e-002  
6.188e-002  
4.125e-002  
2.063e-002  
0.000e+000

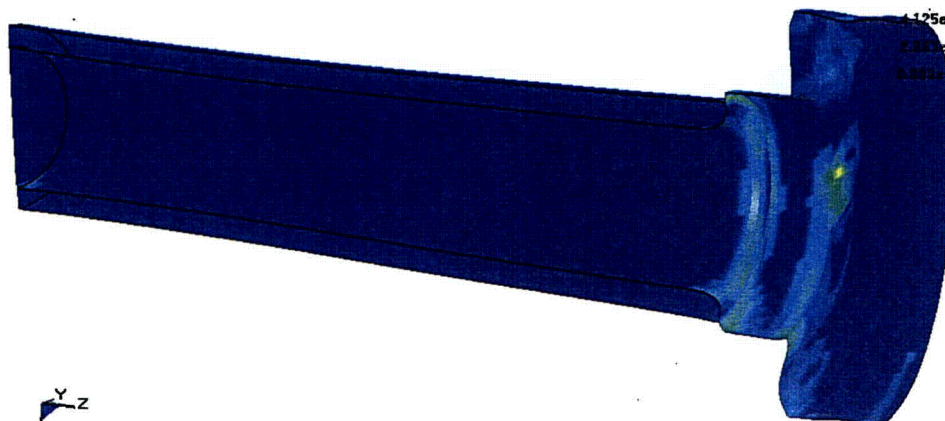


Figure 3.1.25 - Run1g, Crush Impact, Effective Plastic Strain in the Drum Inner Liner

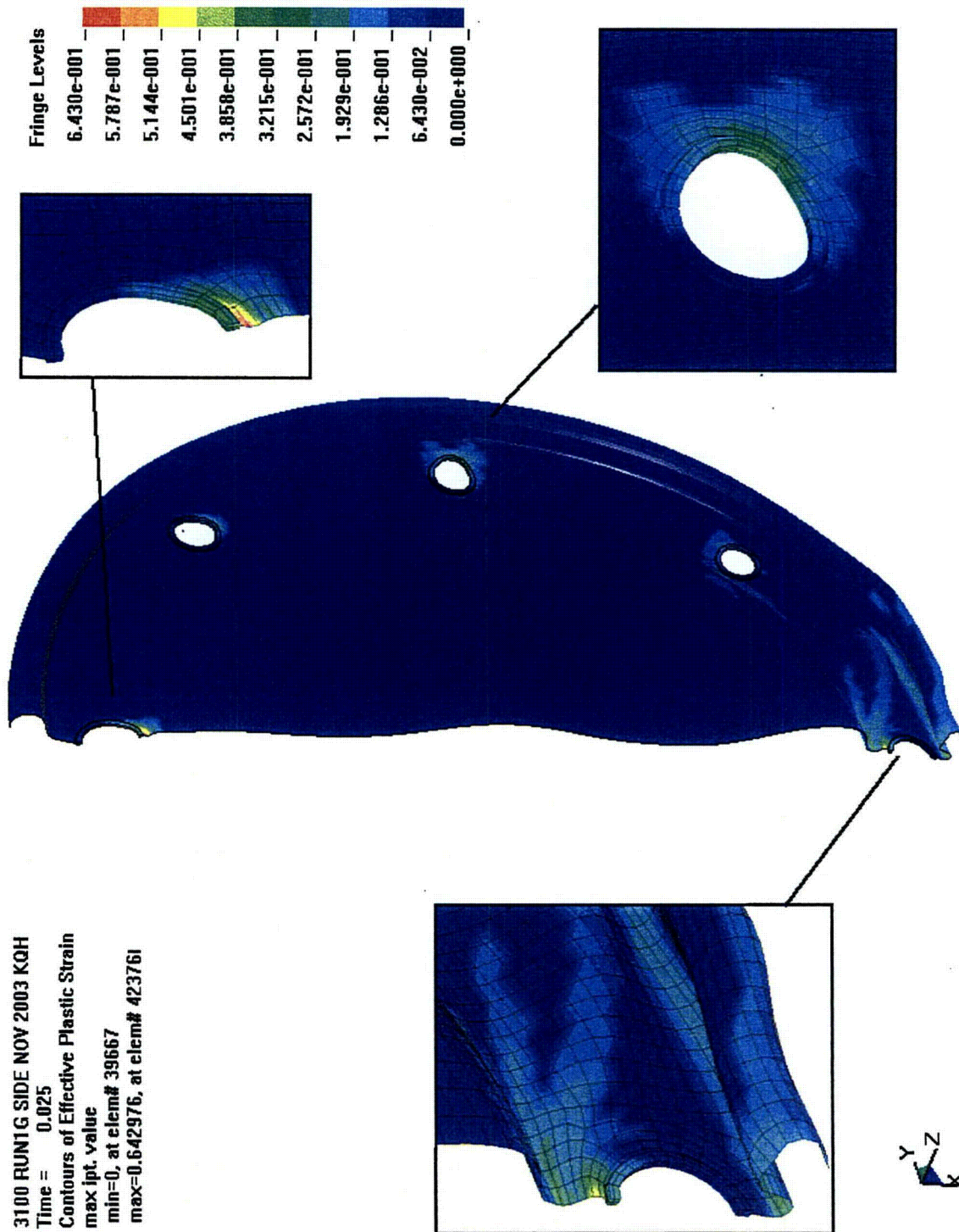


Figure 3.1.26 - Run1g, Crush Impact, Effective Plastic Strain in the Drum Lid

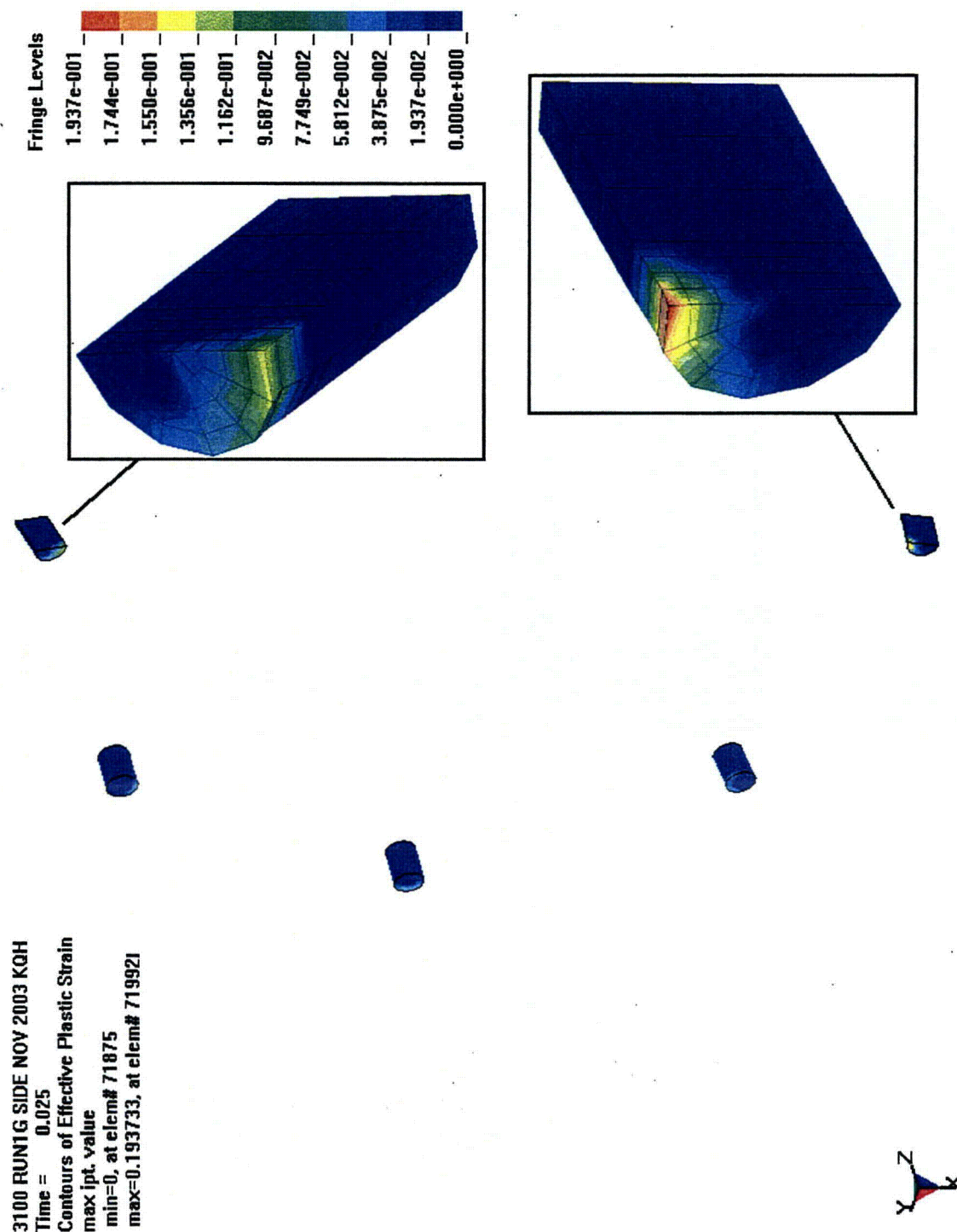


Figure 3.1.27 - Run1g, Crush Impact, Effective Plastic Strain in the Drum Studs



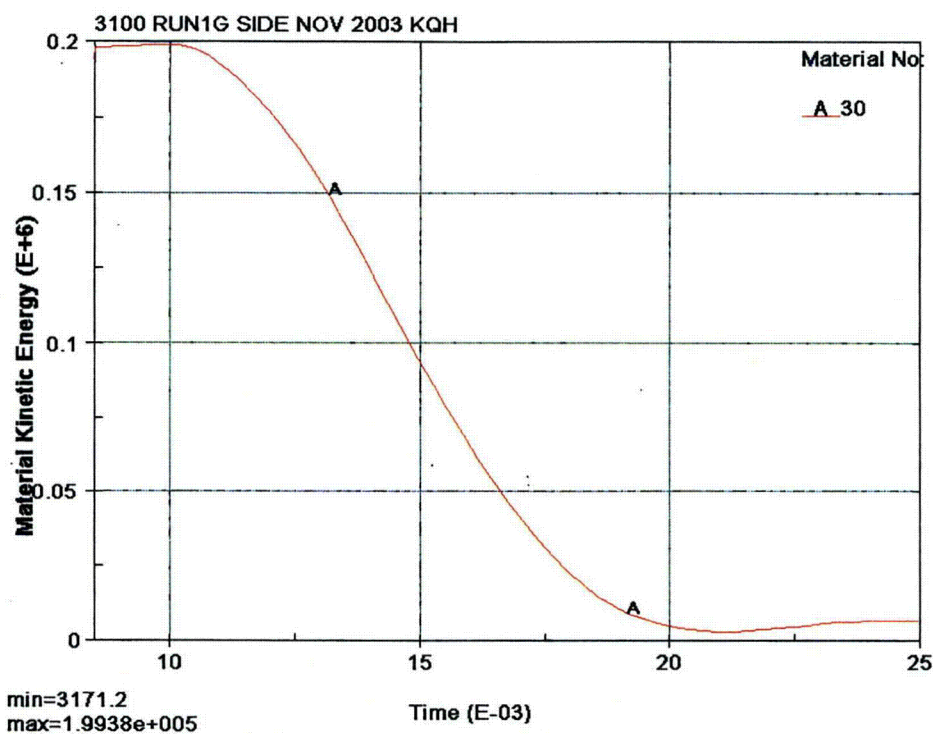


Figure 3.1.28 - Run1g, Crush Impact, Kinetic Energy Time History of the Crush Plate

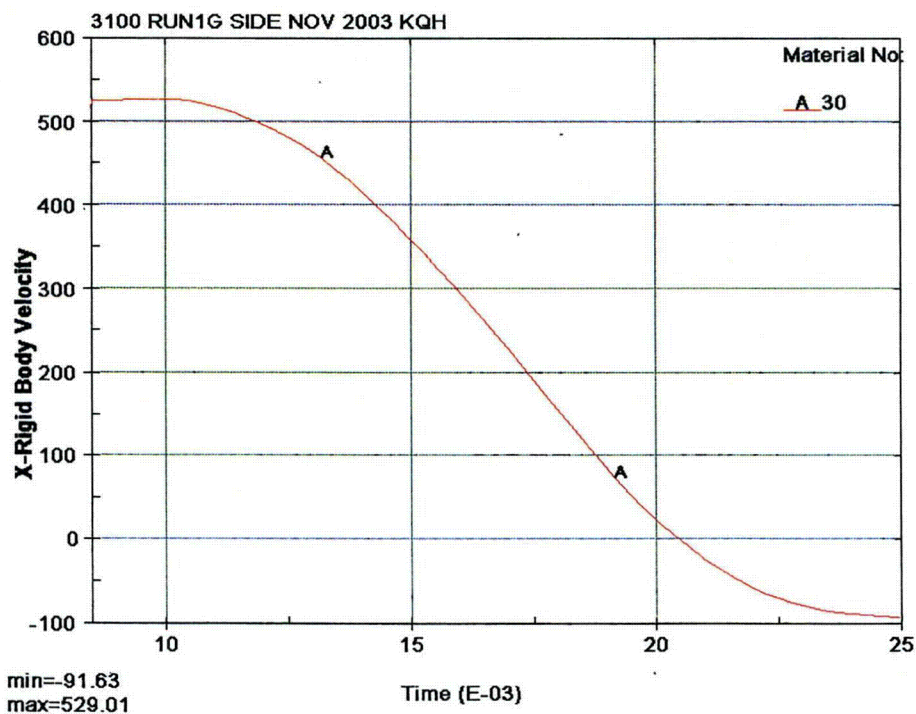


Figure 3.1.29 - Run1g, Crush Impact, X Velocity Time History of the Crush Plate

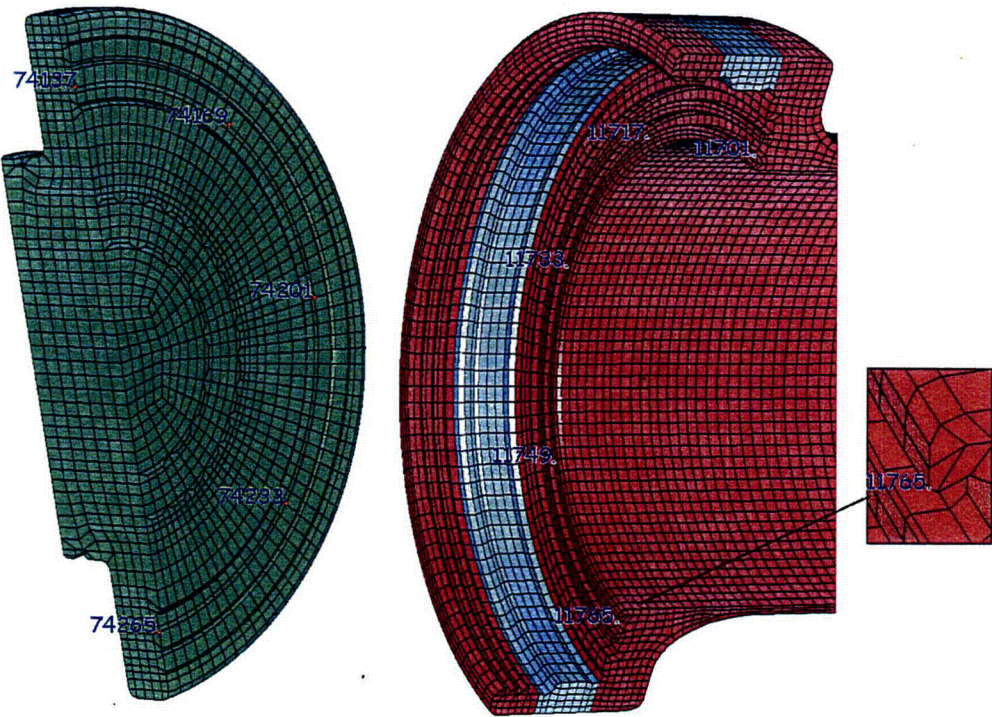


Figure 3.1.30 - Run1g, Nodes on CV Lid and Body Flange for Separation Time History

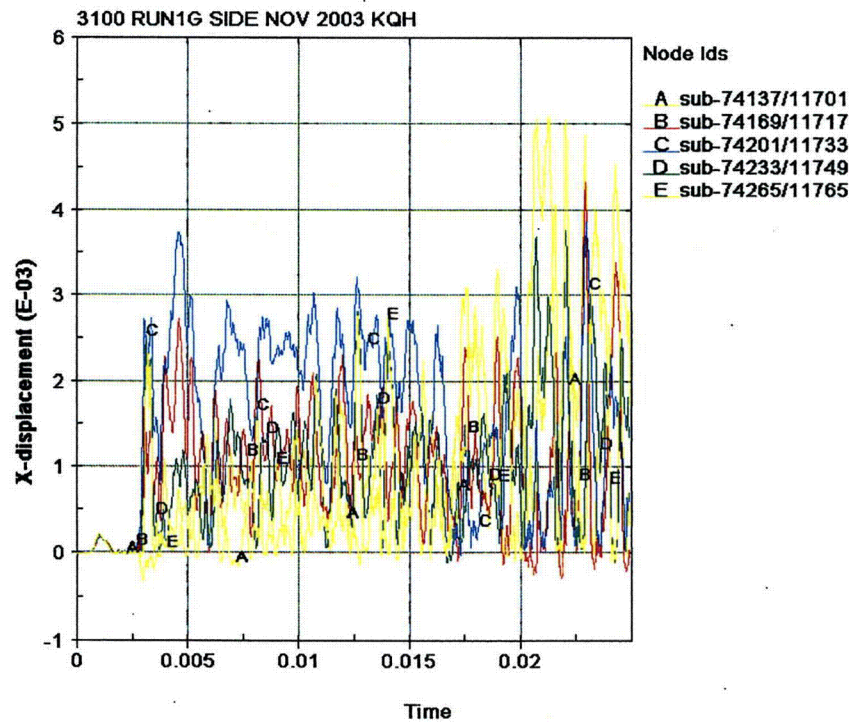


Figure 3.1.31 - Run1g, CV Flange Separation Time History

3100 RUN1G SIDE NOV 2003 KQH  
Time = 0

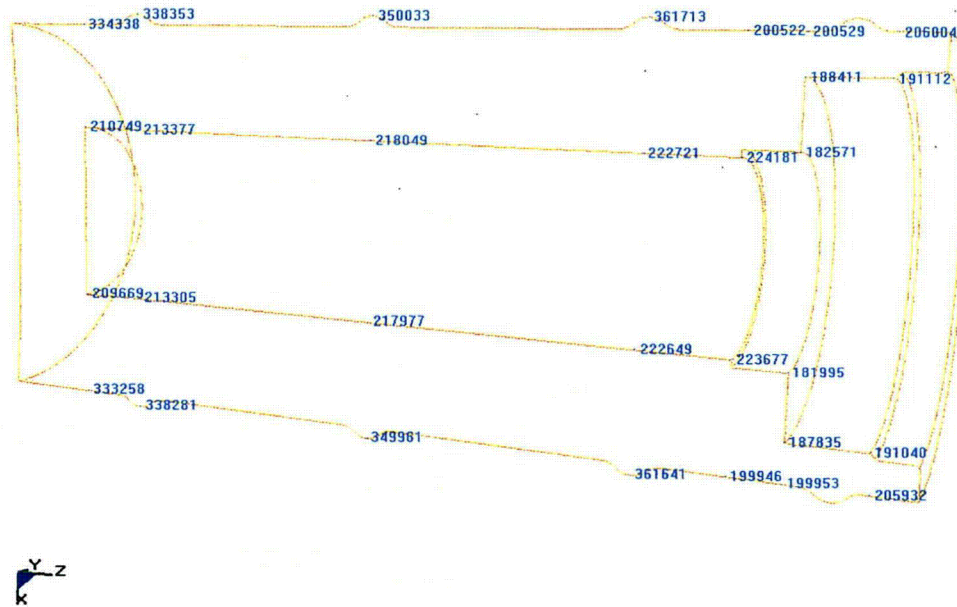


Figure 3.1.32 - Run1g, Drum Kaolite Nodes Used for Thickness Time Histories

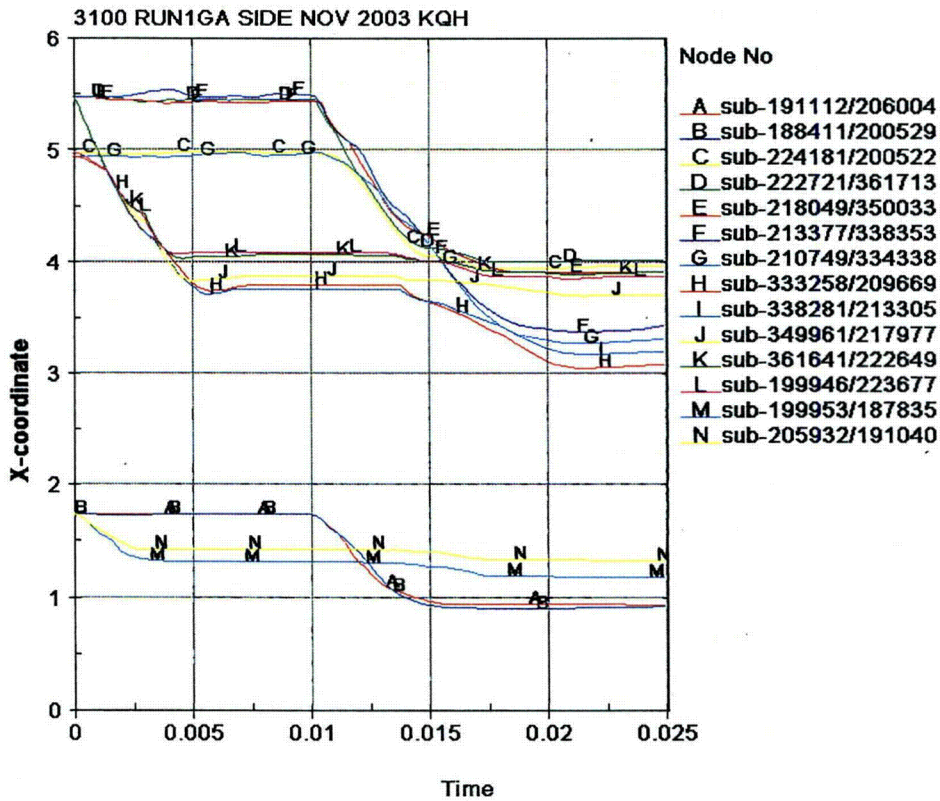


Figure 3.1.33 - Run1g, Drum Kaolite Thickness Time History



3100 RUN1G SIDE NOV 2003 KQH  
Time = 0



Figure 3.1.34 - Run1g, Drum Nodes Used to Measure Deformation Time Histories

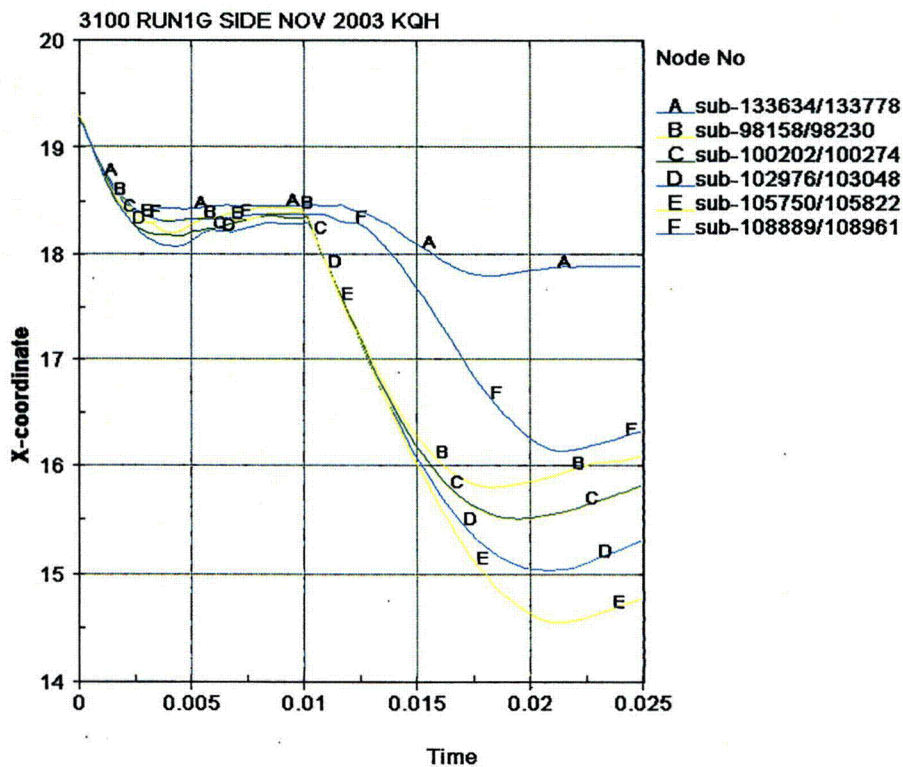


Figure 3.1.35 - Run1g, Drum Measurement Time History in the X-Direction

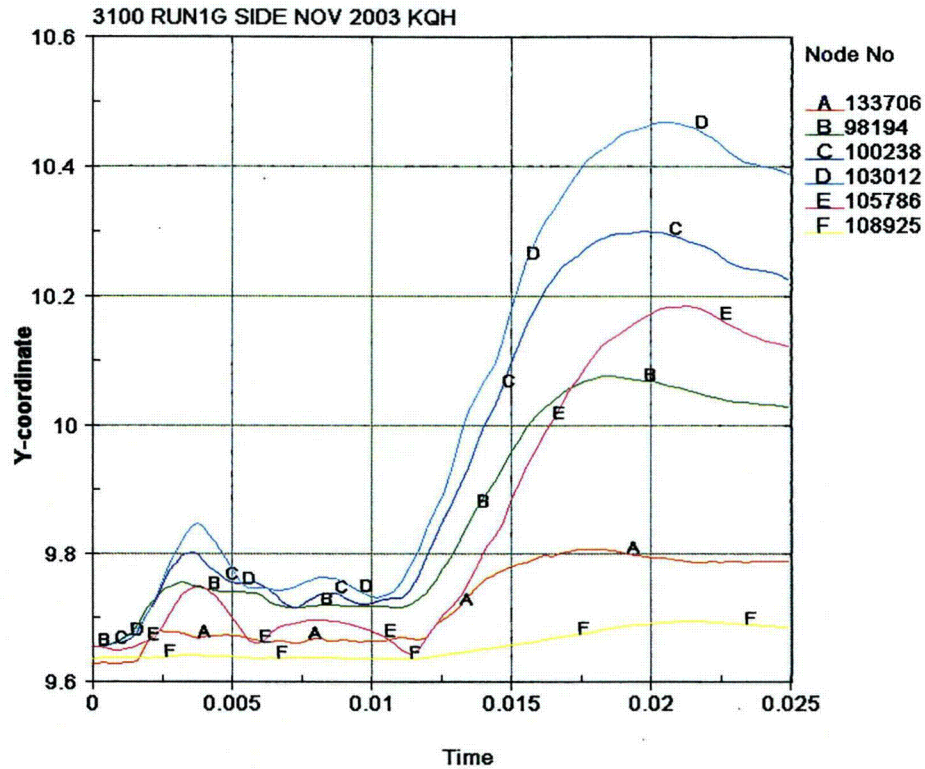


Figure 3.1.36 - Run1g, Drum Measurement Time History in the Y-Direction

3100 RUN1G SIDE NOV 2003 KQH  
Time = 0

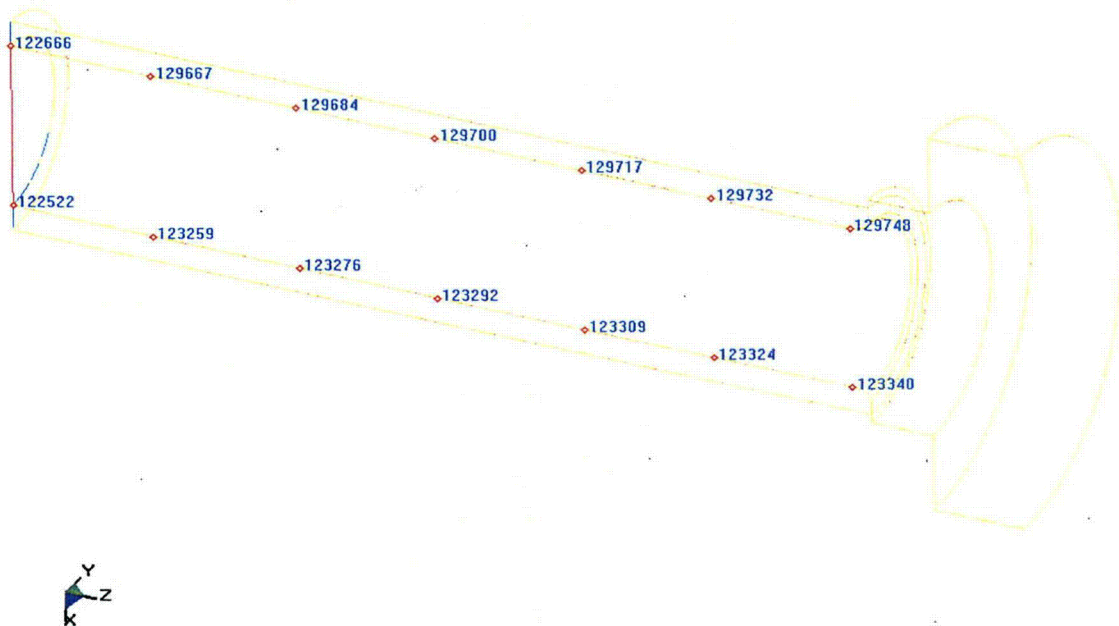


Figure 3.1.37 - Run1g, Position of Inner Liner Nodes Used for Diameter Time History

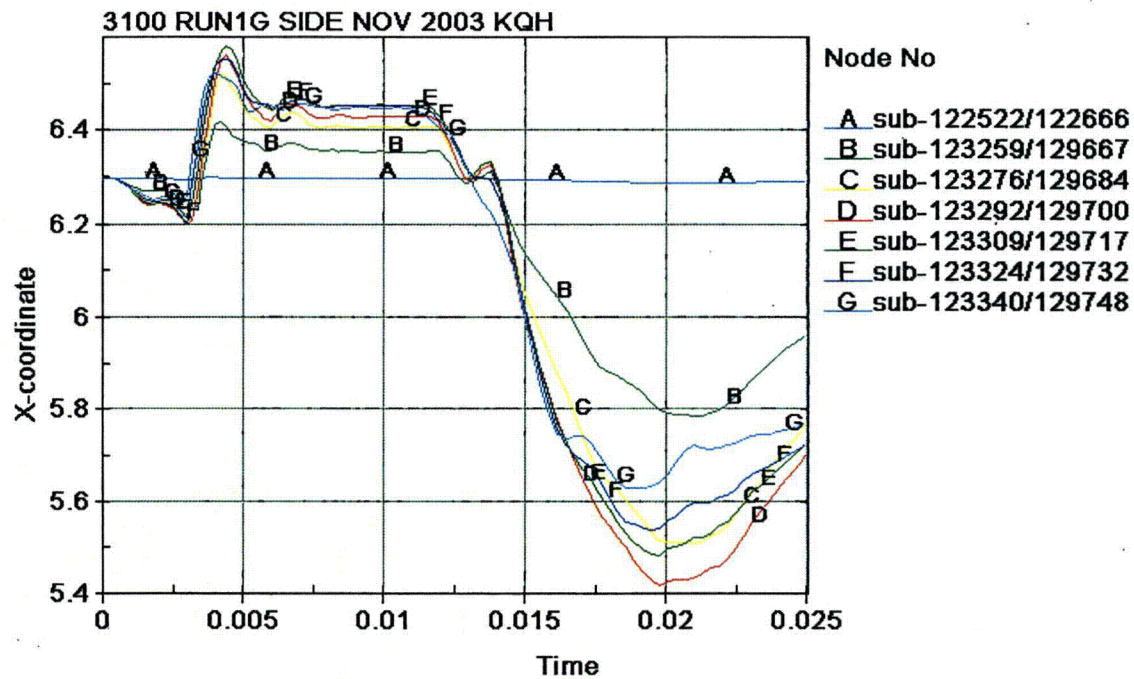


Figure 3.1.38 - Run1g, Inner Liner Diameter Time History



### 3.2 Run1ga - Side

The run1ga is a 30-foot impact followed by a crush impact, with the crush plate centered above the CV flange. The run1g 30-foot impact restart file was used and the crush plate was moved during the restart phase so that its centerline was approximately above the CV flange. The 30-foot impact was from time 0.0 to 0.0085 sec. The crush plate translation to center it above the CV flange was from time 0.0085 sec to 0.0086 sec. The run1ga crush occurred from 0.0086 sec to 0.027 sec. Therefore, the 30-foot impact results for this run would be the Section 3.1, 30-foot results for run1g, and the crush results for run 1ga (offset crush) are presented in this section.

Figure 3.2.1 shows the configuration of the model after the crush plate was moved above the CV flange (time = 0.0086 sec). Figure 3.2.2 shows the model configuration after the run1ga crush impact. Figure 3.2.3 through Figure 3.2.6 show enlarged views in the lid and bottom regions of the package assembly.

Figure 3.2.7 shows that the maximum strain in the CV body for the run1ga crush impact is 0.0348 in/in. The effective plastic strain in the CV lid is 0.0002 in/in and is shown in Figure 3.2.8. The CV nut ring remains elastic for the crush impact of run1ga.

The maximum effective plastic strain in the drum angle is shown in Figure 3.2.9 to be 0.1058 in/in. The maximum effective plastic strain in the drum is 0.3818 in/in and occurs in the top drum roll near the crush plate (Figure 3.2.10).

Figure 3.2.11 gives the maximum effective plastic strain in the lid to be 1.1345 in/in. This is a relatively high strain level and the maximum occurs near the stud hole at the 90° position (initially along Y axis). Another high region of strain is near the upper stud nearest the crush plate. The solid elements (used for contact bearing on the studs) around the stud holes show effective plastic strain maximum of 0.8745 in/in. The membrane effective plastic strain in the shell elements is a maximum of 0.8057 in/in and is highly localized near the stud hole at the 90° position. Some tearing of the lid could occur in the lid hole at the 90° position and at the lid hole nearest the crush plate (180°).

Figure 3.2.12 shows the effective plastic strain levels in the drum studs. The maximum is shown to be 0.5207 in/in and occurs in the stud at the 90° position. From Figure 3.2.12 it is seen that the elevated strain occurs near the outer extreme of the stud, and that the through thickness strain levels between 0.3170 and 0.3802 in/in exist.

A study of the timing of the elevated effective plastic strain levels in the lid and the drum studs shows that the lid reaches failure magnitudes before the studs. At the stud hole in the drum lid nearest the crush plate (180°), the bending strain crosses the 0.57 in/in

strain at about 0.0122 seconds in the crush impact. The membrane strain in the lid elements at 180° reaches a maximum of .5295 in/in. The stud at 180° does not experience elevated strain levels (final maximum in this stud is 0.17 in/in). So at the 180° position, only the lid experiences relatively high levels of effective plastic strain.

At the 90° position in the lid, the membrane effective plastic strain exceeds the 0.57 in/in level near 0.0164 seconds in the crush impact. The surface maximum effective plastic strain exceeds 0.57 in/in at about 0.0161 seconds, slightly ahead of the membrane. At time 0.0164 seconds, the effective plastic strain levels in the stud at 90° is about 0.35 in/in maximum, with the through thickness levels between 0.104 in/in to 0.136 in/in. Therefore, at the 90° position, the lid reaches the failure level of 0.57 in/in before the stud.

From this timing data, it is shown that the lid would reach failure levels in bending and membrane before the stud effective plastic strain levels become relatively high. Therefore, it would be expected that the lid would locally tear before the bolting reached elevated effective plastic strain levels, thus possibly reducing the loadings on the studs. Due to the extent of the relatively high levels of effective plastic strain in the drum lid, it would be expected that any lid tearing would be localized and that the large washers would restrain the drum lid.

The effective plastic strain contour patterns for the other components are not shown in figures. The maximum effective plastic strain in the drum bottom is 0.2444 in/in; in the liner it is 0.2853 in/in; in the lid stiffener it is 0.1116 in/in; in the drum stud nuts it is 0.0103 in/in; in the drum stud washers it is 0.1685 in/in and in the plug liner it is 0.2181 in/in.

The kinetic energy time history for the crush plate impact is shown in Figure 3.2.13. The X velocity time history is shown in Figure 3.2.14.

The lid separation time history is shown in Figure 3.2.15 (nodes defined in Figure 3.1.30). From Figure 3.2.15 it is seen that the spike separation of just under 0.004 inches can occur with a final nominal separation of less than 0.002 inches expected.

The kaolite thickness time histories for the nodes defined in Figure 3.1.32 are given in Figure 3.2.16 for run1ga. The drum diameter time histories are given in Figures 3.2.17 and 3.2.18. The nodes defining this response are shown in Figure 3.1.34. As shown in Figure 3.2.17, the bottom head and the bottom drum roll remain at, or near 30-foot impact diameters for the crush impact. This response is expected as qualitatively shown in Figure 3.2.2. The response in the Y-direction is shown in Figure 3.2.18.

Figure 3.2.19 shows the diameter time history for various locations along the liner length. Figure 3.1.37 and Table 3.1.3 define the locations at which the diameters are obtained.



3100 RUN1GA SIDE NOV 2003 KQH  
Time = 0.0086

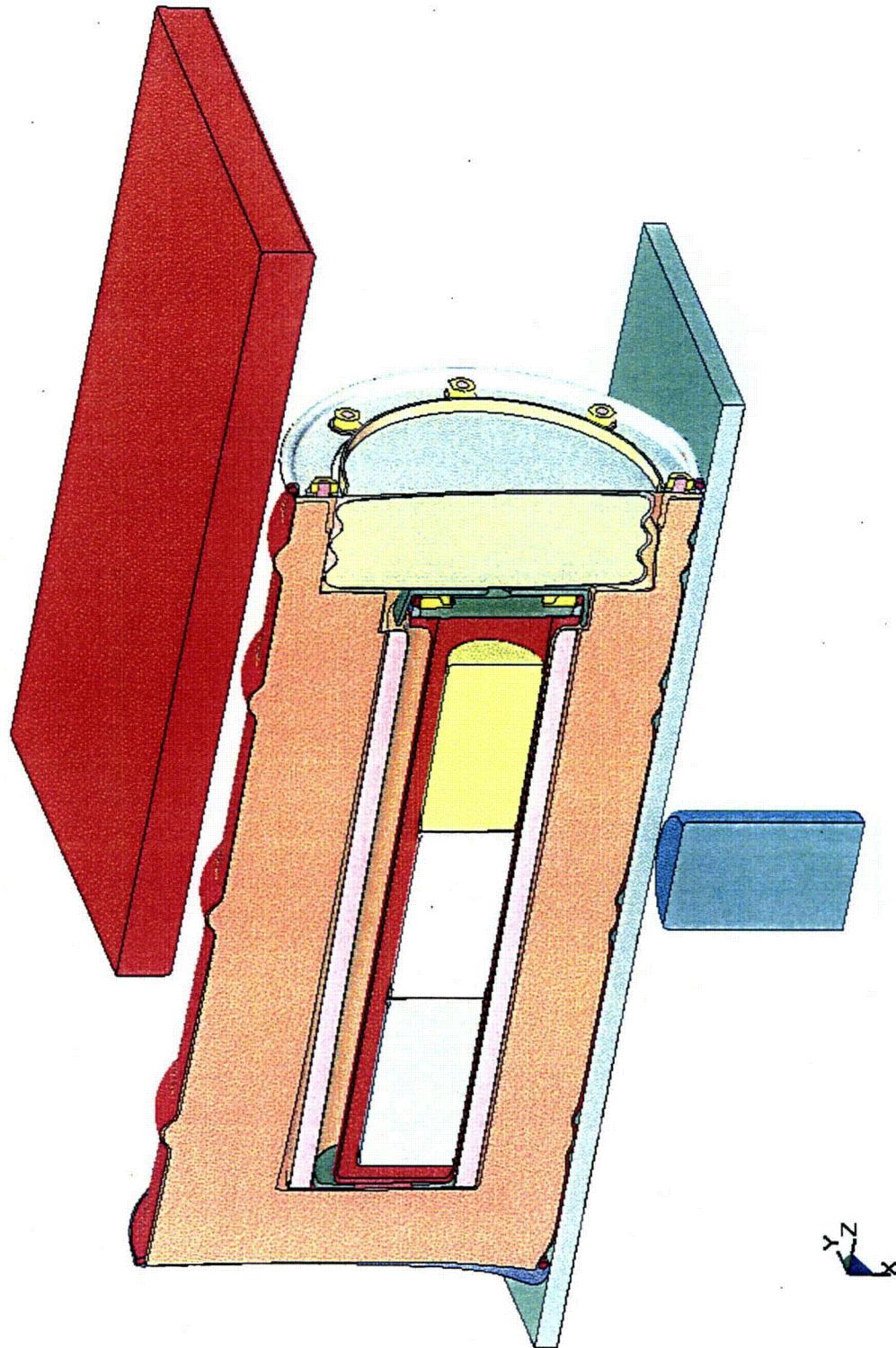


Figure 3.2.1 - Run1ga, Crush Impact, Initial Configuration for the Crush Impact

3100 RUN1GA SIDE NOV 2003 KQH  
Time = 0.027

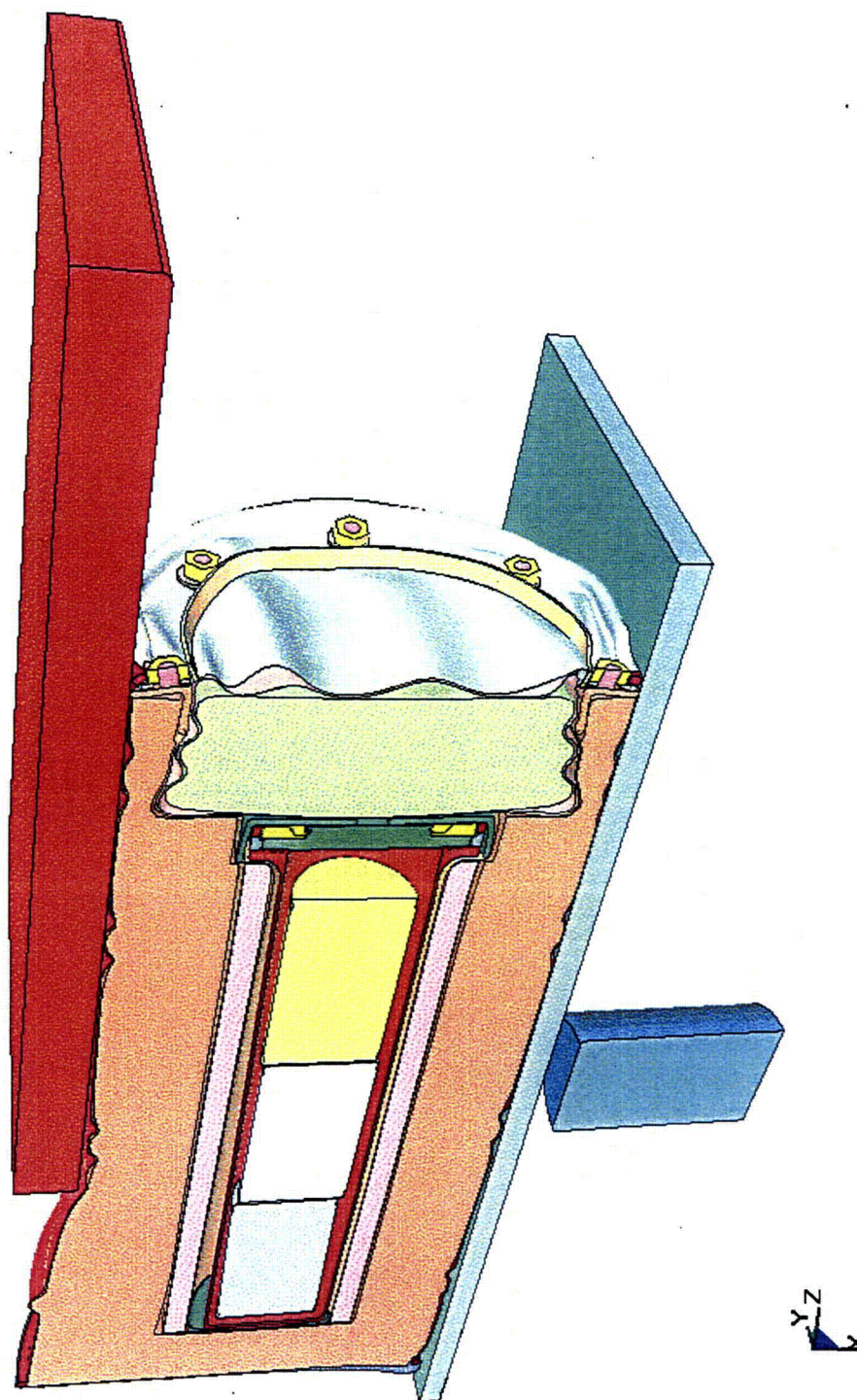


Figure 3.2.2 - Run1ga, Crush Impact, Configuration of the ES-3100 After the Crush Impact



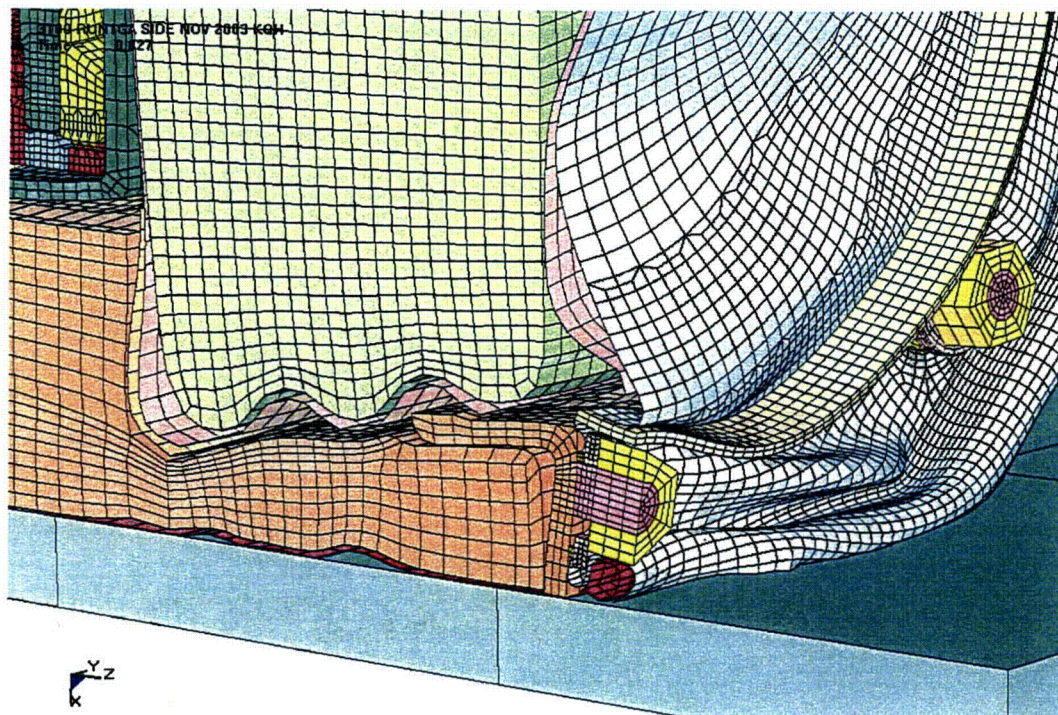


Figure 3.2.3 - Run1ga, Crush Impact, Configuration of the Lid Region Near the Rigid Plane

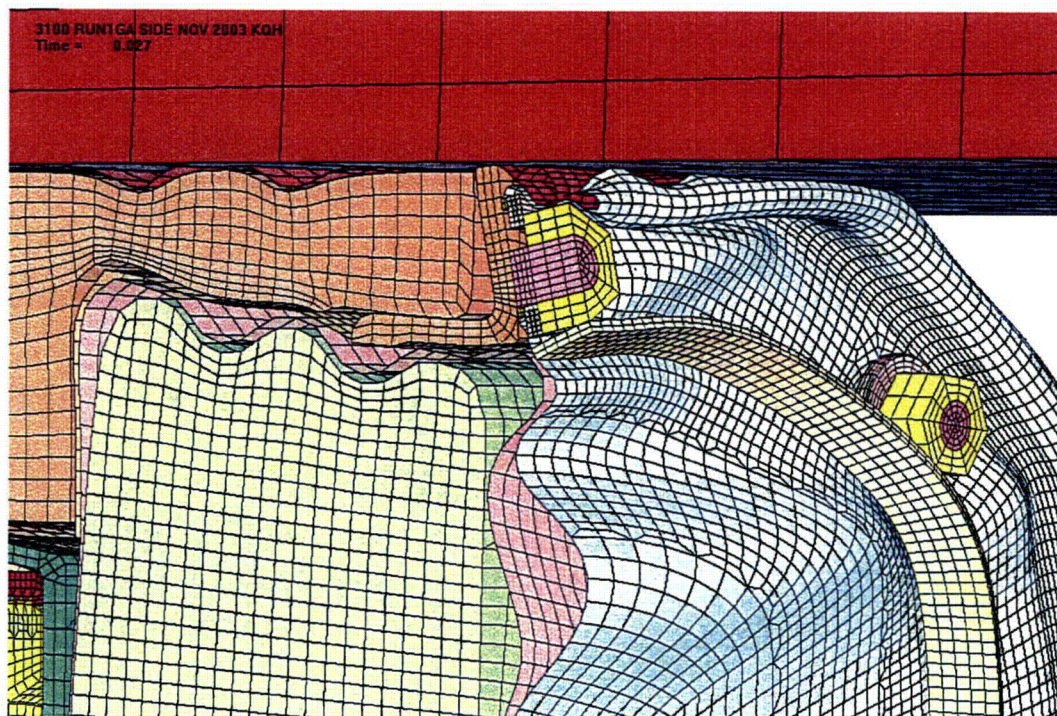


Figure 3.2.4 - Run1ga, Crush Impact, Configuration of the Lid Region Near the Crush Plate



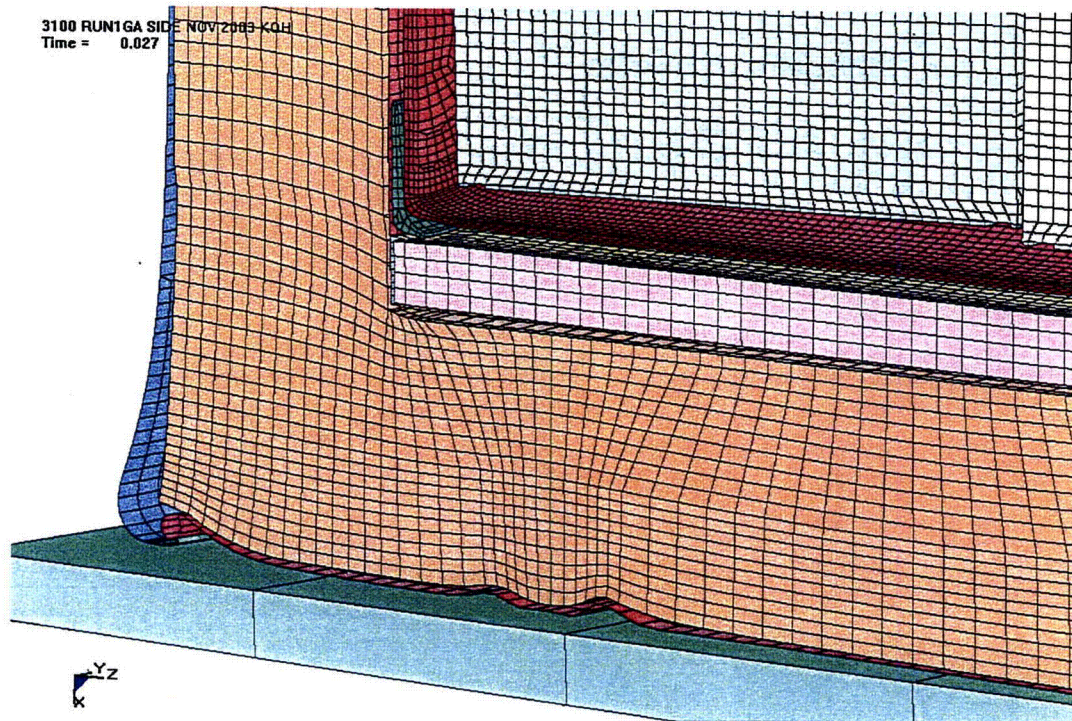


Figure 3.2.5 - Run1ga, Crush Impact, Configuration of the Bottom Near the Rigid Plate

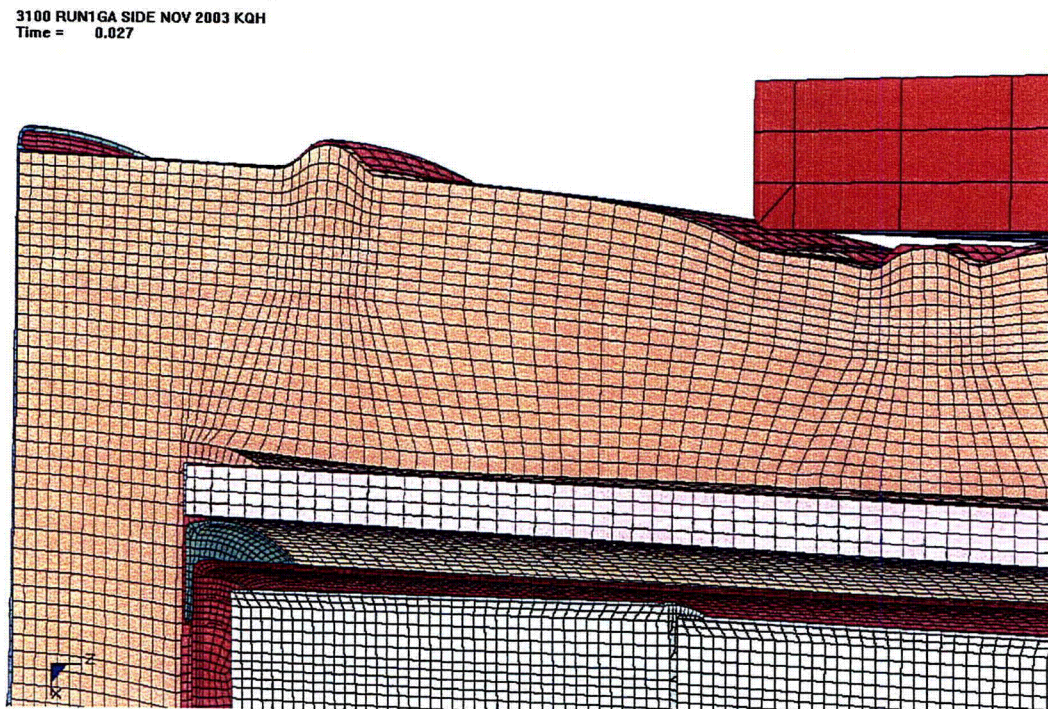


Figure 3.2.6 - Run1ga, Crush Impact, Configuration of the Bottom Near the Crush Plate



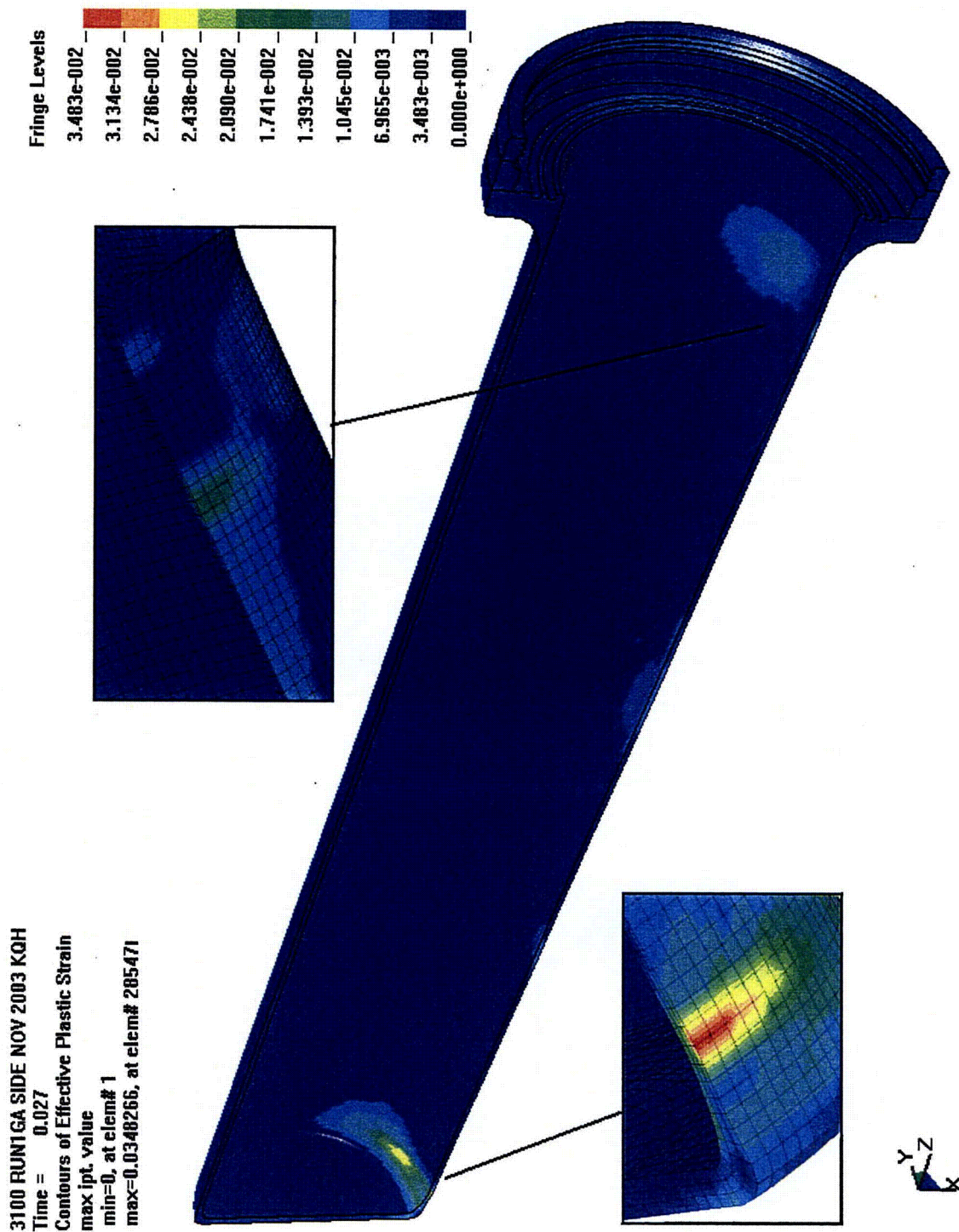
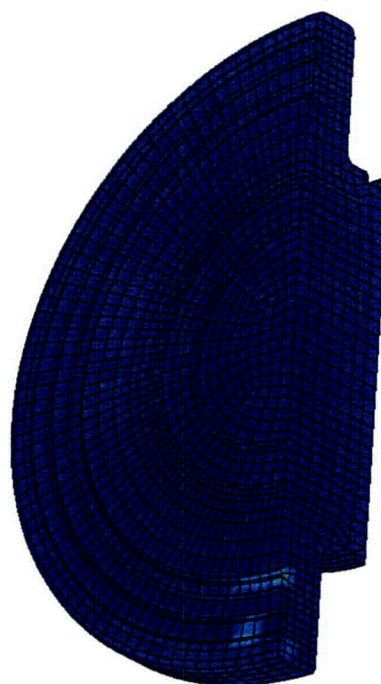


Figure 3.2.7 - Run1ga, Crush Impact, Effective Plastic Strain in the CV Body

3100 RUN1GA SIDE NOV 2003 KQH  
Time = 0.027  
Contours of Effective Plastic Strain  
max ipt. value  
min=0, at elem# 51809  
max=0.000174097, at elem# 565471

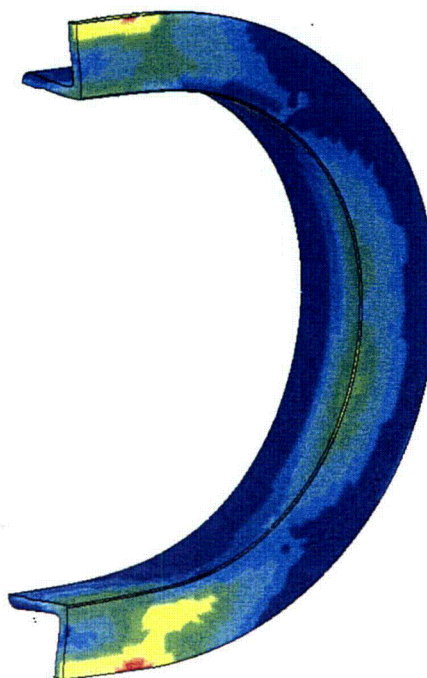


Fringe Levels

1.741e-004  
1.567e-004  
1.393e-004  
1.219e-004  
1.045e-004  
8.705e-005  
6.964e-005  
5.223e-005  
3.482e-005  
1.741e-005  
0.000e+000

Figure 3.2.8 - Run1ga, Crush Impact, Effective Plastic Strain in the CV Lid

3100 RUN1GA SIDE NOV 2003 KQH  
Time = 0.027  
Contours of Effective Plastic Strain  
max ipt. value  
min=0, at elem# 61157  
max=0.10579, at elem# 679231



Fringe Levels

1.058e-001  
9.521e-002  
8.463e-002  
7.405e-002  
6.347e-002  
5.289e-002  
4.232e-002  
3.174e-002  
2.116e-002  
1.058e-002  
0.000e+000

Figure 3.2.9 - Run1ga, Crush Impact, Effective Plastic Strain in the Drum Angle



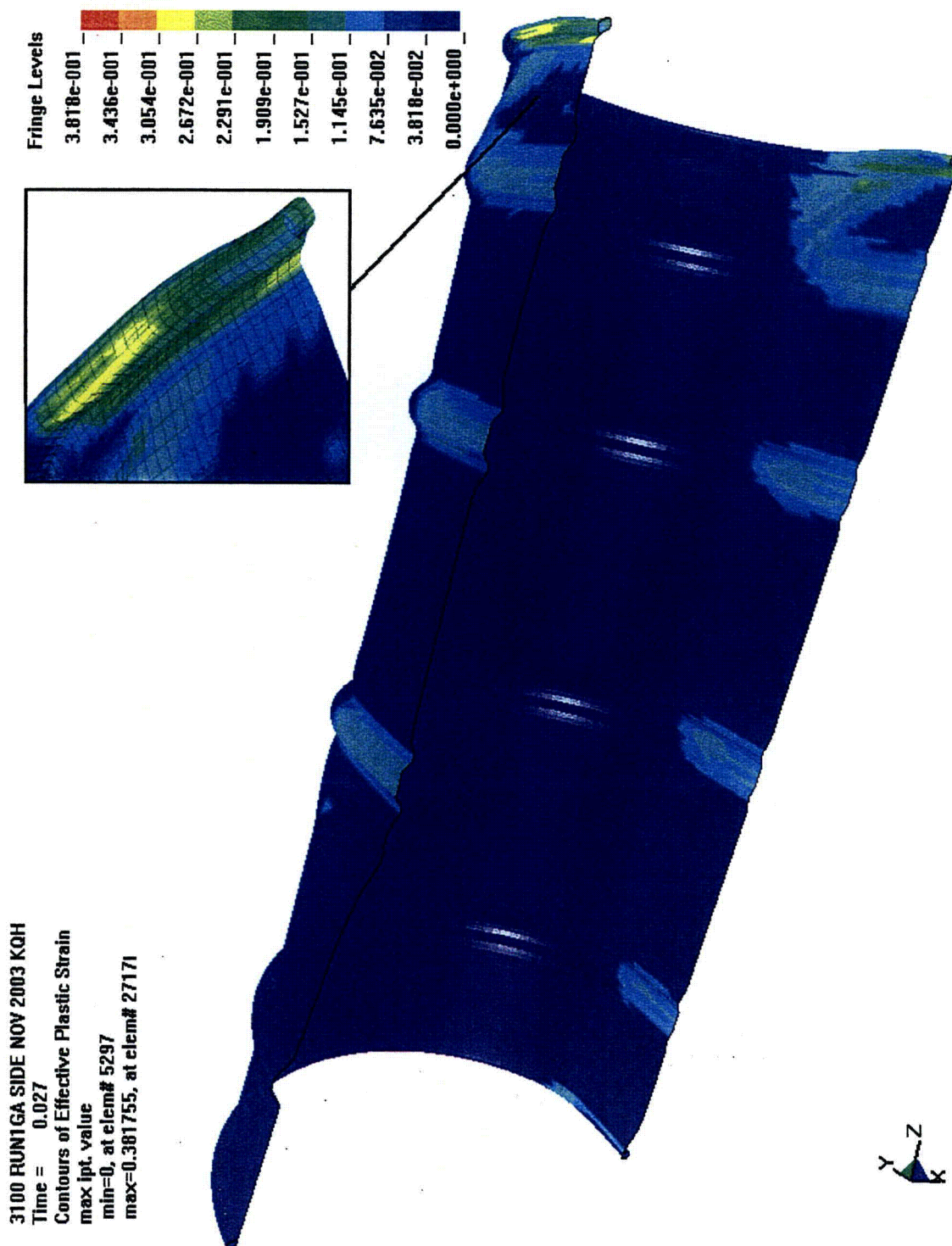


Figure 3.2.10 - Run1ga, Crush Impact, Effective Plastic Strain in the Drum

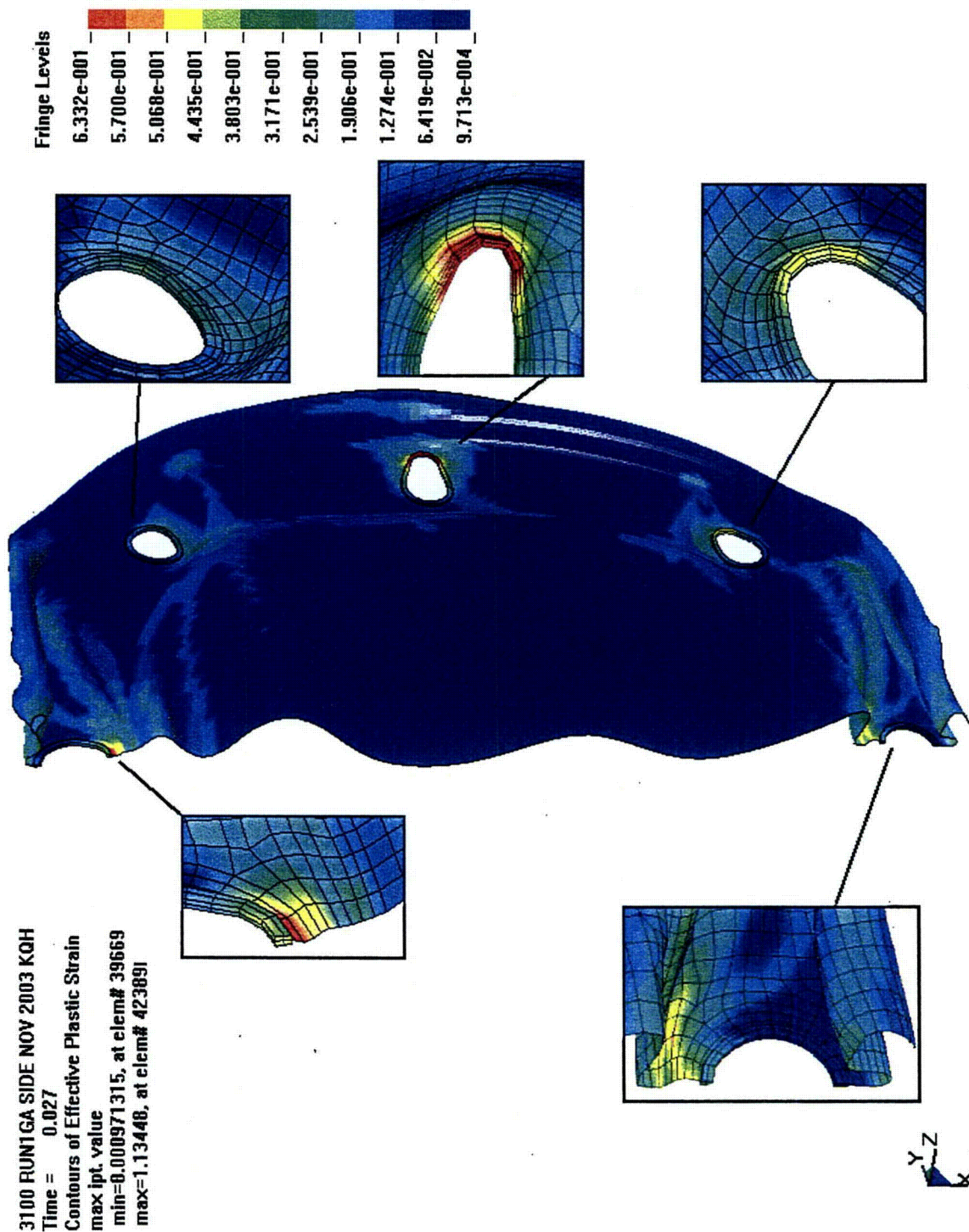
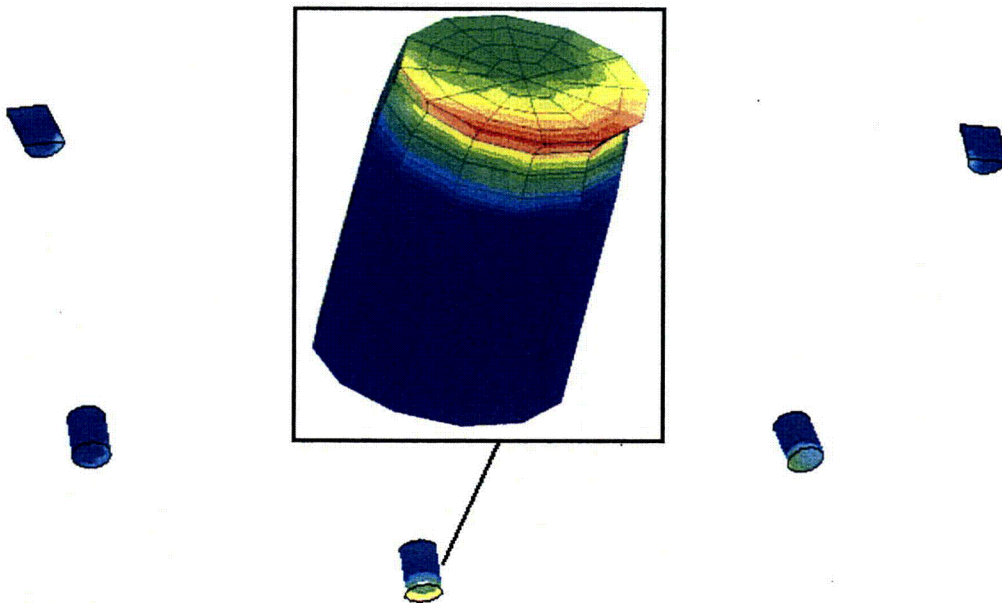
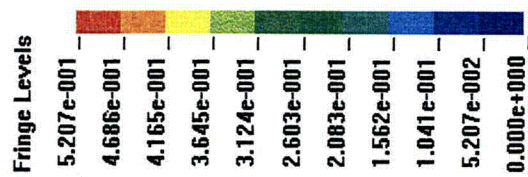


Figure 3.2.11 - Run1ga, Crush Impact, Effective Plastic Strain in the Lid



3100 RUN1GA SIDE NOV 2003 KQH  
 Time = 0.027  
 Contours of Effective Plastic Strain  
 max ipt. value  
 min=0, at elem# 71878  
 max=0.520685, at elem# 726501



Figure 3.2.12 - Run1ga, Crush Impact, Effective Plastic Strain in the Drum Studs



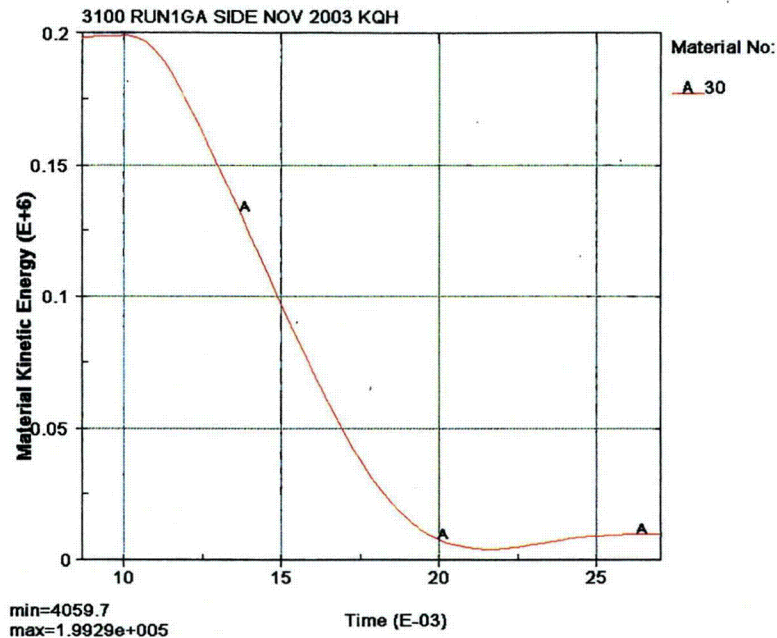


Figure 3.2.13 - Run1ga, Crush Impact, Kinetic Energy Time History

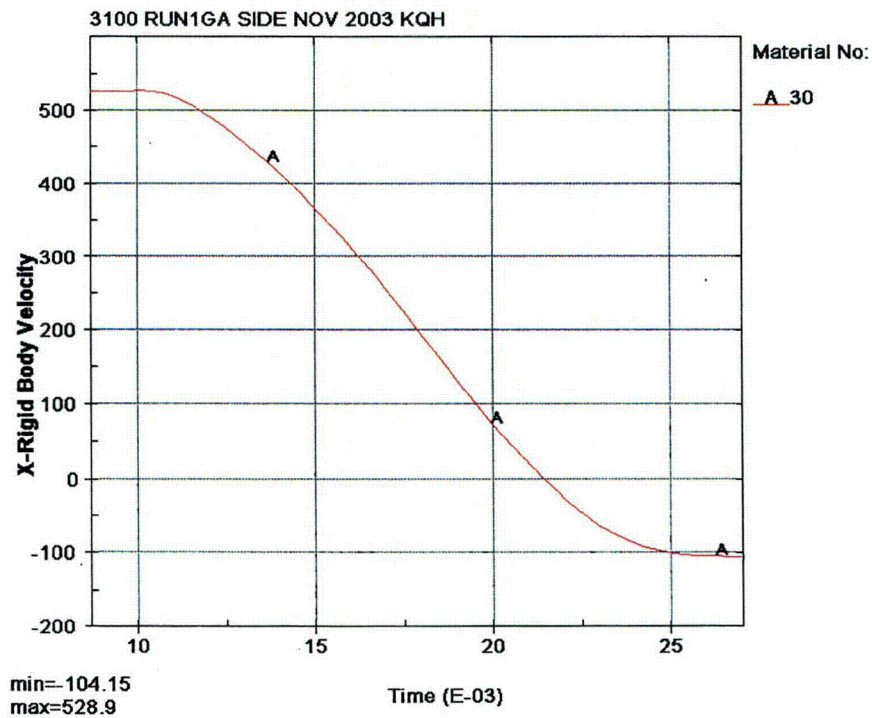


Figure 3.2.14 - Run1ga, Crush Impact, X Velocity Time History

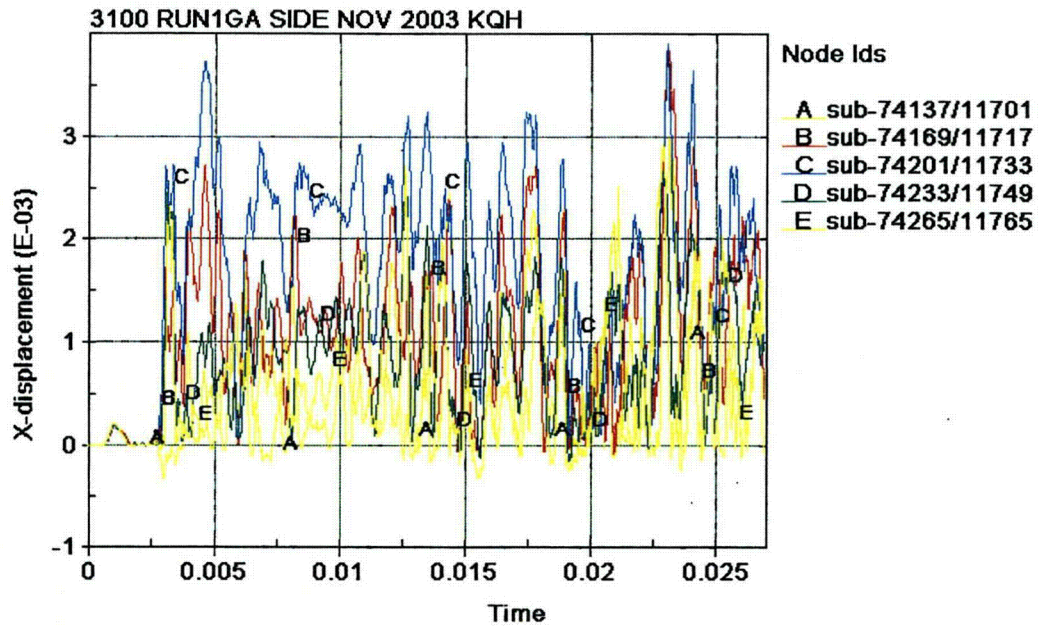


Figure 3.2.15 - Run1ga, Lid Separation Time History

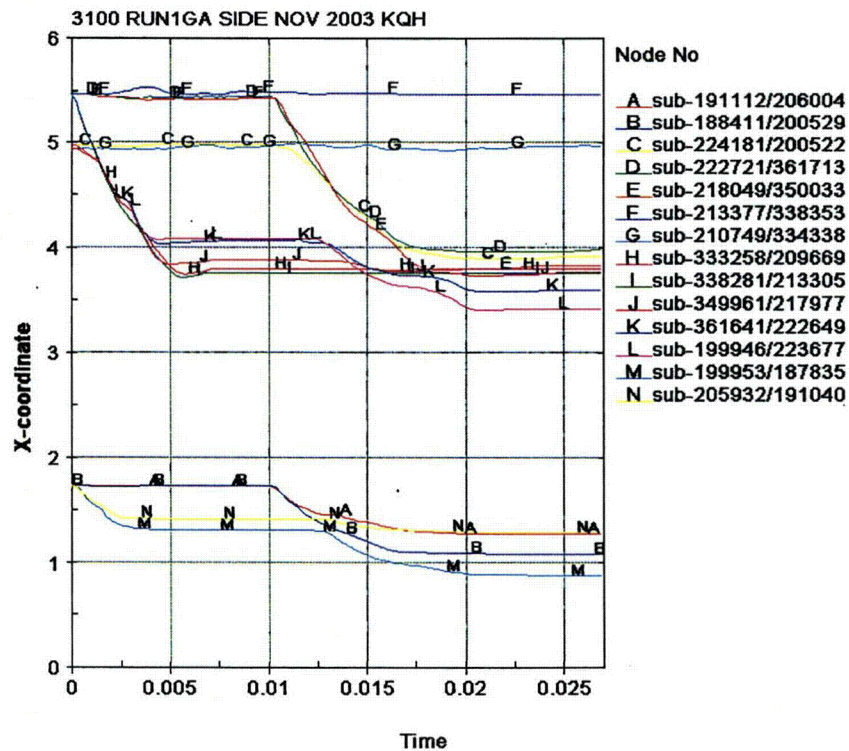


Figure 3.2.16 - Run1ga, Drum Kaolite Thickness Time Histories

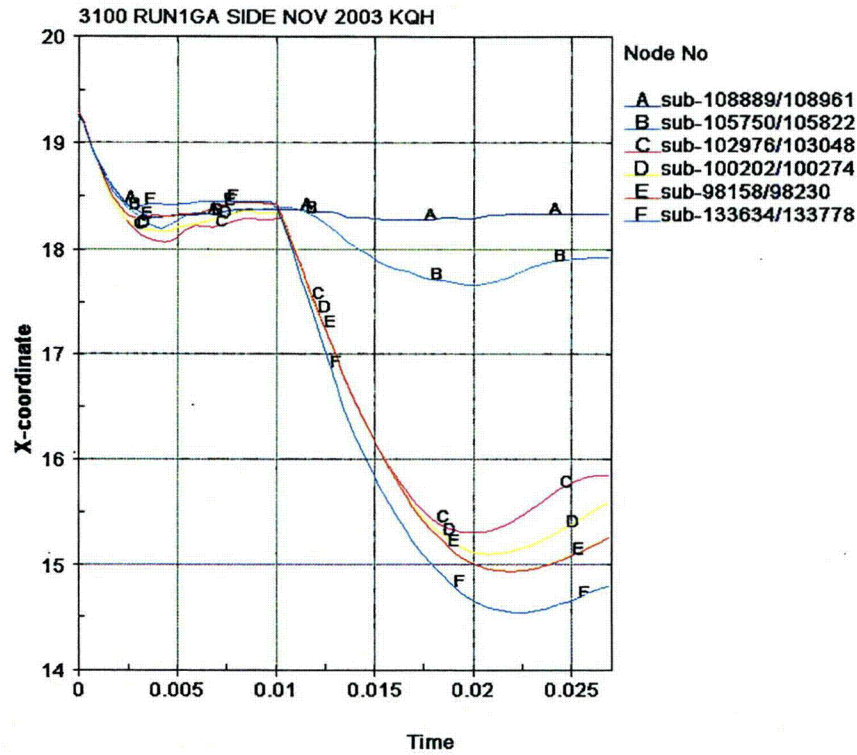


Figure 3.2.17 - Run1ga, Drum Dimension Time History in the X-Direction

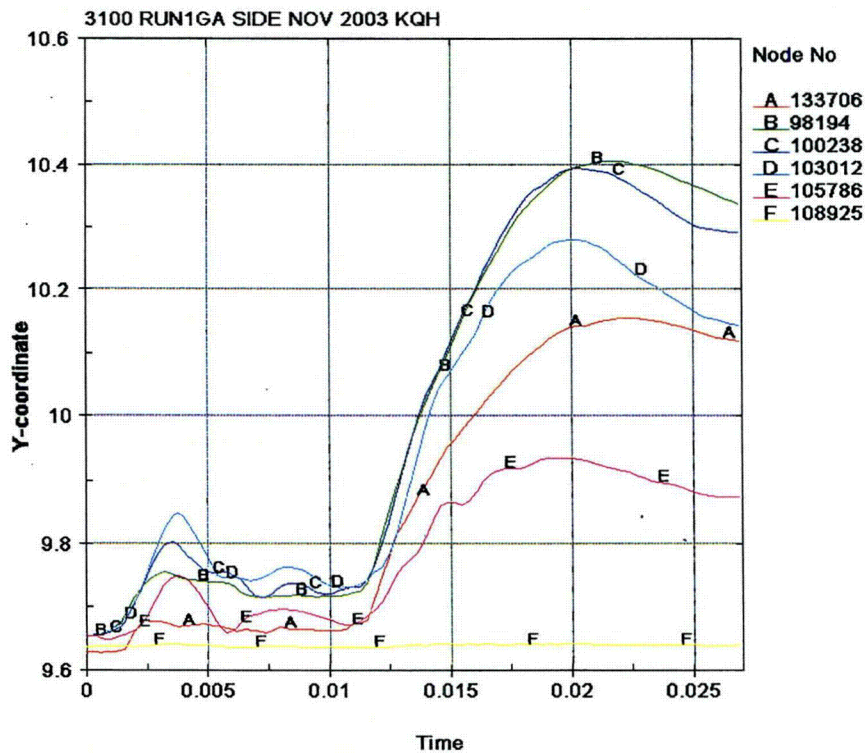


Figure 3.2.18 - Run1ga, Drum Dimension Time History in the Y-Direction



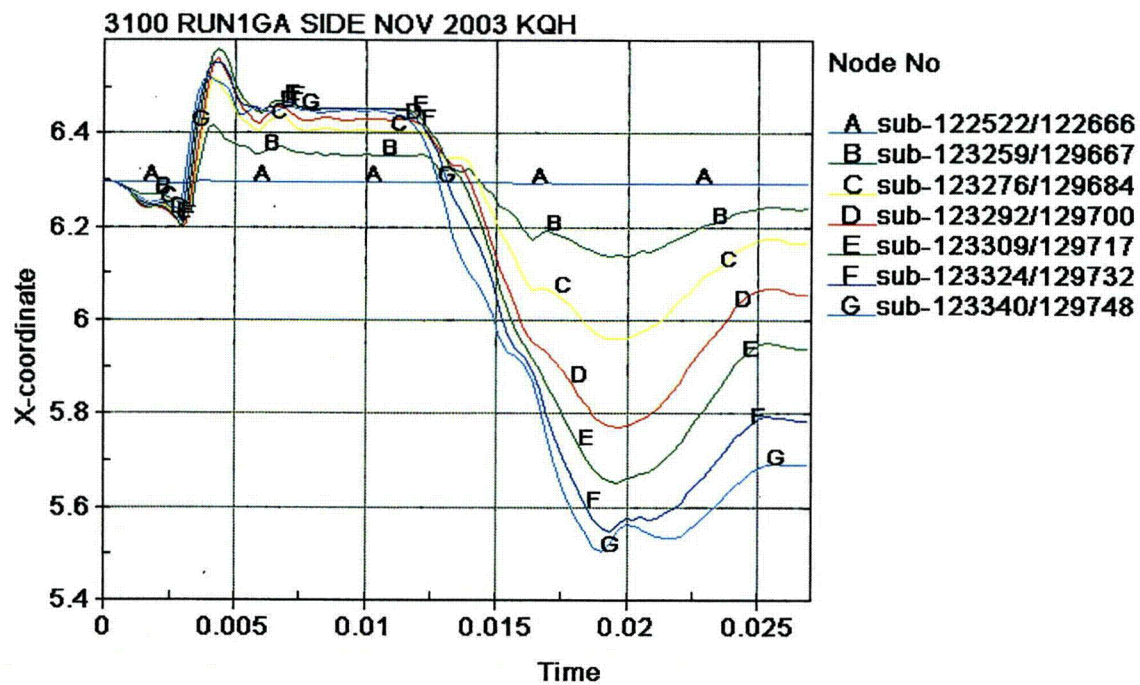


Figure 3.2.19 - Run1ga, Liner Diameter Time History